Structural Insights into Viral Membrane Fusion Machinery via Cryo-Electron Tomography: Influenza Virus and Human Parainfluenza Virus

Long Gui

A dissertation submitted

in partial fulfillment of the requirements

for the degree of

Doctor of Philosophy

University of Washington

2016

Reading Committee:

Kelly Lee, Chair

Abhinav Nath

Liguo Wang

Program Authorized to Offer Degree:

Medicinal Chemistry

University of Washington

Abstract

Structural Insights into Viral Membrane Fusion Machinery via Cryo-Electron Tomography: Influenza Virus and Human Parainfluenza Virus

Long Gui

Chair of the Supervisory Committee:

Associate Professor Kelly K. Lee

Department of Medicinal Chemistry

Enveloped viruses such as influenza virus and human parainfluenza virus use specialized protein machinery to fuse their membrane with the cellular membrane of target host cells and thus deliver their genome for replication. This protein-mediated membrane fusion is also a ubiquitous and key event that underlies many fundamental cellular processes. Despite its biological significance, the states that drive the fusion process have been refractory to classical structure determination, and the interplay of fusion proteins and membranes remains exclusive. My dissertation focused on direct structural characterization of viral fusion proteins and interplay between fusion proteins and membrane during fusion, using a combined approach of cryo-electron tomography (cryo-ET) and fluorescence spectroscopy. Firstly, in Chapter 2, I have investigated the 3-dimensional organization and population kinetics of the intermediates during fusion of influenza virus with membranes. I observed that progression of membrane reorganization proceeded through an extended contact zone with tightly apposed virus-target

membrane interactions and this study provided the first demonstration of the sequence of membrane deformations during fusion. In Chapter 3, influenza virus fusion peptide-induced membrane deformation for isolated fusion proteins was compared with the behavior on whole viruses. I also examined the influence of cholesterol on the type of membrane deformations that were induced by activated influenza virus fusion protein. This study showed that isolated, soluble influenza virus fusion protein by itself could induce significant membrane deformation and that cholesterol had a very noticeable effect in stabilizing the target membrane against fusion protein-induced membrane deformation. Finally, I examined a parallel enveloped virus system to influenza virus by studying the organization of surface glycoproteins on human parainfluenza virus 3 (HPIV3) in Chapter 4. Using a combination of negative-staining and cryo-ET I was able to resolve the distributions of receptor binding protein and fusion protein, even to identify the conformational states of these proteins on the virus surface in some cases. My observations are consistent with a model for fusion in which prefusion fusion proteins associate with receptor binding proteins prior to receptor engagement. In conclusion, my studies have shown that a combination of biophysical and structural approaches can provide new insights into the process of protein-mediated membrane fusion.

Table of Contents

List of Figures

List of Tables

Acknowledgements

This dissertation would not have been attempted, let alone completed, without the unstinted support from so many people in so many ways. I shall therefore seize this opportunity to express my greatest thanks and utmost respects for all those who have helped during my journey to Ph.D.

To start with, my sincere gratitude goes to my supervisor and mentor, Dr. Kelly Lee, who has provided tremendous help and guidance in my graduate research. Because I am one of the first graduate students in the lab, he has spent a lot of time teaching me basic experimental protocols such as sample preparation, electron microscope operation, data analysis, and so on. Besides the laboratory skills, he has also provided consistent support and generous assistance on my way to becoming a scientist. He encouraged me to think deeply about the biological sense of our experiments and how we could improve our knowledge based on our results. Finally, he always served as a great source of enthusiasm and inspiration. There are many pretty memorable and wonderful moments that will never decrease over time. I would also like to thank the other members of my doctoral and dissertation reading committees: Dr. Sarah Keller, Dr. Abhinav Nath, Dr. William Atkins, and Dr. Liguo Wang. Without their guidance and support, this dissertation would never have been possible. I thank them especially for guiding me to understand what the research and scholar can be and should be. Dr. Keller has been continually encouraging and has introduced me the amazing field of membrane lipids. Dr. Nath has provided tremendous help in my thesis writing and I am greatly thankful for his guidance on statistical analysis of biological data. Dr. Atkins has encouraged me and extended my vision by kinetics studies. Dr. Wang, who is so supportive and caring, has provided generous assistant and suggestions about electron microscope.

I also want to extend my appreciation to scholars who have helped me during my graduate studies at University of Washington. I would like to thank Dr. David Baker and Dr. Phil Bradley for providing rotation opportunities at my first year of graduate school. Many thanks go to Dr. Rachel

Klevit, Dr. Trisha Davis and Dr. Wenqing Xu who have kindly provided teaching assistant positions. I also want to thank Dr. Carlos Catalano (now at University of Colorado) who was my committee member from 2012 to 2015.

I would like to express my sincere and humble thanks to my colleagues, friends and peers at the University of Washington over the years: Natalie Garcia, Tad Davenport, Mike Guttman, James Williams, Jamie Ebner, Alex Mileant, Mark Benhaim, Modestas Filipavicius, Yan Han, Yu-ruei Wang, and Scott Delbecq. It has been a wonderful experience to work, play, and live with such passionate, stimulating and friendly people. Their friendship and company have carried me through many difficult times of research and writing and will still support me.

At last, I reserve my deepest gratitude to my loving family members. I am mostly thankful for my parents (Daolin Wang and Yuping Wang), who have sacrificed many things and been continuously supporting me throughout the years. Although most of the time we are separated by the ocean and can only communicate via video chat, their priceless love and spiritual support have always companied me.

Dedication

To my beloved family

for their constant support and unconditional love

Chapter 1. Introduction

Membrane fusion is the process whereby two separate lipid membrane bilayers merge into a single continuous one. It occurs widely in almost all biological systems including the entry of enveloped virus, synaptic signaling, intracellular vesicle trafficking, membrane repair, vacuole fusion, cell-cell fusion and even fertilization of eggs by sperms (Martens & McMahon, 2008; Harrison, 2008; Jahn *et al*, 2003). Despite intensive studies, the basic mechanism of how fusion proteins interact with lipid membranes to induce their fusion has largely eluded characterization. In this introductory chapter, I will start with a concise introduction of the shared motifs of protein-mediated membrane fusion. Then I will also briefly discuss how components of lipid bilayers could affect membrane fusion. The viral fusion protein machinery from influenza virus and human parainfluenza virus 3 (HPIV3) will be introduced as an example. Finally, I will present the technique, cryo-electron tomography, used in my research and recent advances of this technique.

1.1 Mechanism of protein-mediated membrane fusion

Fusion of two separate bilayers is thermodynamically favorable, but must overcome some energy barriers. One energetically demanding process is to bring the membranes into close proximity where a repulsive “hydration force” needs to be overcome. The energy barriers are also related to curvature deformations during the membrane fusion (Jahn *et al*, 2003; Chernomordik & Kozlov, 2008; Harrison, 2008). The role of fusion proteins is to lower these energy barriers at the appropriate time and place to regulate the fusion process (Figure 1.1A)(Jahn *et al*, 2003; Martens & McMahon, 2008; White *et al*, 2008). The accumulated evidence from numerous membrane-fusion studies suggests that in different biological reactions, membrane fusion is controlled by distinct fusion proteins. Intracellular membrane fusion plays a significantly important role in distribution of building blocks into various organelles and deliver of signaling molecules. The cellular fusion machinery consists of two matching halves, v-SNAREs on the vesicle and

cognate t-SNAREs on the target, which will later fuse and drive membrane fusion. In contrast to intracellular fusion, viral membrane fusion is exclusively mediated by the viral fusion proteins (Söllner, 2004; White *et al*, 2008).

However, numerous studies of membrane fusion suggest that there are general principles and conserved motifs in many disparate fusion reactions (Chernomordik & Kozlov, 2008; 2005). For instance, many biological fusion events proceed through a “hemifusion intermediate”, in which the proximal leaflets have merged, but not yet the distal ones (Figure 1.1B). As shown in Figure 1.1B, membrane fusions start with the dehydration step in which two lipid membrane bilayers approach. Then a point-like membrane protrusion minimizes the energy of the hydration repulsion between the proximal leaflets of the membranes coming into immediate contact, followed by the formation of a narrow “stalk” with proximal leaflets fused and distal leaflets unfused. Stable arrays of such stalk have been observed in block copolymer melts (Disko *et al.,* 1993) and in lipid systems (Yang and Huang, 2002). The pathway by which the hemifused stalk proceeds into open fusion pores is still not well understood. The hypothesis of hemifusion diaphragm, proposed 30 years ago by Kozlov and Markin, was mostly accepted as the standard pathways of membrane fusion (Kozlov and Markin, 1983). In this hypothesis, the stalk expands axially as the tension causes the inner leaflets to recede, resulting in a hemifusion diaphragm that consists of the two outer leaflets of the opposing bilayers. Then this single bilayer needs to be punctured in order to open a fusion pore. An alternative hypothesis consisting of a leaky pathway that progresses through the formation of a stalk-hole complex is proposed about ten years ago in a few of molecular dynamics simulations. In this model, the initial step of the stalk formation was the same as the hemifusion diaphragm hypothesis. However, instead of expanding axially, the stalk elongated linearly and began to wander. The presence of the stalk tended to destabilize the membranes causing a hole to appear near the stalk in at least one of the bilayer. Elongation of the stalk-hole complex resulted into the formation of final open pore. Direct imaging approaches such as cryo-electron tomography (will be introduced later) towards fusion events have just begun

to shed a light on this debate. For example, one model based upon real-time fluorescence microscopy and cryo-electron microscopy imaging of SNARE-mediated fusion in an *in vitro* system reconstituted from components and liposomes suggested that SNARE-mediated fusion proceeds via point-like, dimpled contacts while hemifusion diaphragm appeared be kinetic traps, which were less efficient in achieving full fusion (Diao *et al*, 2012). Another study indicated that tightly docked membranes spanning large areas of the two opposing membranes lead to hemi-fusion as the primary route to SNARE-mediated fusion pore formation (Hernandez *et al*, 2012). More direct structural characterization of protein-mediated membrane fusion events under a range of conditions and covering the nascent initial stages of membrane deformation through formation of fusion pores will improve our understanding of this complex, dynamic process.

Lipid composition of membrane bilayers plays an important role in membrane fusion. The propensities of membrane to deform, hemifuse and develop to fusion pores have been found to depend on lipid structure and its spontaneous curvature (Chernomordik & Kozlov, 2008). The area of dioleoylphosphatidylcholine (DOPC) polar heads and hydrocarbon chains are similar so that the lipid has the overall shape of a cylinder. Thus monolayers formed by DOPC are almost flat at room temperature (Figure 1.2A). However, lysophosphatidylcholine (LPC), a modified form of DOPC where one fatty acid residue is removed, has a smaller hydrophobic chain and inverted-cone shape. Monolayers formed by inverted cone-shaped lipids tend to self-assemble into curved monolayers whose surface bulge in the direction of polar heads (Figure 1.2B). Finally, lipids including phosphatidylethanolamine (PE) and bis(monoacylglycero)phosphate (BMP) with smaller headgroups compared to their wider fatty side chains tend to form monolayers with surfaces bulging in the direction of the hydrocarbon chains. Lipids could either promote or inhibit the formation of a particular fusion intermediate depending on the net curvature of that intermediate. For instance, cone-shaped PE promotes, but inverted core-shaped LPC inhibits the formation of hemifusion stalk when added to the proximal leaflets of the fusing membranes (Figure 1.2C) (Chernomordik & Kozlov, 2008).

Another important fusion factor that affects membrane fusion is the presence of cholesterol (Figure 1.3A). Cholesterol is universally present in large amounts (about 20 – 40%) in eukaryotic plasma membranes (Mouritsen & Zuckermann, 2004). The unique structure of cholesterol consists of a small polar headgroup and a rigid hydrophobic body(Maxfield & Tabas, 2005; Mouritsen & Zuckermann, 2004). Cholesterol is known to increase lipid order in fluid membranes through the effects of its rigid body and the ability to fill interstitial spaces between neighboring phospholipids. Also the smaller headgroup of cholesterol compared to the headgroup of other phospholipids makes it easier to flip-flop between leaflets of the membrane (Figure 1.3B) (Bruckner *et al*, 2009). Thus, cholesterol is believed to play a crucial role in the lateral membrane organization on a small scale. This idea is especially important within the so-called raft hypothesis that differential small-scale regions in biological membranes appear to be particular domains for a variety of cell functions, such as signaling and influenza virus assembly (Simons & Toomre, 2000). Recent reports examining the effect of altering cholesterol content in the virus envelope or in the cellular membranes have provided evidence that cholesterol also plays a significant role in the membrane fusion by influenza virus (Mouritsen & Zuckermann, 2004; Epand, 2006; Biswas *et al*, 2008; Sun & Whittaker, 2003; Domanska *et al*, 2013). For instance, previous studies have shown that removal of cholesterol from influenza virus envelope resulted in the decrease of influenza virus fusion while the influenza virus morphology, binding, and internalization were not affected (Sun & Whittaker, 2003). In another study of fusion between human erythrocytes and HA-expressing insect cells that were engineered to incorporate different levels of cholesterol in the membrane, Biswas and his colleagues showed that cholesterol enrichment on the HA-presenting membrane facilitated faster membrane merging and greater content transfer (Biswas *et al*, 2008). Thus cholesterol has been shown to have a significant effect on membrane fusion, but the underlying structural basis for the observed effects has eluded characterization. Using a combination of fluorescence assay and cryo-electron tomography, I aim to investigate the influence of cholesterol composition during influenza virus HA-mediated membrane fusion.

1.2 Viral membrane fusion proteins

Enveloped viruses with lipid bilayers derived from the host cell membranes require fusion of viral and host-cell membranes to enter the cells (White *et al*, 2008; Harrison, 2008; 2015; Kielian, 2014). Because lipid bilayer fusion requires catalysis to overcome the energy barrier, viral fusion proteins on the surface of viral envelope serve to fulfill this catalytic function. Several such proteins have been studied in great detail, and their crystal structures were determined both before virus-cell interaction ("prefusion" conformation) and in the form of the protein after the fusion is complete ("postfusion" conformation) (Wilson *et al*, 1981; Chen *et al*, 1998; Yin *et al*, 2005; 2006). Though their architectures vary greatly, all seem to converge the same overall strategy, in which a ligand-triggered, large-scale structural rearrangement is coupled with membrane approaching and merging. The initiating ligand can be a proton, in the case of low-pH triggered membrane fusion (example: influenza virus); it can be a host receptor on the cell surface that binds to the fusion proteins (example: HIV); or it can be a distinct protein on the viral envelope. After host cell receptors bind to a viral receptor binding protein, the information is somehow relayed to the fusion protein, which is then triggered to undergo conformational changes and to induce membrane fusion (example: human parainfluenza virus). Examples of viral fusion proteins are influenza virus hemagglutinin (HA) and human parainfluenza virus 3 fusion (F) protein (Figures 1.4 & 1.5).

Influenza A virus is an enveloped, single-stranded, negative-sense RNA virus of the Orthomyxoviridae family. The virus's segmented genome is packed inside the envelope, which the virus acquires during budding from cholesterol-enriched microdomains of the host plasma membrane. Influenza particles have two glycoproteins projecting outward from the surface lipid bilayer. Hemagglutinin (HA) is responsible for mediating virus attachment through interactions with sialic acid on the cell surface, which leads to endocytosis of the particle (Huang *et al*, 1981; Maeda & Ohnishi, 1980). The other surface glycoprotein, neuraminidase (NA), has sialidase

activity that trims away cell-surface sialic acids that could bind HA, allowing newly formed virus particles to be released from infected cells.

Influenza HA is expressed as a single precursor polypeptide called HA0. Each 225kDa HA spike is a homotrimer of HA0 subunits (Wilson *et al*, 1981). Host proteases cleave the HA0 into the receptor binding subunit, HA1 and the fusion subunit, HA2 (Figure 1.4A). After attachment to sialic acid receptors at the cell surface, influenza virus enters the cell via endocytosis. Exposure to acidic pH in the maturing endosome triggers a series of conformational changes, which drive the viral envelope to fuse with host cell membrane (Figure 1.4B) (Chen *et al*, 1998; Bullough *et al*, 1994; Fontana *et al*, 2012). Though the detailed structures for HA in the beginning and ending states have been determined by crystallography, the structure of fusion intermediates and the interplay between lipid bilayers and fusion proteins are still largely unknown (Wilson *et al*, 1981; Chen *et al*, 1998). A significant body of indirect evidence indicates that HA populates at least one stable intermediate state during fusion. Upon acidification, protonation of key residues in HA1 and HA2 results in dissociation the HA1 head domain and exposure of the amphipathic, membrane-active fusion peptide at the N-terminus of the HA2 domain (Garcia *et al*, 2015). Once exposed, the hydrophobic fusion peptide insert into target membrane. At this stage, HA2 spans the distance between viral envelope and target cell membranes, which probably corresponds to the “prehairpin” intermediates. Subsequently, a portion of the helix becomes an unstructured linker, allowing the C-terminal region of HA2 to fold back against the long N-terminal helix. This movement forms the postfusion “hairpin” structure and merges the attached viral with target membranes (Fig. 1.4B). Studies of intermediates are useful for the development of fusion inhibitors. For example, fusion-inhibitory peptides that are conjugated by cholesterol to locate on the cell membrane are able to trap HA in a transient intermediate before completion of the post-fusion conformation (Lee *et al*, 2011).

Compared with influenza virus that utilizes a single trimeric fusion protein for both receptor binding and membrane fusion functions, human parainfluenza virus 3 (HPIV3) employs two

specialized proteins to mediate cell entry: the fusion protein (F) and the receptor binding protein, hemagglutinin-neuraminidase (HN). HPIV3 is an enveloped, ssRNA virus of the Paramyxovirus family and can cause serious respiratory illness, especially in children. A receptor binding protein HN binds to the sialic acid-containing molecules on the host cell plasma membrane. A separate membrane fusion protein F, once activated by the receptor binding protein, mediates the fusion of virus and host membranes in order to deliver the viral ribonucleoprotein into the host cell(Jardetzky & Lamb, 2014; Lamb & Jardetzky, 2007; Russell & Luque, 2006). HPIV3 F protein, like most other type-I fusion proteins, undergoes conformational changes broadly analogous to those of influenza HA (Figure 1.5A) (Yin *et al*, 2006; 2005). Numerous studies have provided evidence that interaction of HN with its receptor is necessary in order for F to promote membrane fusion during HPIV3 infection (Hu *et al*, 1992; Yao *et al*, 1997; Porotto *et al*, 2012; Jardetzky & Lamb, 2014; Lamb & Jardetzky, 2007). However, the detailed organization and interactions between the two glycoproteins still elude direct visualization using structural methods. Proposed models of paramyxovirus surface glycoprotein interaction during fusion activation and viral entry posit that either (a) the HN-F interaction occurs in the absence of a receptor and "clamps" the two proteins together until the proper time, when F is released to proceed towards fusion, or (b) the HN-F interaction occurs only upon receptor binding and the receptor-binding protein provides the "trigger" after which F proceeds to fusion, which is also known as "provocateur" hypothesis (Figure 1.5B) (Jardetzky & Lamb, 2014). Previous studies by Porotto and Moscona have shown that HPIV3 HN receptor binding protein associates with F protein before and during fusion activation, suggesting that HN contributes to maintaining F in its pre-triggered state until the correct time and place for entry (Porotto *et al*, 2012; 2011). However, another study using bimolecular fluorescence complementation examining HN-F interaction in parainfluenza virus 5 indicated that HN is not required to stabilize the pre-fusion F trimer, and alternatively HN may only associated with F after receptor binding (Connolly *et al*, 2009). Moreover, recent data show that parainfluenza virus 5, measles virus and henipavirus F are all expressed in the pre-fusion form in the absence of HN

and later heat converts pre-fusion to post-fusion F, supporting one of the principal tenets of the "provocateur" hypothesis that pre-fusion F is not stabilized by receptor binding protein (Brindley *et al*, 2012; Ader *et al*, 2012; Chan *et al*, 2012). Comprehensive, direct structural characterization of protein-protein interaction on the viral envelop is needed to help resolve the apparent conflicting information and fill the critical gaps in our understanding of this complex, dynamic process.

1.3 Cryo-electron Tomography (Cryo-ET)

Cryo-electron tomography has been widely used in both virology and cellular biology at nanometer scale since it can provide a three-dimensional (3D) structural map of an unperturbed, vitrified sample (Baumeister *et al*, 1999; Lučić *et al*, 2013). Also, the flash freezing step required for cryo-ET sample preparation makes it possible to trap transient intermediates and observe dynamic processes in a close-to-physiological state. Recent advances in image recording as well as in processing software help to obtain three-dimensional reconstructions of macromolecular assemblies at near-atomic resolution (Nogales & Scheres, 2015; Campbell *et al*, 2012; Liao *et al*, 2014; Grant & Grigorieff, 2015).

The basic principles of cryo-ET include sample freezing, data collection and 3D reconstruction. The initial step in preparing biological samples for cryo-ET is vitrification, which is typically performed by rapidly plunging the sample into liquid ethane (cooled by liquid nitrogen) to ensure the preservation and imaging of the fine, delicate or transient structures. Then the vitrified sample of suitable thickness (<1 μm) is transferred into a transmission electron microscope (TEM) and rotated around a defined tilt axis, covering a maximal range of 140° between +70° to -70°. A series of two-dimensional projections, i.e., a "tilt-series", is collected under low electron dose conditions (typically total dose <100 electrons/$Å^2$) to avoid radiation damage to the sample. The tilt-series is subsequently aligned to a common frame using fiducial markers such as 5-10 nm colloidal golden particles. The aligned tilt-series is then used to reconstruct the final 3D volume of the specimen, also called a tomogram using back-projection method or simultaneous iterative

reconstruction technique (SIRT). Usually the tomogram is de-noised by Gaussian filter and frame averaging due to low signal-to-noise ratio (Lee, 2010).

Since early 2013, rapid progress in cryo-electron microscopy (cryo-EM), including the development of a new generation of electron detectors and improved image processing procedures, started a revolution in the field of cryo-EM. The new-generation “direct electron detection devices” (DDD) are able to detect individual incident electrons and to yield data of high signal-to-noise ratio. Given that electron doses used in cryo-EM with DDD could be spread over multiple frames, Grigorieff and colleagues were able to demonstrate, using rotavirus particles, that DDDs allow splitting the total dose (typically 20 electrons/$Å^2$ over a couple of seconds) into short frames (e.g., 20, with typically 1 electrons/$Å^2$ 2 dose each), where the blurring due to beam-induced movement is minimized, and where frame alignment is carried out computationally after data collection (Campbell *et al*, 2012). At the same time, powerful classification methods of maximum-likelihood approach were introduced to yield clean, high-resolution single particle reconstructions with a minimum of user intervention (Scheres, 2012; Grigorieff, 2007).

Compared with single-particle cryo-EM which produces tens of thousands of particles in one experiment, cryo-ET contains a much smaller data set of ~60 frames in a tilt-series. So most visualization of irregular complexes, viruses or whole cells by cryo-ET has been limited in the nanometer resolution. However, if macromolecular complexes are present in multiple and homogeneous copies, 3D volumes can be subsequently identified within the tomogram, computationally extracted, and averaged to obtain higher resolution 3D structures. This method, called subtomogram averaging or subvolume averaging, allows structures of macromolecular complexes to be resolved at higher resolution (Lučić *et al*, 2013; Schur *et al*, 2015b). For instance, subtomogram averaging combined with cryo-ET is applied to obtain a subnanometer structure of *in vitro*-assembled, immature virus-like Rous sarcoma virus (RSV) Gag particles at the resolution of ~8 Å, in which all the alpha-helices in Gag are clearly resolved (Schur *et al*, 2015a).

Influenza virus entry and ultrastructure have been investigated by cryo-ET in a large number of studies (Booy *et al*, 1985; Vijayakrishnan *et al*, 2013; Fontana & Steven, 2013; Fontana *et al*, 2012; Lee, 2010; Harris *et al*, 2006; Fontana & Steven, 2015). Briefly, cryo-ET was used to image influenza virus at neutral pH soon after this technique was introduced, providing the first glimpse of the virus's structure (Booy *et al*, 1985). Continued studies of cryo-ET combined with subtomogram averaging have shown intermediate conformations of HA in its transition towards the post-fusion conformations and the dissociation of matrix layer from viral envelope when influenza virus particles are exposed to low pH (Fontana *et al*, 2012)2. Cryo-ET has also been used to visualize elongated Udorn viral particles budding from infected cells as well as broadly neutralizing antibodies on intact influenza virions (Vijayakrishnan *et al*, 2013). In a recent study, we have used cryo-ET to image the initiating stages of fusion process by mixing influenza virions with liposomes under fusogenic conditions (Lee, 2010). However, the nature and sequence of membrane deformations during fusion have been poorly understood and yet to be directly imaged. In this dissertation, I imaged the 3D organization of intact influenza virions at different stages of fusion with liposomes by means of cryo-ET, from the initial states of membrane fusion to the completion of open fusion pores.

Compared with extensive structural studies of influenza virus, HPIV3 ultrastructure as well as other paramyxovirus ultrastructure has eluded detailed characterization until recently. A recent advance where the use of an engineered measles receptor binding protein (H) with an elongated stalk allows visualization of the envelope glycoproteins on the paramyxovirus envelope provides evidence that direct contact between F and the head domain of H may not be required for activation of measles virus fusion (Brindley *et al*, 2013). In my thesis, I aim to apply cryo-ET to visualize the relative distribution, conformation and interactions of the HN and F proteins on a HPIV3 surface prior to receptor binding.

Reference:

Ader N, Brindley M, Avila M, Orvell C, Horvat B, Hiltensperger G, Schneider-Schaulies J, Vandevelde M, Zurbriggen A, Plemper RK & Plattet P (2012) Mechanism for Active Membrane Fusion Triggering by Morbillivirus Attachment Protein. *J. Virol.* **87:** 314–326

Baumeister W, Grimm R & Walz J (1999) Electron tomography of molecules and cells. *Trends Cell Biol.* **9:** 81–85

Biswas S, Yin SR, Blank PS & Zimmerberg J (2008) Cholesterol promotes hemifusion and pore widening in membrane fusion induced by influenza hemagglutinin. *J. Gen. Physiol.* **131:** 503–513

Booy FP, Ruigrok R & Van Bruggen E (1985) Electron microscopy of influenza virus: a comparison of negatively stained and ice-embedded particles. *J Mol Biol.* **184**:667-76.

Brindley MA, Suter R, Schestak I, Kiss G, Wright ER & Plemper RK (2013) A stabilized headless measles virus attachment protein stalk efficiently triggers membrane fusion. *J. Virol.* **87:** 11693–11703

Brindley MA, Takeda M, Plattet P & Plemper RK (2012) Triggering the measles virus membrane fusion machinery. *Proc. Natl. Acad. Sci. USA* **109:** E3018–27

Bruckner RJ, Mansy SS, Ricardo A, Mahadevan L & Szostak JW (2009) Flip-Flop-Induced Relaxation of Bending Energy: Implications for Membrane Remodeling. *Biophys. J.* **97:** 3113–3122

Bullough PA, HUGHSON FM, Skehel JJ & Wiley DC (1994) Structure of influenza haemagglutinin at the pH of membrane fusion. *Nature* **371:** 37–43

Campbell MG, Cheng A, Brilot AF, Moeller A, Lyumkis D, Veesler D, Pan J, Harrison SC, Potter CS, Carragher B & Grigorieff N (2012) Ways & Means. *Structure* **20:** 1823–1828

Chan Y-P, Lu M, Dutta S, Yan L, Barr J, Flora M, Feng Y-R, Xu K, Nikolov DB, Wang L-F, Skiniotis G & Broder CC (2012) Biochemical, conformational, and immunogenic analysis of soluble trimeric forms of henipavirus fusion glycoproteins. *J. Virol.* **86:** 11457–11471

Chen J, Lee KH, Steinhauer DA, Stevens DJ, Skehel JJ & Wiley DC (1998) Structure of the hemagglutinin precursor cleavage site, a determinant of influenza pathogenicity and the origin of the labile conformation. *Cell* **95:** 409–417

Chernomordik LV & Kozlov MM (2005) Membrane hemifusion: Crossing a chasm in two leaps. *Cell* **123:** 375–382

Chernomordik LV & Kozlov MM (2008) Mechanics of membrane fusion. *Nat. Struct. & Mol. Biol* **15:** 675–683

Connolly SA, Leser GP, Jardetzky TS & Lamb RA (2009) Bimolecular complementation of paramyxovirus fusion and hemagglutinin-neuraminidase proteins enhances fusion: implications for the mechanism of fusion triggering. *J. Virol.* **83:** 10857–10868

Diao J, Grob P, Cipriano DJ, Kyoung M, Zhang Y, Shah S, Nguyen A, Padolina M, Srivastava A, Vrljic M, Shah A, Nogales E, Chu S & Brunger AT (2012) Synaptic proteins promote calcium-triggered fast transition from point contact to full fusion. *eLife* **1:** e00109–e00109

Domanska MK, Wrona D & Kasson PM (2013) Multiphasic Effects of Cholesterol on Influenza Fusion Kinetics ReflectMultiple Mechanistic Roles. *Biophys. J.* **105:** 1383–1387

Epand RM (2006) Cholesterol and the interaction of proteins with membrane domains. *Progs in Lipid Res.* **45:** 279–294

Fontana J & Steven AC (2013) At low pH, influenza virus matrix protein M1 undergoes a conformational change prior to dissociating from the membrane. *J. Virol.* **87:** 5621–5628

Fontana J & Steven AC (2015) Influenza virus-mediated membrane fusion: Structural insights from electron microscopy. *Arch Biochem Biophys.* **581:** 1–12

Fontana J, Cardone G, Heymann JB, Winkler DC & Steven AC (2012) Structural Changes in Influenza Virus at Low pH Characterized by Cryo-Electron Tomography. *J. Virol.* **86:** 2919–2929

Garcia NK, Guttman M, Ebner JL & Lee KK (2015) Dynamic Changes during Acid-Induced Activation of Influenza Hemagglutinin. *Structure* **23:** 665–676

Grant T & Grigorieff N (2015) Measuring the optimal exposure for single particle cryo-EM using a 2.6 Å reconstruction of rotavirus VP6. *eLife* **4**: e06980

Grigorieff N (2007) FREALIGN: high-resolution refinement of single particle structures. *J Struct. Biol.* **157:** 117–125

Harris A, Cardone G, Winkler DC, Heymann JB, Brecher M, White JM & Steven AC (2006) Influenza virus pleiomorphy characterized by cryoelectron tomography. *Proc. Natl. Acad. Sci. U.S.A.* **103:** 19123–19127

Harrison SC (2008) Viral membrane fusion. *Nat. Struct. & Mol. Biol.* **15:** 690–698

Harrison SC (2015) Viral membrane fusion. *Virology* **479-480:** 498–507

Hu XL, Ray R & Compans RW (1992) Functional interactions between the fusion protein and hemagglutinin-neuraminidase of human parainfluenza viruses. *J. Virol.* **66:** 1528–1534

Huang RT, Rott R & Klenk HD (1981) Influenza viruses cause hemolysis and fusion of cells. *Virology* **110:** 243–247

Jahn R, Lang T & Südhof TC (2003) Membrane fusion. *Cell* **112:** 519–533

Jardetzky TS & Lamb RA (2014) Activation of paramyxovirus membrane fusion and virus entry. *Curr. Opin. in Virol.* **5:** 24–33

Kielian M (2014) Mechanisms of Virus Membrane Fusion Proteins. *Annu. Rev. Virol.* **1:** 171–189

Lamb RA & Jardetzky TS (2007) Structural basis of viral invasion: lessons from paramyxovirus F. *Curr. Opin. in Struct.l Biol.* **17:** 427–436

Lee KK (2010) Architecture of a nascent viral fusion pore. *EMBO J.* **29:** 1299–1311

Lee KK, Pessi A, Gui L, Santoprete A, Talekar A, Moscona A & Porotto M (2011) Capturing a fusion intermediate of influenza hemagglutinin with a cholesterol-conjugated peptide, a new antiviral strategy for influenza virus. *J. Biol. Chem.* **286:** 42141–42149

Liao M, Cao E, Julius D & Cheng Y (2014) Structure of the TRPV1 ion channel determined by electron cryo-microscopy. *Nature* **504:** 107–112

Lučić V, Rigort A & Baumeister W (2013) Cryo-electron tomography: The challenge of doing structural biology in situ. *J. Cell Biol.* **202:** 407–419

Maeda T & Ohnishi S (1980) Activation of influenza virus by acidic media causes hemolysis and fusion of erythrocytes. *FEBS Lett.* **122:** 283–287

Martens S & McMahon HT (2008) Mechanisms of membrane fusion: disparate players and common principles. *Nat Rev Mol Cell Biol* **9:** 543–556

Maxfield FR & Tabas I (2005) Role of cholesterol and lipid organization in disease. *Nature* **438:** 612–621

Mouritsen OG & Zuckermann MJ (2004) What's so special about cholesterol? *Lipids.* **39**:1101-13.

Nogales E & Scheres SHW (2015) Cryo-EM: A Unique Tool for the Visualization of Macromolecular Complexity. *Mol. Cell* **58:** 677–689

Porotto M, Devito I, Palmer SG, Jurgens EM, Yee JL, Yokoyama CC, Pessi A & Moscona A (2011) Spring-loaded model revisited: paramyxovirus fusion requires engagement of a receptor binding protein beyond initial triggering of the fusion protein. *J. Virol.* **85:** 12867–12880

Porotto M, Salah ZW, Gui L, Devito I, Jurgens EM, Lu H, Yokoyama CC, Palermo LM, Lee KK & Moscona A (2012) Regulation of paramyxovirus fusion activation: the hemagglutinin-neuraminidase protein stabilizes the fusion protein in a pretriggered state. *J. Virol.* **86:** 12838–12848

Russell CJ & Luque LE (2006) The structural basis of paramyxovirus invasion. *Trends Microbiol.* **14:** 243–246

Scheres S (2012) RELION: implementation of a Bayesian approach to cryo-EM structure determination. *J Struct. Biol.* **180**:519-30

Schur FKM, Dick RA, Hagen WJH, Vogt VM & Briggs JAG (2015a) The Structure of Immature virus-like rous Sarcoma virus gag particles reveals a structural role for the p10 domain in assembly. *J. Virol.* **89:** 10294–10302

Schur FKM, Hagen WJH, Rumlová M, Ruml T, Müller B, Kräusslich H-G & Briggs JAG (2015b) Structure of the imma ture HIV-1 capsid in intact virus particles at 8.8 A resolution. *Nature* **517:** 505–508

Simons K & Toomre D (2000) Lipid rafts and signal transduction. *Nat Rev Mol Cell Biol* **1:** 31–39

Söllner TH (2004) Intracellular and viral membrane fusion: a uniting mechanism. *Curr. Opin. Cell Biol.* **16:** 429–435

Sun X & Whittaker GR (2003) Role for Influenza Virus Envelope Cholesterol in Virus Entry and Infection. *J. Virol.* **77:** 12543–12551

Vijayakrishnan S, Loney C, Jackson D, Suphamungmee W, Rixon FJ & Bhella D (2013) Cryotomography of budding influenza A virus reveals filaments with diverse morphologies that mostly do not bear a genome at their distal end. *PLoS Pathog* **9:** e1003413

White JM, Delos SE, Brecher M, Schornberg K (2008) Structures and mechanisms of viral membrane fusion proteins: multiple variations on a common theme. *Crit. Rev. Biochem. Mol. Biol.* **43**: 189-219

Wilson IA, Skehel JJ & Wiley DC (1981) Structure of the haemagglutinin membrane glycoprotein of influenza virus at 3 A resolution. *Nature* **289:** 366–373

Yao Q, Hu X & Compans RW (1997) Association of the parainfluenza virus fusion and hemagglutinin-neuraminidase glycoproteins on cell surfaces. *J. Virol.* **71:** 650–656

Yin H-S, Paterson RG, Wen X, Lamb RA & Jardetzky TS (2005) Structure of the uncleaved ectodomain of the paramyxovirus (hPIV3) fusion protein. *Proc. Natl. Acad. Sci. U.S.A.* **102:** 9288–9293

Yin H-S, Wen X, Paterson RG, Lamb RA & Jardetzky TS (2006) Structure of the parainfluenza virus 5 F protein in its metastable, prefusion conformation. *Nature* **439:** 38–44

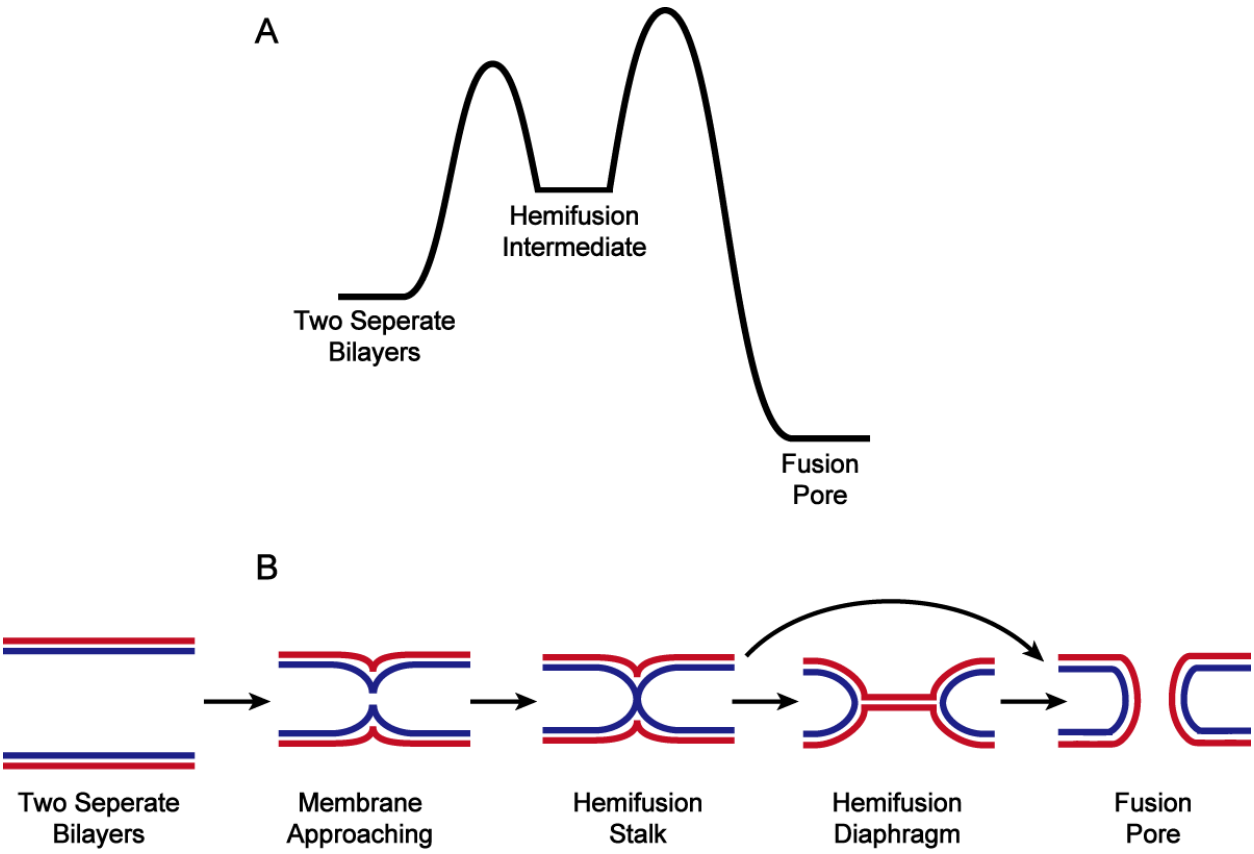

Figure 1.1 (A) Schematic diagram showing the free energy changes during membrane fusion. The relative heights of the various barriers are arbitrary. Fusion proteins accelerate the fusion process by overcoming the energy barrier. **(B) Steps including hemifusion of lipid bilayer fusion**. Apposed leaflets in blue; distal leaflets in red.

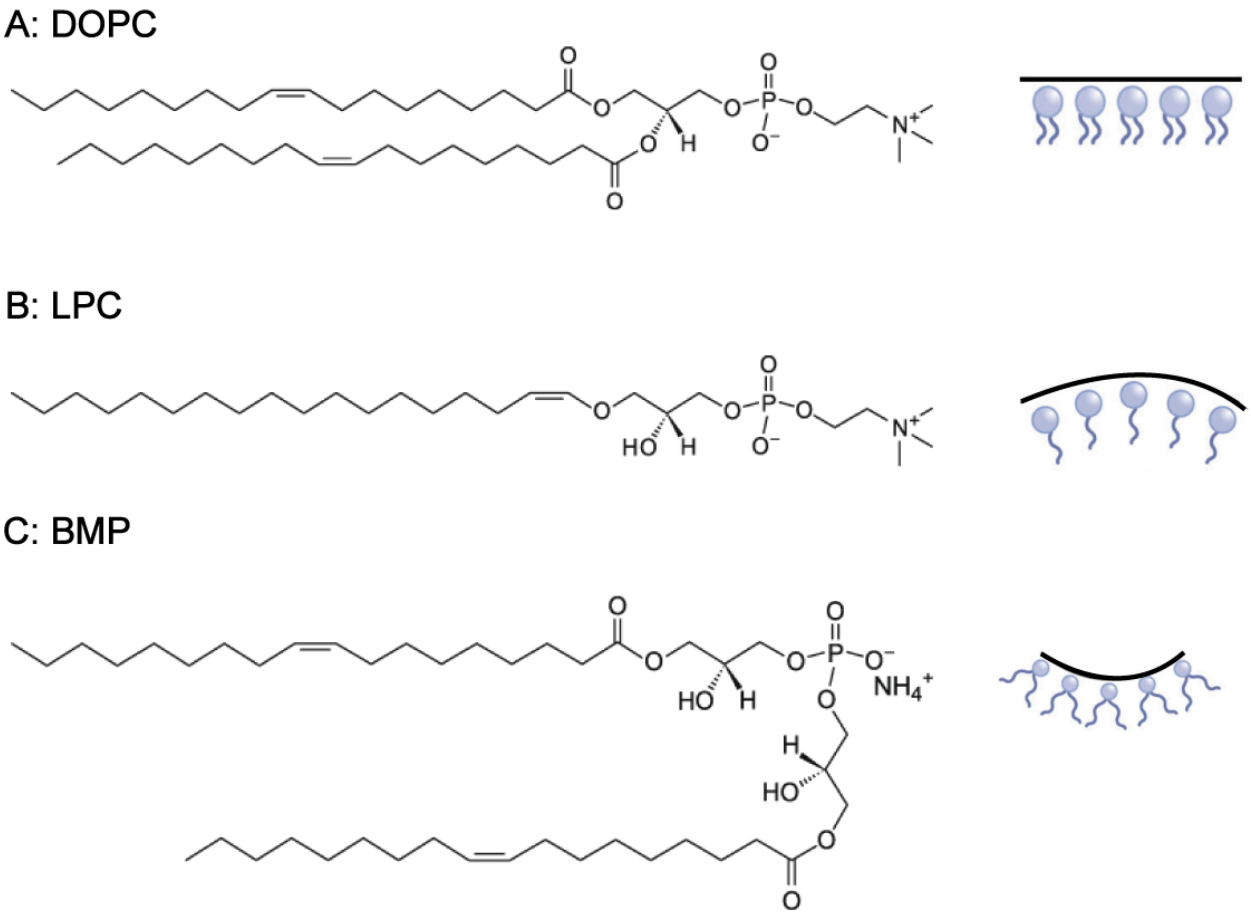

Figure 1.2 Different lipids, depending on their molecular shapes, spontaneously form monolayers of different curvatures. **(A)** Cylindrical DOPC forms an almost flat monolayer. **(B, C)** Monolayer formed by inverted-cone shaped LPC and cone-shaped BMP bulge in the direction of the polar heads or in the opposite direction of the hydrocarbon tails.

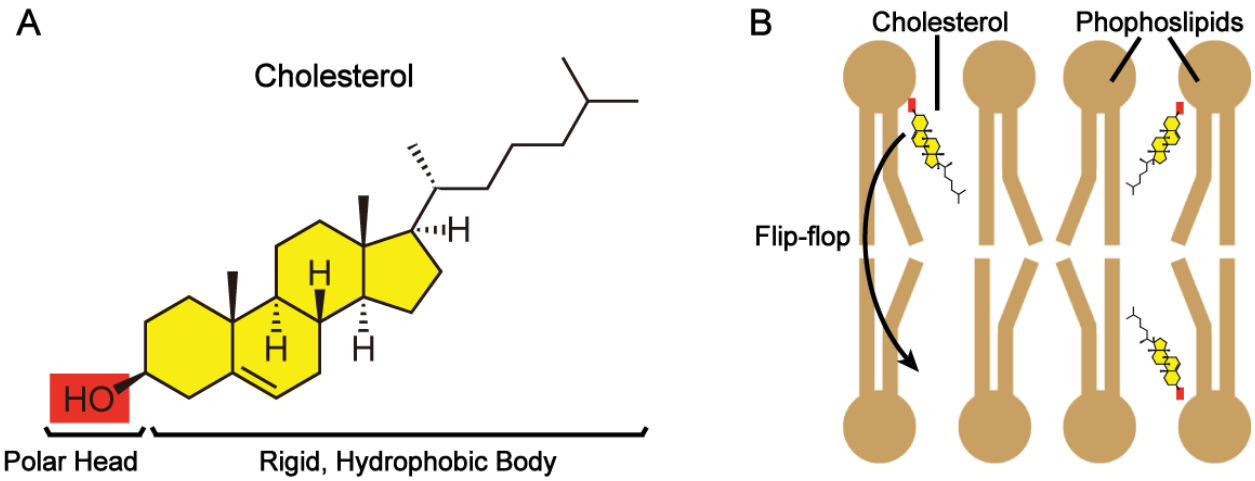

Figure 1.3 (A) The unique structure of cholesterol consists of a series of fused and rigid carbon rings, as well as a hydrophilic hydroxyl group at the end of the planar rings. **(B) Cholesterol is able to fill interstitial spaces between adjunct phospholipids and easily flip-flop between the double leaflets of lipid membranes.** Thus cholesterol has an ordering effect on lipid bilayers.

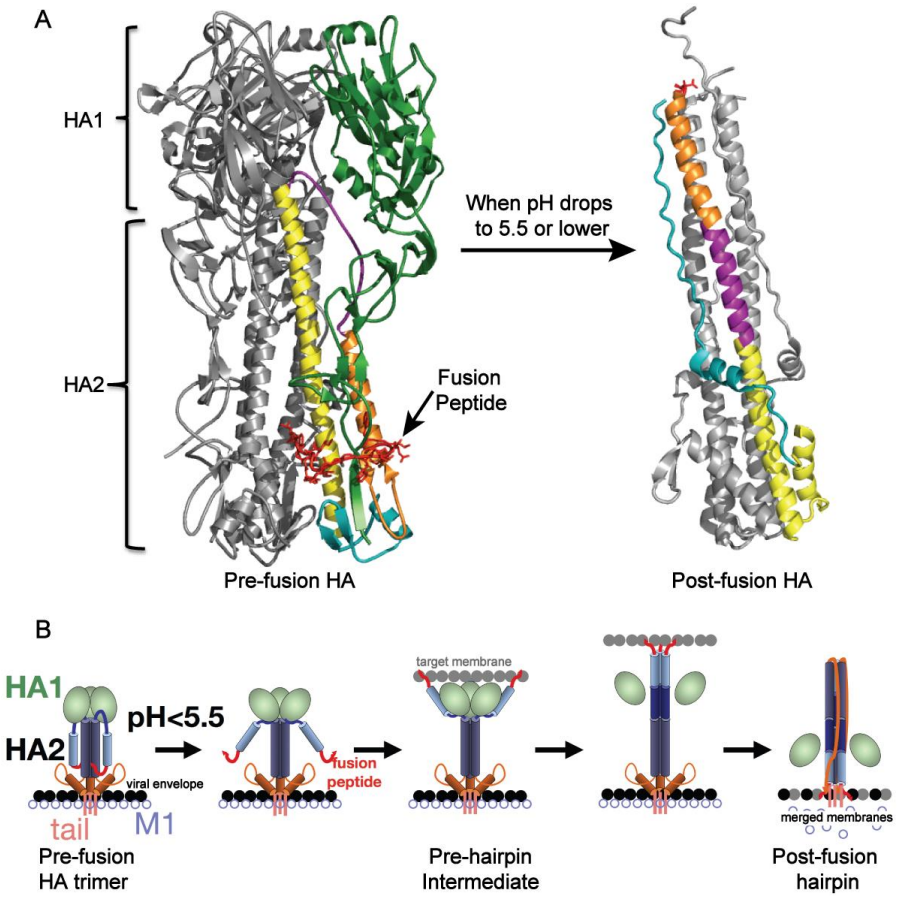

Figure 1.4 (A) Crystal structures of influenza hemagglutinin trimers reveal a significant conformational change before and after fusion. Left: The pre-fusion bromelain-cleaved hemagglutinin (BHA) at pH 7.4 (PDB code: 1RUZ) does not contain the transmembrane domain nor the C-terminal tail. Only one subunit of the homotrimer has been labeled with color: the intact HA1 domain in green, HA2 fusion peptide in red, the helix-to-loop region in yellow and HA2 N-terminal in orange. Right: The post-fusion structure has been heavily truncated (PDB code: 1HTM). Both HA1 domain and fusion peptide are absent in the post-fusion structure. After the structural rearrangements, N-terminal helixes form coiled coil center with the C-terminal outside. **(B) Current working model of HA conformational changes upon exposure to endocytic pH (modified from Lee, 2010 and Garcia *et al*, 2015).** (1) Fusion peptides become accessible at ~pH 5.5; partial relaxation of HA1 domain interactions but not complete dissociation (2) Fusion peptides bind host cell membrane (3) HA1 domains dissociate from each other and from HA2 stem; HA2 undergoes a largest conformational change involving refolding and an extension of the central coiled coil (4) C-terminal tail of HA2 which attaches to the viral membrane anchor refolds and zippers along the coiled coil to draw the two membranes together.

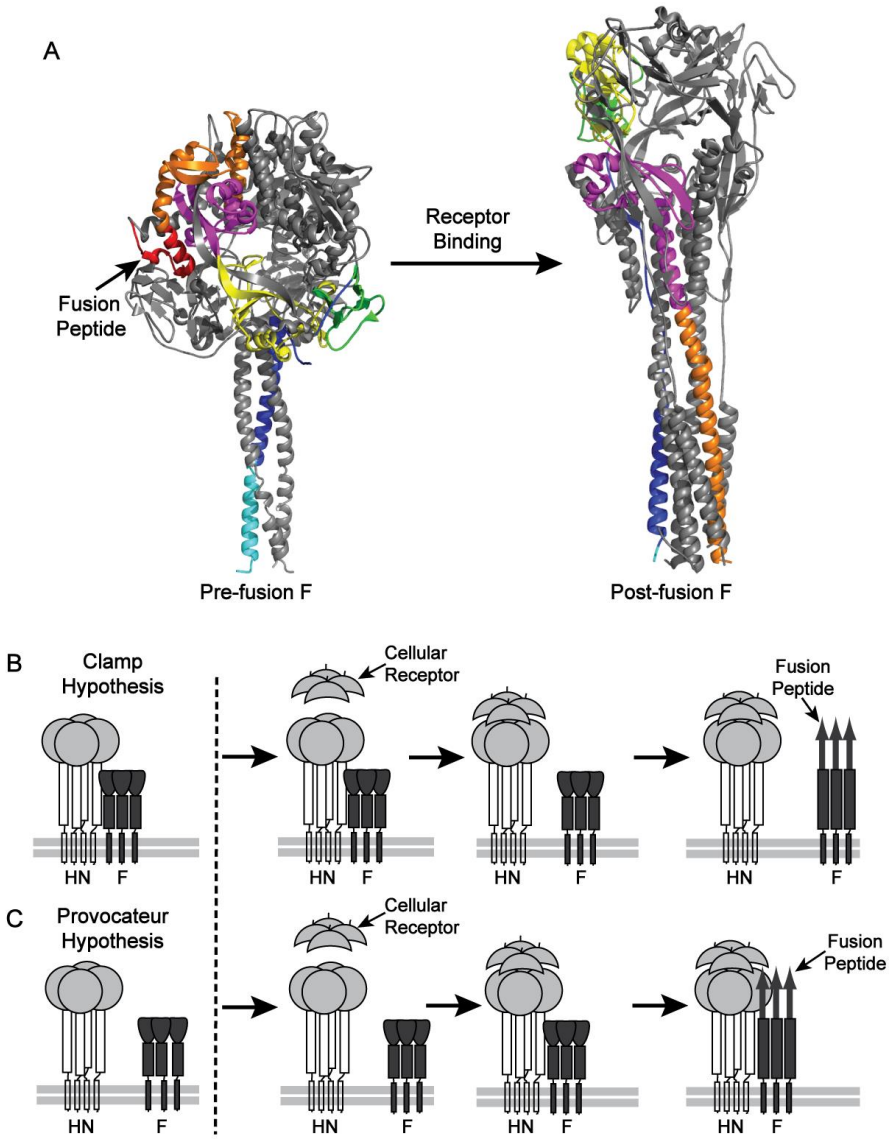

Figure 1.5 (A) Crystal structures of Paramyxovirus F fusion protein in the pre-fusion states (left, parainfluenza virus 5 F protein, PDB code: 2B9B) and the post-fusion states (right, human parainfluenza virus 3 F protein, PDB code: 1ZTM). DIII domain (highlighted in orange) plays an essential role during the structure changes, in which multiple distinct segments (including several α-helixes, loops and β-sheets, highlighted in orange color) in the pre-fusion conformation fold into a single helix of ~120 Å in the post-fusion form. **(B, C) Schematic diagram illustrating first step of fusion activation of the "Clamp" hypothesis (B) and the "Provocateur" hypothesis (C).** In the clamp hypothesis, HN tetramer is tightly associated with F protein prior to membrane fusion. Receptor engagement induces "dissociation" between HN and F proteins, allowing the release of fusion peptides of F proteins. Alternatively, in the provocateur hypothesis, following binding of the receptor, HN "associates" with the fusion protein inducing it to undergo the conformational changes.

Chapter 2. Visualization and Sequencing of Membrane Remodeling during Influenza Virus Fusion

2.1 Introduction

Membrane fusion is a crucial step in cell entry by enveloped virus. In influenza virus, endosomal acidification causes irreversible structural rearrangements of the viral glycoprotein hemagglutinin (HA), leading to exposure of fusion peptides that insert into host endosomal membrane and mediate membrane merging (Wilson *et al*, 1981; Skehel *et al*, 1982; Chen *et al*, 1998; Skehel & Wiley, 2000). This dynamic process has been previously studied by monitoring lipid and content exchanges of fluorescent probes between fusion partners. For example, lipid-anchored influenza HA expressed on the cell surface permits lipid exchange but no content exchange, suggesting that HA lacking transmembrane domains only promotes hemifusion, not complete fusion (Kemble *et al*, 1993). Moreover, mutagenesis studies have identified that residue changes in the region of high coiled-coil propensity completely block membrane fusion activity (Qiao *et al*, 1998). Despite extensive studies, the fusion mechanisms of influenza HA fusion proteins still remain uncharacterized. There are still a number of unanswered questions: How many HA molecules are required to induce efficient membrane fusion? How does the HA conformational change bring the target membrane towards the viral envelope and finally merge them? What are the structures and properties of the fusion intermediates during the fusion process? In order to answer all these questions, a more direct imaging method will be needed.

Cryo-electron microscopy (cryo-EM) and cryo-electron tomography (cryo-ET) are ideal to study the influenza virus fusion system (Baumeister *et al*, 1999; Lučić *et al*, 2013; Lee, 2010; Bonnafous *et al*, 2014; Chlanda *et al*, 2016). The flash-freeze method is able to trap the intermediate states of the continuous membrane fusion process. And the nanometer resolution is sufficient to resolve the surface protein spikes as well as membrane deformations during influenza

virus membrane fusion. In fact, cryo-EM/ET have been applied to investigate membrane fusion mediated by SNARE fusion protein from eukaryotic cells in several recent studies (Xu *et al*, 2011; Hernandez *et al*, 2012; Diao *et al*, 2012). In these studies, *in vitro* liposome fusion mediated by SNARE protein was imaged by cryo-EM and different stages of fusion process such as vesicle docking, point-like membrane contacts between liposomes and hemifusion diaphragms were found. Since the maximum thickness of specimen that can be imaged cryo-EM/ET is limited to around 0.5 – 1 μm, direct imaging of influenza virus entry inside eukaryotic cells is infeasible. Although new strategies using a combination of focused ion beam milling (to thin the sample around the point of interest) and cryoET allow researchers to observe intracellular events, this procedure is still quite time-consuming and challenging (Lučić *et al*, 2013). Instead, using liposomes as artificial target membranes, researchers directly imaged fusion process of influenza virus under full control of environmental parameters (e.g. pH, temperature, incubation times and liposome lipid compositions). In our previous cryo-ET experiment, we have imaged the membrane fusion between influenza virus and liposomes at pH 5.5, focusing the earliest stage of membrane remodeling by influenza virus (Lee, 2010). Tomographic reconstructions show the formation of a pinched liposomal funnel that may impinge on the apparently undisturbed viral envelope. We posit that M1 matrix layer may be still rigid and serve as an endoskeleton during fusion. However, the detailed mechanism of the transition from the funnel-shaped membrane deformation to the final open fusion pore is still largely unknown.

To gain inside into the overall fusion process, here I aim to characterize the full pathway and identify the kinetics of fusion intermediate evolution over the course of fusion. Using combined approaches of fluorescence assays and cryo-ET, I aim to investigate (1) whole influenza virus interacting with liposomes of different lipid compositions; (2) influenza virus with liposomes at different pH (pH 5.5 as the early maturing endosomes and pH 5.1 as the late maturing endosomes); (3) influenza virus fusing with liposomes at different time scales. The majority of this chapter is adapted from our previous publication titled “Visualization and sequencing of

membrane remodeling leading to influenza virus fusion" (accepted by Journal of Virology, not yet published).

2.2 Methods and Materials

2.2.1 Influenza virus preparation

X31 (H3N2) influenza A virus grown in embryonated chicken eggs was purchased from Charles River Laboratories. Virus stocks were first centrifuged at 2,320 relative centrifugal force (rcf) for 5 min to remove precipitates formed by egg proteins. Then the virus supernatant was concentrated to 10-12 mg/ml by centrifugation at 21,000 rcf and stored in 150 mM NaCl, 10 mM HEPES, 50 mM sodium citrate (pH 7.5), 0.02% NaN_3 buffer. Labeling with the lipophilic dye 1,1'-dioctadecyl-3,3,3'3'-tetramethylindodicarbocyanine (DiD) was performed by adding 400 µL of approximately 1 mg/ml X31 virus-diluted solutions to 20 µL of 1 mM DiD Vybrant solution (Invitrogen) followed by a 2-h incubation at 37 °C with gentle rocking. The DiD-labeled virus was harvested by ultracentrifugation and concentrated to 10-12 mg/ml X31 virus, then stored at 4 °C and used within 1 to 10 days. Virus from the same batch was used for each series of experiments where a parameter such as pH or cholesterol concentration was varied. This enabled us to avoid batch-to-batch variability in virus fusion activity in determining the effect of varying each particular parameter. Such variation between batches was typically in the range of 5-10% activity and different batches showed the same trends.

2.2.2 Liposome preparations

Liposomes composed of 1,2-dioleoyl-sn-glycero-3-phosphatidylcholine (DOPC) and cholesterol with 0%, 5%, 9%, 20%, and 33% molar fraction of cholesterol (both from Avanti Polar Lipids) were prepared by lipid extrusion method. We elected to use target liposomes lacking sialic acid in order to monitor membrane remodeling that results from HA's fusion activity, without confounding interactions. Previous studies have reported that the presence of receptor such as

gangliosides on target membranes primarily influences kinetics of adhesion but not the fusion process itself (Stegmann *et al*, 1989).

DOPC and cholesterol were combined from chloroform stock solutions then dried overnight under nitrogen gas. The lipid films were resuspended in 150 mM NaCl, 10 mM HEPES, 50 mM sodium citrate (pH 7.5), 0.02% NaN_3, and extruded 21 times through a 100 nm polycarbonate membrane (Avanti Polar Lipids) after 6 liquid nitrogen freeze/thaw cycles. The resulting liposomes were passed over a PD-10 desalting column (GE Healthcare) and stored in the same pH 7.5 HEPES-citrate buffer for virus storage. Dynamic light scattering (DLS) with a DynaPro NanoStar analyzer (Wyatt Tech, CA) was used to characterize the average dimensions and polydispersity of the liposomes at room temperature. The liposomes were of similar diameter regardless of cholesterol content and ranged from 135 to 145 nm, with low polydispersity. Bis(monoacylglycero)phosphate (BMP) was purchased from Echelon Biosciences Inc (Salt Lake City, UT) and mixed with DOPC in a 80%:20% DOPC:BMP molar ratio, then liposomes were prepared as described above.

2.2.3 Fluorescence spectroscopy monitoring membrane fusion

For fluorescence-monitored membrane fusion assays, DiD-labeled virus and liposomes were mixed in a volumetric ratio of 1:10 with liposomes in excess. The reaction mixture was incubated at neutral pH, 37 °C for 10 min to allow the liposomes and virus to equilibrate. To initiate the fusion reactions, the pH was dropped to 5.5, pH 5.25, or pH 5.1 by the addition of aliquots of 150 mM NaCl, 10 mM HEPES, 50 mM sodium citrate (pH 3.0), 0.02% NaN_3 buffer. Fluorescence spectroscopy was carried out in a Varian Cary Eclipse spectrophotometer using excitation/emission pairing of λ_{Ex} = 644 nm, λ_{Em} = 665 nm with 2.5 nm slit widths while the cuvette was kept at 37 °C. The extent of dequenching was calculated as [F(t) – F(0)] / [F(max) – F(0)], where F(0) is the fluorescence reading before acidification and F(max) is the fluorescence reading

after complete dequenching achieved by the addition of Triton X-100 detergent to a final concentration of 1% (v/v).

2.2.4 FI6v3 broadly neutralizing antibody for fusion control experiments

To test whether the DiD dequenching signal was reliably reporting on HA-mediated membrane fusion and lipid mixing, we also performed a control experiment in which the fusion assay at pH 5.5 was run in the presence of a HA fusion-inhibitory neutralizing antibody, FI6v3 that binds to the HA stem and prevents its fusion activation (Corti *et al*, 2011). The FI6v3 IgG was expressed in a stable HEK 293 cell line and purified from media using protein A column (Pierce Protein A Plus Agarose, Thermofisher Scientific). IgG was concentrated to ~9.0 mg/mL by centrifugal filtration using a vivaspin concentrator (GE Healthcare). Fi6v3 purity was assessed by SDS/PAGE prior to use in the fusion experiments. The FI6v3 IgG was preincubated on ice with DiD-labeled X31 influenza virus at a 3:2 IgG:HA molar ratio prior to transferring the mixture into the cuvette. The fluorescence experiment was then performed as described above.

2.2.5 Cryo-EM and tomography processing

Purified virus, 10 nm colloidal gold beads (Electron Microscopy Sciences) and pure DOPC liposomes or DOPC liposomes containing 20% cholesterol were mixed at a volumetric ratio of 1:1:10 and incubated at 37 °C for 10 min. The combined solution was then mixed with a pH 3.0 HEPES-citrate buffer to produce a final pH of 5.5, 5.25, or 5.1. Samples were incubated at 37 °C. 10 min after acidification, 3 µL of the solution was added to glow-discharged holey carbon-coated grids (C-flat, 200 mesh; Electron Microscopy Sciences) and plunge frozen in liquid ethane using a Vitrobot Mark IV (FEI Co.). Vitrobot settings were 25 °C, 100% humidity and the blotting time was 6 seconds.

For the time-dependent kinetics studies, virus and 10 nm colloidal gold as well as 20%-cholesterol DOPC liposomes were mixed at a ratio of 1:1:10 and acidified to pH 5.5 or 5.25. From

the common stock solution that was incubated at 37 ˚C, aliquots were drawn at 30 s, 3 min, 10 min and 30 min postincubation and flash frozen.

Vitrified grids were mounted on a Gatan 626 single-tilt cryo transfer holder and imaged at 200 kV in a FEI Tecnai F20 transmission electron microscope. Images were captured using a Gatan Ultrascan 4000 charge-coupled device (CCD) camera at a nominal magnification of 50,000X (and binned by a factor of 2, yielding a scaling of 4.4 Å per pixel), or using a Gatan K2 Summit direct detector in counting mode at a calibrated magnification of 11,500X (yielding a scaling of 3.2 Å per pixel). Images were acquired at 2 to 4 µm underfocus, and specimens were tilted from 58° to -58° in 2° steps or from 48° to -48° in 3° steps using the Leginon software package (Suloway *et al*, 2009). A dose rate of 8 electrons/pixel/s and 120 ms exposure per frame were used in the counting mode with the K2 Summit detector. The exposure at 0° was 1.56 s long and imaged as a movie of 13 frames while 58° exposure was 2.64 s long and recorded as a movie of 22 frames. Total electron dose for the entire tilt series was estimated ~100 electrons/Å^2 for datasets gathered with the CCD, and ~70 electrons/Å^2 with the K2 Summit detector. The K2 image frames were aligned prior to tomographic reconstruction (Li *et al*, 2013). Tomograms were reconstructed using the back-projection method in the IMOD package (Kremer *et al*, 1996). Images were denoised as previously described (Lee, 2010).

2.3 Results

2.3.1 Lipid composition effects on influenza fusion probed by fluorescence spectroscopy

To establish a robust *in vitro* fusion system that is amenable to cryo-electron tomography as well as fluorescence spectroscopy, we employed liposomes that could be generated with a range of lipid compositions and combined with influenza X31 H3N2 virions under controlled pH and solution conditions. To begin with, we have first investigated the impact of lipid compositions on membrane remodeling and influenza virus fusion efficiency using a fluorescence dequenching assay that enables lipid mixing to be monitored. Here, the viral membrane was labeled with a

lipophilic fluorophore, DiD, at self-quenching concentration. When the lipid mixing commences, the dye disperses over a larger membrane area and the fluorescence quenching is relieved (Figure 2.1A). The fluorescence-dequenching signal was normalized to the total detergent-quenched intensity. As a control, we performed the fusion assay in the presence of a fusion inhibitory neutralizing antibody, FI6v3, that targets the HA stem and prevents it from undergoing pH-dependent conformational changes (Corti *et al*, 2011). As was clearly evident in the fluorescence experiment with FI6v3 (blue trace in Figure 2.1B), the antibody indeed inhibited HA-mediated lipid mixing (Figure 2.1B). This control experiment confirmed that the fluorescence dequenching signal reports on HA-mediated membrane fusion and the fusion protein's activity could be abrogated by the monoclonal antibody.

Cholesterol is a major component in animal cell membranes that has been shown to have a significant effect on membrane properties and HA-mediated fusion (Mouritsen & Zuckermann, 2004; Epand, 2006; Biswas *et al*, 2008; Sun & Whittaker, 2003; Domanska *et al*, 2013). A series of liposomes composed of 1,2-dioleoyl-sn-glycero-3-phosphatidylcholine (DOPC) and 0%, 5%, 9%, 20%, and 33% molar fraction of cholesterol were prepared by freeze-thaw and extrusion methods. When the DOPC:Chol liposomes were mixed with DiD-labeled influenza virus at pH 5.5, increases in fluorescence intensity as a result of DiD fluorescence dequenching could be detected indicating that fusion was taking place. At pH 5.5, the magnitude of the DiD signal increase correlated with the increase in cholesterol concentration, roughly doubling when the cholesterol molar fraction was increased from 0 to 33% (Figure 2.1B).

2.3.2 Organization of fusion contacts between influenza virus and target liposomes

Cryo-electron tomography (cryo-ET) was next used to image the 3-dimensional organization of influenza viruses fusing with liposomes. Influenza X31 virus particles were combined with liposomes composed purely of DOPC or including 20% cholesterol in order to determine whether membranes of different lipidic compositions exhibited distinct remodeling

phenotypes when they undergo fusion with influenza virus. In each case, the virus-liposome mixture was plunge frozen after 10 minutes incubation at pH 5.5, 37 ˚C. Similar types of virus-liposome contact organizations were observed for the two formulations of liposomes (Figure 2.2). Interactions were classified as the following 4 main types:

Type I (HA bridging contacts): In this type of contact, relatively well-ordered HA spikes bridge the virus and target membrane surfaces (Figure 2.3). The target membranes did not appear to be significantly deformed at this stage. The sizes of the HA-bridged contact zones varied from several to 100 nm. HA density in the interstitial zone was similar to densities in regions of the virus that were not coordinating the target membranes, indicating that the fusion proteins were not significantly enriched or depleted at these sites. At the resolution of our tomograms, it was not possible to distinguish whether HA was in the neutral pH, prefusion structure or a similar fusion-primed conformation that has been reported (Fontana *et al*, 2012). A previous cryo-ET study of influenza virus at low pH found evidence that HA can adopt a conformation in which HA1 domains remain associated but the stem of the spike showed differences consistent with the fusion peptide subdomain of HA2 being released (Fontana *et al*, 2012). Structural mass spectrometry studies from our lab also indicated that as pH approaches 5.5, the fusion peptide and associated regions in the stem become significantly more dynamic, suggesting they may be at least transiently released, while the HA1-HA1 interface remains well-ordered (Garcia *et al*, 2015). Based on those previously reported studies, it thus appears that HA can adopt a type of fusion-peptide primed state. We note that in general, in the absence of virus, liposomes tend to not localize efficiently in the EM grid holes. The fact that they were seen in complex with virus suggests they were drawn to the holes through interactions mediated by HA and most likely its membrane-active fusion peptides.

Type II (Localized pinching contacts): In the second primary type of virus-liposome contact, pinched target membranes were observed in which the target liposomal membrane dimple was drawn to the virus surface where it formed a nearly point-like contact (Figure 2.4). This type of contact was consistent with our previous reports that examined the early stages of membrane remodeling and fusion induced by influenza HA (Lee, 2010). The target membrane dimples were ~5 nm-wide (yellow arrowheads in Figure 2.4), and density we attribute to HA could be observed forming a fringe around the dimple.

Type III (Extended, tightly-docked membrane-membrane contacts): In the third type of virus-liposome contact, extended interfaces in which the target membrane was tightly docked with the viral envelope were observed (Figures. 2.5&2.6). In these types of contacts, the target membranes were observed to run parallel with the viral envelope for up to 100 nm, in most cases without apparent gaps between the two proximal leaflets. Indeed, the proximal leaflets (virus and liposome outer leaflets) were in general drawn close enough that the width of the observed density layer was no greater than that expected for a single leaflet (Figures. 2.5&2.6). In rarer cases (*e.g.* Figures. 2.6K-P), docked liposomal and viral leaflets at sub-portions of the contact zones exhibited narrow gaps of ~1.3-2.6 nm separation, alternating with regions in which separation of the proximal leaflets was not visible.

Extended contact zones were observed for both the typical matrix-bearing and less common matrix-lacking particles (Figure 2.5). For the dominant matrix-bearing particles, the target liposomal membranes appeared to conform to the topography of the virus surface, whereas docking with matrix-lacking particles yielded a more planar organization for the contact zone (Figure 2.5). We infer that the matrix layer, which bolsters the virus envelope, imposes an asymmetric membrane perturbation as previously reported for localized interactions at the early dimpling stages of membrane remodeling (Lee, 2010).

No density that could be attributable to glycoprotein was observed in the Type III extended contact zones, suggesting HA and NA were excluded from the membrane-membrane contact sites. Instead, punctate density features attributed to end-on views of HA spikes were identified in slices from the top and bottom of the contact zones while spike-like density at the edges in the central tomogram slices revealed lateral views of HA at the peripheral junction of the two membranes. These data indicated that the membranes were docked together by a fringe of HA ringing the contact zone periphery (Figures 2.5 B&C, highlighted by arrows). In some instances, as in our previous study (Lee, 2010), the HA density at the periphery of the contact zone exhibited a “Y” or “V”-shape that is consistent with an intermediate state in which a portion of HA2 had yet to complete the transition to the hairpin, postfusion bundle conformation where the C-terminal part of HA2 zippers along the N-terminal central HA2 helical bundle (Figure 2.5B, arrows in central panel) (Gruenke *et al*, 2002; Park *et al*, 2003).

Type IV (Postfusion): The final major type of virus-liposome contact were postfusion complexes. These terminal states of the fusion process were recognizable by the presence of internal electron dense clumps presumably composed of M1 protein that had dissociated from the viral membrane and aggregated with the ribonucleoprotein segments (Figure 2.7) (Calder *et al*, 2010; Lee, 2010; Fontana & Steven, 2013); these were often accompanied by additional smaller vesicles encapsulated inside the outer limiting membrane (Bonnafous *et al*, 2014). The internal vesicles originated from inner layers of multi-lamellar liposomes where the outermost layer had fused with the virus membrane, and the inner liposomal vesicles ended up inside the fused membrane.

Uncategorized complexes: Lastly, due to limitations of the tomographic data collection, a relatively small complement, generally less than ~5-10%, of liposome-virus interactions could not be unambiguously characterized. In these cases where the primary contact site was oblique relative to the sample plane, it was difficult to clearly identify membrane and protein density. In addition

shadowing arising from colloidal gold beads that were included in the samples in some cases obscured the electron density near regions of interest.

2.3.3 *The extended, docking interface is enriched at the presence of cholesterol*

While the types of contacts between liposomes with and without cholesterol were similar regardless of lipid composition (Figure 2.2), we found that the relative abundance of the contact types was highly dependent on the lipid composition of target membrane (Figure 2.8, Table 2.1). Of the 453 complexes between virus and pure DOPC liposomes observed after 10 min acidification at pH 5.5, more than half, 245, were found with well-ordered HA spikes bridging the virus and target membranes (Type I). 35% (159 cases) were observed with pinched membrane dimples (Type II), and 9% (43 cases) exhibited an extended interface (Type III). The sample counts by contact Type for this and all the experiments involving cryo-ET are presented in Table 2.1. When 20% Chol was present in the target membranes, a shift towards complexes with Type III extended contact zones was observed (Figure 2.8). For these liposomes, at pH 5.5, 40% (174 of 436) of these virus-liposome interactions involved HA bridging (Type I), 27% (117 cases) exhibited membrane dimpling (Type II), and 27% (116 cases) showed large, extended interaction zones (Type III) with closely apposed membranes. The 3-fold increase in relative abundance of Type III extended membrane-membrane contacts was the most notable difference between pure DOPC liposomes and those containing cholesterol.

2.3.4 pH dependence of influenza virus membrane fusion

In addition to exhibiting sensitivity to target membrane lipid composition, influenza membrane fusion is highly pH sensitive due to HA's pH-dependent activity. For X31 influenza virus, this activity peaks as pH approaches 5.0 (White & Wilson, 1987). While *in vitro* fusion assays often employ an abrupt pH drop to 5.0 where fusion activity is high, during endocytosis the virus experiences stages of acidification (Lakadamyali *et al*, 2003), and priming of HA and

virus takes place under more elevated pH conditions found in early to maturing endosomes (Lee *et al*, 2011; Garcia *et al*, 2015; Fontana *et al*, 2012). We sought to determine whether the relative populations and abundance of the types of fusion contacts shift as the pH was lowered towards more fusion-optimal conditions. To examine the pH-dependence of the fusion reaction, we carried out a series of fluorescence fusion assays with influenza virus and 20% cholesterol-containing liposomes at pH 5.5, 5.25, and 5.1. The fluorescence data showed that as solution pH was decreased, membrane merging was dramatically increased (Figure 2.9A).

When virus-liposome contacts at pH 5.5 and pH 5.25 were imaged by cryo-ET, it was apparent that the types of contacts fell into similar categories including Type I (bridging), Type II (pinching or dimpling), Type III (extended, tightly docked interfaces) and Type IV (postfusion complexes), but a systematic shift in population of virus-liposome contacts was evident. Namely, Type III (extended interfaces) and Type IV (postfusion complexes) became increasingly prevalent as pH was lowered (Figure 2.9B, Table 2.1).

After 10 minutes incubation at pH 5.5 (Figure 2.9C), most of the HA spikes on the virus surface retained well-defined density similar to that of the prefusion trimer. Recent EM reports (Lee, 2010; Fontana *et al*, 2012), hydrogen/deuterium exchange data data (Garcia *et al*, 2015), and epitope mapping by monoclonal antibodies (White & Wilson, 1987) have revealed an HA state in which the HA1-HA1 receptor binding domains remained clasped together, but the fusion peptide region gains conformational freedom. By cryo-ET these closely resemble the prefusion conformation. It is possible that the HA we observe at pH 5.5 may have adopted such a fusion-primed conformation, but at the resolution of our tomograms, at this time we cannot definitively distinguish between that and the untriggered, prefusion state. In nearly all virus particles (>90%) under the moderately acidic pH 5.5 conditions, the internal M1 matrix layer remained closely associated with the inner leaflet of the viral membrane (Lee, 2010; Calder *et al*, 2010; Fontana & Steven, 2013).

After pH was lowered to 5.25 (Figure 2.9D), a subset of the HA spikes had adopted a more disorganized form, as inferred from the loss of the well-ordered spike density that typifies prefusion HA. We note that at the resolution of our tomograms we cannot definitively attribute the variable surface density features on the virus to post-fusion HA, and it is possible that some of the density reflects an additional intermediate conformation distinct from both the prefusion, fusion peptide-primed and the postfusion HA conformations that have been described (Fontana *et al*, 2012). Most HA at pH 5.25 however maintained an organization resembling the organized trimer spike. Matrix layers in some particles started to dissociate from the viral membrane at this pH as well.

As depicted in Figure 2.9E, when pH was lowered to 5.1, most of the HA spikes on the surface of viruses had adopted a more disorganized morphology than those observed at higher pH, and after 10 minutes at pH 5.1, the M1 matrix layers were largely dissociated from viral envelope.

2.3.5 Rarity of stable hemifused complexes

In cryo-ET datasets of virus-liposome complexes gathered at pH 5.5 and pH 5.25, no instances of hemifused intermediates were found. It is plausible that the hemifusion diaphragm is a transient intermediate during influenza virus membrane fusion, which might be unstable and may readily proceed to an open fusion pore. A single hemifused complex was identified in a data set gathered at pH 5.1 (Figure 2.9F). In contrast to the tightly docked, extended contacts that are more abundant and exhibit three apparent layers of membrane density (plus a layer for the M1 matrix) due to the close juxtaposition of the proximal leaflets, here the two proximal leaflets of lipid bilayers have joined and no matrix layer was present. The diaphragm thus was composed of only the two remaining leaflets at approximately 3.5 nm head group separation as measured peak-to-peak in a radial density plot (Figure 2.9G). The fused leaflets show what appear to be gaps or

regions of weak density, indicating that the hemifusion state may have been collapsing into an open fusion pore. The span of this diaphragm was ~100 nm.

2.3.6 Time-dependent population kinetics of influenza virus fusion intermediates

In order to characterize the pathway of membrane remodeling and determine whether states such as pinching and extended contact interfaces are on-pathway intermediates or terminal dead ends of the HA-mediated fusion process, the population of the different contact types were tracked over time at pH 5.5 and pH 5.25. In these kinetics experiments, influenza virus and DOPC liposomes containing 20% Chol were incubated at the given pH and frozen for cryo-ET analysis after 30 s, 3 min, 10 min and 30 min following acidification (Figure 2.10, Table 2.1).

At pH 5.5, the HA-bridging arrangement was the most predominant form at early time points. Over the 30-minute time course, this state decreased in population as pinching and extended interface complexes increased in abundance. Relatively few cases of clearly identifiable post-fusion complexes were identified at pH 5.5, consistent with the low efficiency of lipid mixing, even with cholesterol present under these nascent fusion conditions.

At pH 5.25, a very different evolution of virus-liposome complexes was seen. In this case, bridging interactions were less abundant at the first time point, while the HA-induced target membrane pinching was highly populated at the initial time point. This population of locally dimpled membranes peaked at 3 min following acidification to pH 5.25, then decreased monotonically until 30 min post-acidification. The extended interfaces by contrast increased in abundance with a peak at 10 min after acidification, then diminished in population by 30 min post-acidification. Post-fusion complexes showed a systematic increase in abundance over the time course, reaching ~50% of the total virus-liposome complexes at 30 minutes. The matrix layer in these complexes was no longer associated with the viral membranes, while the influenza virus particles that had yet to fuse still exhibited intact matrix layers beneath the viral envelope (Figure 2.7).

The sequential waxing and waning of the populations of distinct fusion contact types suggests that bridging, pinching and extended contact interactions are on-pathway intermediates leading to the post-fusion end-state.

2.3.7 Additional fusion-promoting conditions also enrich for extended contact zones.

Bis(monoacylglycero)phosphate (BMP) is a lipid component that is enriched in late endosomes and has been reported to produce highly fusogenic membranes (Kobayashi *et al*, 2002). Fluorescence assays monitoring fusion of DiD-labeled influenza virus with DOPC liposomes containing either 0% or 20% BMP showed that as with cholesterol, lipid mixing reported by DiD fluorescence was significantly enhanced with BMP included in the target membrane (Figure 2.11). As in the case of cholesterol-enriched liposomes, the BMP-containing liposomes exhibited a significantly greater abundance of extended virus-liposome contact zones than liposomes composed purely of DOPC (Figure 2.11C, Table 2.1). The overall organizations of these extended contact zones were similar to the cholesterol-containing liposomes, i.e. the proximal leaflets were indistinguishable from each other, suggesting a tight packing. and protein was excluded from the contact zone, but was localized in a fringe around the perimeter of the contact region. In summary, with BMP as with all the fusion-promoting conditions examined, an enrichment of tightly docked, extended membrane-membrane contacts was observed.

2.4 Discussion

Biological membrane fusion is mediated by the action of fusion proteins that manipulate and remodel the membranes to overcome barriers to spontaneous fusion. Here we have resolved membrane organizations as well as demonstrated that the relative populations of these species follow a progression over time. These results suggest a sequence of events that take place during hemagglutinin-mediated fusion (Figure 2.12). The kinetics data following populations of fusion states indicate that the fusion commences with the formation of HA-mediated bridging contacts

(Type I) between influenza virus and liposomes (Lee, 2010; Floyd *et al*, 2008; Danieli *et al*, 1996). This occurs even in the absence of sialic acid receptor when the fusion peptides become accessible for membrane binding at the earliest stages of HA activation but prior to HA undergoing the full extent of its spring-loaded conformational change (White & Wilson, 1987; Lee, 2010; Garcia *et al*, 2015).

Next, as the fusion reaction progresses, the kinetics analysis at pH 5.25 demonstrates that Type II dimpled target membranes increase in population up to 3 minutes, then diminish in abundance. The highly focused dimpling of the target membrane was observed with the dimple being drawn to the unperturbed virus surface through the refolding action of a small number of clustered HA spikes, as observed in our previous study (Lee, 2010). Localized dimpling may serve to minimize the initial penalty of dehydrating the two membranes, allowing a small contact zone to form and then nucleate expansion as additional HAs are recruited to ring the zone's periphery (Leikina *et al*, 2004). The point-like contacts then transition to Type III large, extended contact zones with tightly docked proximal leaflets. The extended contact zones increase in population, then diminish over the course of the experiment in a manner consistent with intermediate state kinetics.

We note that extended, tightly docked membrane-membrane interfaces have also been observed in vesicle fusion mediated by SNARE proteins (Christensen *et al*, 2011; Diao *et al*, 2012; Hernandez *et al*, 2012; Imig *et al*, 2014). In addition, similar tightly "zippered" opposing membranes have been reported for fusion-primed membranes tethered by the atlastin GTP-driven fusion machinery (Saini *et al*, 2014). Moreover, it appears that during yeast vacuolar fusion, large extended membrane contacts form, though resolution of bilayers was not attained in that case (Wang *et al*, 2002). Such tightly docked membrane contacts thus appear to be ubiquitous during fusion reactions. Our results indicate that these states are key on-pathway intermediates in influenza virus fusion.

Surface glycoproteins were excluded from the extended contact zones, suggesting that

the proteins must have some degree of lateral mobility allowing them to be pushed aside from the membrane-apposed zone. Interactions are believed to exist between HA's cytoplasmic tail and the M1 matrix layer that would need to be weakened in order to displace HA at the membrane contact zones (Enami & Enami, 1996; Jin *et al*, 1997; Lee, 2010). As pH is lowered towards 5.0, the M1 matrix layer dissociates from the viral envelope (Lee, 2010; Calder *et al*, 2010; Fontana & Steven, 2013). M1 release from the inner leaflet of the viral membrane would result in greater lateral mobility of the glycoprotein spikes whose tails would no longer be constrained by interactions with the matrix layer. Once the cytoplasmic tail is released from its interactions with the matrix layer at low pH, the HA transmembrane domain (TMD) would also be less restrained. It has been proposed that the TMD and fusion peptide, initially anchored in opposing membranes, need to associate in the merging membranes in order to complete the fusion process (Kemble *et al*, 1994). The association of the TMD with N-terminal fusion peptides may help to lock in the hairpin, postfusion form of HA, resulting in the two membranes being pinched together at the periphery of the contact zones where HA is localized in a fringe of spikes that clasp the extended contact zones together (Figure 2.5). The fusogens at the periphery also imposes strain and acute curvature discontinuity on the target membrane at the edge of the contact zones. These sites of HA coordination and membrane strain at the edge of the extended contact zones may serve as focal points where bilayer defects originate and propagate as the tightly docked extended contacts transition to stalk or hemifused states as has been suggested in the SNARE-mediated fusion system (Diao *et al*, 2012; Hernandez *et al*, 2012). Coarse-grained simulations of liposome-liposome fusion have also identified the edges of flat contact zones as likely fusion initiation sites (Stevens *et al*, 2003).

This release of M1 from the membrane also confers greater plasticity to the viral membrane, allowing it to bend under HA's action (Lee, 2010). Indeed the vast majority of postfusion complexes we observed lacked M1 layers associated with the fused membranes, suggesting the matrix likely dissociated prior to fusion (Figure 2.7). Based upon the data at hand,

we conclude that the increased efficiency of extended contact zones transitioning to postfusion states at the lower pH conditions is due to a combination of the dissociation of the M1 matrix layer from the viral membrane, freeing the membrane to bend and fuse, and activation of greater amounts of HA that are also able to refold fully to the postfusion, hairpin conformation.

The process of membrane fusion is dependent on the composition of the membranes (Stegmann *et al*, 1989; Chernomordik *et al*, 1997; Biswas *et al*, 2008; Domanska *et al*, 2013), however, the underlying physicochemical and structural bases for such effects are only beginning to be directly characterized. In this study, we observed that fusion-promoting lipid compositions (higher cholesterol or BMP content) increased the abundance of extended contact zones on the pathway to formation of postfusion complexes. This suggests that these lipids may facilitate close apposition of membranes, which may promote subsequent stages leading to fusion pore formation. Experimental support for this model of lipid dependence in membrane-membrane interactions is found in previously reported X-ray diffraction studies that indicated that formation of a lipidic stalk intermediate and the first stages of lipid mixing become permissive when two DOPC:Cholesterol bilayers are brought within 0.9±0.05 nm, requiring their partial dehydration (Aeffner *et al*, 2012). The dimensions of the central docked membrane layer in the extended contact zones we observe are consistent with the X-ray diffraction measurements. From that study, Aeffner and colleagues deduced that components such as cholesterol and phosphatidylethanolamine, common fusion-promoters, have the effect of reducing barriers to membrane dehydration, allowing them to approach more closely, which would facilitate subsequent stalk formation. Like cholesterol, the BMP head group consists of a phosphate and two hydroxyl moieties, forming a squat hydrophilic face of the molecule that may permit close apposition of membranes. It is also conceivable, though beyond our ability to resolve at this stage, that membrane components such as cholesterol may become enriched in contact zones (or that the more polar phospholipids such as phosphatidylcholine may become excluded from the zone) and further faciliate tight docking and dehydration of extended membrane areas. The virus

envelope itself is also enriched in cholesterol (Takeda *et al*, 2003; Rossman & Lamb, 2011), which would further facilitate tight docking with target membranes.

Based upon computational simulations, Kasson et al. and Smirnova et al. found that when two liposomes approach, the water layer between vesicle membranes thinned until a transition state was attained in which the two lipid tails could be splayed with one tail in each membrane and the head group positioned between the two (Kasson *et al*, 2010; Smirnova *et al*, 2010). Notably, insertion of influenza HA fusion peptides into the membranes increased the probability of splayed tail configurations of lipid (Kasson *et al*, 2010). Whether such a lipid organization can be demonstrated to exist and abundantly populated at the extended contact zones will require further studies with additional methodologies, but we note that this type of organization may be consistent with the extended contact zones we observed.

In contrast to the relatively well-populated, tightly docked membrane contacts, hemifused states, appeared to be minimally populated as stable intermediates. This at first glance seems to run counter to numerous previous reports of hemifusion during HA-mediated membrane fusion (Biswas *et al*, 2008; Chernomordik & Kozlov, 2005; Mittal *et al*, 2003). Most of the prior reports of hemifusion were inferred from fluorescence microscopy, which enables lipid exchange and content transfer to be monitored, but without resolution of bilayer leaflets or fusion proteins. We hypothesize the discrepancy in observations may result from the fact that in the cases where hemifusion has been identified, HA was often expressed on cell surfaces at densities and spatial arrangments that may not fully replicate those found on the surface of authentic virions. In addition, the M1 matrix layer, a key player in influenza virus fusion, is absent in those cell-expression systems, while diverse cell surface proteins coexist with the HA that is present and may perturb the normal HA-mediated fusion process. In the authentic influenza fusion system, it appears that true hemifused intermediates may be far more transient and unstable than in the previously studied HA-presenting systems.

Interestingly in reconstituted SNARE-mediated system, hemifused complexes can be

found in abundance, but it is a matter of debate whether hemifusion is an on-pathway intermediate (Diao *et al*, 2012; Hernandez *et al*, 2012). Indeed, in one study of *in vitro* reconstituted SNARE-mediated fusion, the authors concluded that while hemifused complexes can be readily populated, they act as metastable traps (Diao *et al*, 2012), whereas localized point contacts between vesicles provide a more productive staging point leading to efficient membrane fusion and content delivery. In the case of intact influenza virus studied here, however, target membrane dimples that are brought into close contact with the virus envelope are highly populated under moderate acidic conditions (pH 5.5), yet modest levels of lipid mixing were detected, and very few postfusion complexes were observed even after prolonged incubation at this pH condition. It is plausible that between SNARE and viral fusogens, the fusion proteins may perform different specific mechanistic roles and have distinct modes of membrane interaction and manipulation. In the case of viral fusogens, the machinery is consolidated in a single protein on the virus surface with the involvement of a membrane-active fusion peptide, while SNARE fusion proteins employ a coupling of fusion components that are displayed on opposing membranes. The two systems also differ in the concentration of fusogens, with high densities of HA forming a fringe around influenza fusion contacts. Previous studies with cell surface-expressed HA have indicated that cooperative action of a few to several HAs is required to mediate fusion (Danieli *et al*, 1996; Ivanovic *et al*, 2013; Mittal *et al*, 2002; Imai *et al*, 2006; Günther-Ausborn *et al*, 2000). Such figures are consistent with the relatively localized contacts we typically observe at early stages of membrane remodeling (Lee *et al*, 2011). Other studies have demonstrated that additional HA is recruited to promote later stages of fusion (Saini *et al*, 2014), which aligns with our observations that significantly greater numbers of HA spikes ring the periphery of the extended contact zones that follow local dimple formation. In the case of SNARE-mediated fusion it has been reported that a single SNARE complex was all that was needed to initiate fusion, but up to three were required to maintain the pore in its open state (Shi *et al*, 2012). Future studies will further elucidate common as well as disparate traits and pathways of protein-mediated fusion systems.

In summary, using cryo-electron tomography, we have imaged the architecture of virus-target membrane contacts and for the first time deduced the sequence of membrane remodeling that leads to productive fusion between an enveloped virus and a target membrane. These studies highlight the synergy between the HA fusion protein and M1 matrix in directing this sequence of events and illustrate the dynamic interplay between the viral fusion machinery and membrane intermediates during membrane fusion.

References:

Aeffner S, Reusch T, Weinhausen B & Salditt T (2012) Energetics of stalk intermediates in membrane fusion are controlled by lipid composition. *Proc. Natl. Acad. Sci. USA* **109:** E1609–18

Baumeister W, Grimm R & Walz J (1999) Electron tomography of molecules and cells. *Trends Cell Biol.* **9:** 81–85

Biswas S, Yin SR, Blank PS & Zimmerberg J (2008) Cholesterol promotes hemifusion and pore widening in membrane fusion induced by influenza hemagglutinin. *J. Gen. Physiol.* **131:** 503–513

Bonnafous P, Nicolaï M-C, Taveau J-C, Chevalier M, Barrière F, Medina J, Le Bihan O, Adam O, Ronzon F & Lambert O (2014) Biochimica et Biophysica Acta. *BBA - Biomembranes* **1838:** 355–363

Calder LJ, Wasilewski S, Berriman JA & Rosenthal PB (2010) Structural organization of a filamentous influenza A virus. *Proc. Natl. Acad. Sci. USA* **107:** 10685–10690

Chen J, Lee KH, Steinhauer DA, Stevens DJ, Skehel JJ & Wiley DC (1998) Structure of the hemagglutinin precursor cleavage site, a determinant of influenza pathogenicity and the origin of the labile conformation. *Cell* **95:** 409–417

Chernomordik LV & Kozlov MM (2005) Membrane hemifusion: Crossing a chasm in two leaps. *Cell* **123:** 375–382

Chernomordik LV, Leikina E, Frolov V, Bronk P & Zimmerberg J (1997) An early stage of membrane fusion mediated by the low pH conformation of influenza hemagglutinin depends upon membrane lipids. *J. Cell Biol.* **136:** 81–93

Chlanda P, Mekhedov E, Waters H, Schwartz CL, Fischer ER, Ryham RJ, Cohen FS, Blank PS & Zimmerberg J (2016) The hemifusion structure induced by influenza virus haemagglutinin is determined by physical properties of the target membranes. *Nat. Microbiol***:** 16050–8

Christensen SM, Mortensen MW & Stamou DG (2011) Single vesicle assaying of SNARE-synaptotagmin-driven fusion reveals fast and slow modes of both docking and fusion and Intrasample Heterogeneity. *Biophys. J.* **100:** 957–967

Corti D, Voss J, Gamblin SJ, Codoni G, Macagno A, Jarrossay D, Vachieri SG, Pinna D, Minola A, Vanzetta F, Silacci C, Fernandez-Rodriguez BM, Agatic G, Bianchi S, Giacchetto-Sasselli I, Calder L, Sallusto F, Collins P, Haire LF, Temperton N, et al (2011) A neutralizing antibody selected from plasma cells that binds to group 1 and group 2 influenza A hemagglutinins. *Science* **333:** 850–856

Danieli T, Pelletier SL, Henis YI & White JM (1996) Membrane fusion mediated by the influenza virus hemagglutinin requires the concerted action of at least three hemagglutinin trimers. *J. Cell Biol.* **133:** 559–569

Diao J, Grob P, Cipriano DJ, Kyoung M, Zhang Y, Shah S, Nguyen A, Padolina M, Srivastava A, Vrljic M, Shah A, Nogales E, Chu S & Brunger AT (2012) Synaptic proteins promote calcium-triggered fast transition from point contact to full fusion. *eLife* **1:** e00109–e00109

Domanska MK, Wrona D & Kasson PM (2013) Multiphasic Effects of Cholesterol on Influenza Fusion Kinetics ReflectMultiple Mechanistic Roles. *Biophys. J.* **105:** 1383–1387

Enami M & Enami K (1996) Influenza virus hemagglutinin and neuraminidase glycoproteins stimulate the membrane association of the matrix protein. *J. Virol.* **70:** 6653–6657

Epand RM (2006) Cholesterol and the interaction of proteins with membrane domains. *Prog. Lipid. Res.* **45:** 279–294

Floyd DL, Ragains JR & Skehel JJ (2008) Single-particle kinetics of influenza virus membrane fusion. *Proc Natl Acad Sci U S A* **105**: 15382-15387

Fontana J & Steven AC (2013) At low pH, Influenza virus matrix protein M1 undergoes a conformational change prior to dissociating from the membrane. *J. Virol.* **87:** 5621–5628

Fontana J, Cardone G, Heymann JB, Winkler DC & Steven AC (2012) Structural changes in Influenza virus at low pH characterized by cryo-electron tomography. *J. Virol.* **86:** 2919–2929

Garcia NK, Guttman M, Ebner JL & Lee KK (2015) Dynamic Changes during Acid-Induced Activation of Influenza Hemagglutinin. *Structure* **23:** 665–676

Gruenke JA, Armstrong RT, Newcomb WW, Brown JC & White JM (2002) New insights into the spring-loaded conformational change of influenza virus hemagglutinin. *J. Virol.* **76:** 4456–4466

Günther-Ausborn S, Schoen P, Bartoldus I, Wilschut J & Stegmann T (2000) Role of hemagglutinin surface density in the initial stages of influenza virus fusion: lack of evidence for cooperativity. *J. Virol.* **74:** 2714–2720

Hernandez JM, Stein A, Behrmann E, Riedel D, Cypionka A, Farsi Z, Walla PJ, Raunser S & Jahn R (2012) Membrane fusion intermediates via directional and full assembly of the SNARE complex. *Science* **336:** 1581–1584

Imai M, Mizuno T & Kawasaki K (2006) Membrane fusion by single influenza hemagglutinin trimers. Kinetic evidence from image analysis of hemagglutinin-reconstituted vesicles. *J. Biol. Chem.* **281:** 12729–12735

Imig C, Min S-W, Krinner S, Arancillo M, Rosenmund C, Südhof TC, Rhee J, Brose N & Cooper BH (2014) The Morphological and Molecular Nature of Synaptic Vesicle Priming at Presynaptic Active Zones. *Neuron* **84:** 416–431

Ivanovic T, Choi JL, Whelan SP, van Oijen AM & Harrison SC (2013) Influenza-virus membrane fusion by cooperative fold-back of stochastically induced hemagglutinin intermediates. *eLife* **2:** e00333

Jin H, Leser GP, Zhang J & Lamb RA (1997) Influenza virus hemagglutinin and neuraminidase

cytoplasmic tails control particle shape. *EMBO J.* **16:** 1236–1247

Kasson PM, Lindahl E & Pande VS (2010) Atomic-Resolution Simulations Predict a Transition State for Vesicle Fusion Defined by Contact of a Few Lipid Tails. *PLoS Comput Biol* **6:** e1000829

Kemble GW, Danieli T & White JM (1994) Lipid-anchored influenza hemagglutinin promotes hemifusion, not complete fusion. *Cell* **76:** 383–391

Kemble GW, Henis YI & White JM (1993) GPI-and transmembrane-anchored influenza hemagglutinin differ in structure and receptor binding activity. *J. Cell Biol.* **122**:1253-65.

Kobayashi T, Beuchat M-H, Chevallier J, Makino A, Mayran N, Escola J-M, Lebrand C, Cosson P, Kobayashi T & Gruenberg J (2002) Separation and characterization of late endosomal membrane domains. *J. Biol. Chem.* **277:** 32157–32164

Kremer JR, Mastronarde DN & McIntosh JR (1996) Computer visualization of three-dimensional image data using IMOD. *J. Struct. Biol.* **116:** 71–76

Lakadamyali M, Rust MJ, Babcock HP & Zhuang X (2003) Visualizing infection of individual influenza viruses. *Proc. Natl. Acad. Sci. U.S.A.* **100:** 9280–9285

Lee KK (2010) Architecture of a nascent viral fusion pore. *EMBO J.* **29:** 1299–1311

Lee KK, Pessi A, Gui L, Santoprete A, Talekar A, Moscona A & Porotto M (2011) Capturing a fusion intermediate of influenza hemagglutinin with a cholesterol-conjugated peptide, a new antiviral strategy for influenza virus. *J. Biol. Chem.* **286:** 42141–42149

Leikina E, Mittal A, Cho M-S, Melikov K, Kozlov MM & Chernomordik LV (2004) Influenza hemagglutinins outside of the contact zone are necessary for fusion pore expansion. *J. Biol. Chem.* **279:** 26526–26532

Li X, Mooney P, Zheng S, Booth CR, Braunfeld MB, Gubbens S, Agard DA & Cheng Y (2013) Electron counting and beam-induced motion correction enable near-atomic-resolution single-particle cryo-EM. *Nat. Methods* **10:** 584–590

Lučić V, Rigort A & Baumeister W (2013) Cryo-electron tomography: The challenge of doing structural biology in situ. *J. Cell Biol.* **202:** 407–419

Mittal A, Leikina E, Chernomordik LV & Bentz J (2003) Kinetically differentiating influenza hemagglutinin fusion and hemifusion machines. *Biophys. J.* **85:** 1713–1724

Mittal A, Shangguan T & Bentz J (2002) Measuring pKa of activation and pKi of inactivation for influenza hemagglutinin from kinetics of membrane fusion of virions and of HA expressing cells. *Biophys. J.* **83:** 2652–2666

Mouritsen OG & Zuckermann MJ (2004) What's so special about cholesterol? *Lipids.* **39**:1101-13.

Park HE, Gruenke JA & White JM (2003) Leash in the groove mechanism of membrane fusion. *Nat. Struct. Biol.* **10:** 1048–1053

Qiao H, Pelletier SL, Hoffman L & Hacker J (1998) Specific single or double proline substitutions in the 'spring-loaded' coiled-coil region of the influenza hemagglutinin impair or abolish membrane fusion activity. *J. Cell. Biol.* **141**:1335-47.

Rossman JS & Lamb RA (2011) Influenza virus assembly and budding. *Virology* **411:** 229–236

Saini SG, Liu C, Zhang P & Lee TH (2014) Membrane tethering by the atlastin GTPase depends on GTP hydrolysis but not on forming the cross-over configuration. *Mol. Biol. Cell* **25:** 3942–3953

Shi L, Shen Q-T, Kiel A, Wang J, Wang H-W, Melia TJ, Rothman JE & Pincet F (2012) SNARE proteins: one to fuse and three to keep the nascent fusion pore open. *Science* **335:** 1355–1359

Skehel JJ & Wiley DC (2000) Receptor binding and membrane fusion in virus entry: the influenza hemagglutinin. *Annu. Rev. Biochem.* **69:** 531–569

Skehel JJ, Bayley PM, Brown EB, Martin SR, Waterfield MD, White JM, Wilson IA & Wiley DC (1982) Changes in the conformation of influenza virus hemagglutinin at the pH optimum of virus-mediated membrane fusion. *Proc. Natl. Acad. Sci. U.S.A.* **79:** 968–972

Smirnova YG, Marrink S-J, Lipowsky R & Knecht V (2010) Solvent-exposed tails as prestalk transition states for membrane fusion at low hydration. *J. Am. Chem. Soc.* **132:** 6710–6718

Stegmann T, Nir S & Wilschut J (1989) Membrane fusion activity of influenza virus. Effects of gangliosides and negatively charged phospholipids in target liposomes. *Biochemistry* **28:** 1698–1704

Stevens MJ, Hoh JH & Woolf TB (2003) Insights into the molecular mechanism of membrane fusion from simulation: evidence for the association of splayed tails. *Phys. Rev. Lett.* **91:** 188102

Suloway C, Shi J, Cheng A, Pulokas J, Carragher B, Potter CS, Zheng SQ, Agard DA & Jensen GJ (2009) Fully automated, sequential tilt-series acquisition with Leginon. *J. Struct. Biol.* **167:** 11–18

Sun X & Whittaker GR (2003) Role for Influenza Virus Envelope Cholesterol in Virus Entry and Infection. *J. Virol.* **77:** 12543–12551

Takeda M, Leser GP, Russell CJ & Lamb RA (2003) Influenza virus hemagglutinin concentrates in lipid raft microdomains for efficient viral fusion. *Proc. Natl. Acad. Sci. U.S.A.* **100:** 14610–14617

Wang L, Seeley ES, Wickner W & Merz AJ (2002) Vacuole fusion at a ring of vertex docking sites leaves membrane fragments within the organelle. *Cell* **108:** 357–369

White JM & Wilson IA (1987) Anti-peptide antibodies detect steps in a protein conformational change: low-pH activation of the influenza virus hemagglutinin. *J. Cell Biol.* **105:** 2887–2896

Wilson IA, Skehel JJ & Wiley DC (1981) Structure of the haemagglutinin membrane glycoprotein of influenza virus at 3 A resolution. *Nature* **289:** 366–373

Xu Y, Seven AB, Su L, Jiang Q-X & Rizo J (2011) Membrane bridging and hemifusion by denaturated Munc18. *PLoS ONE* **6:** e22012

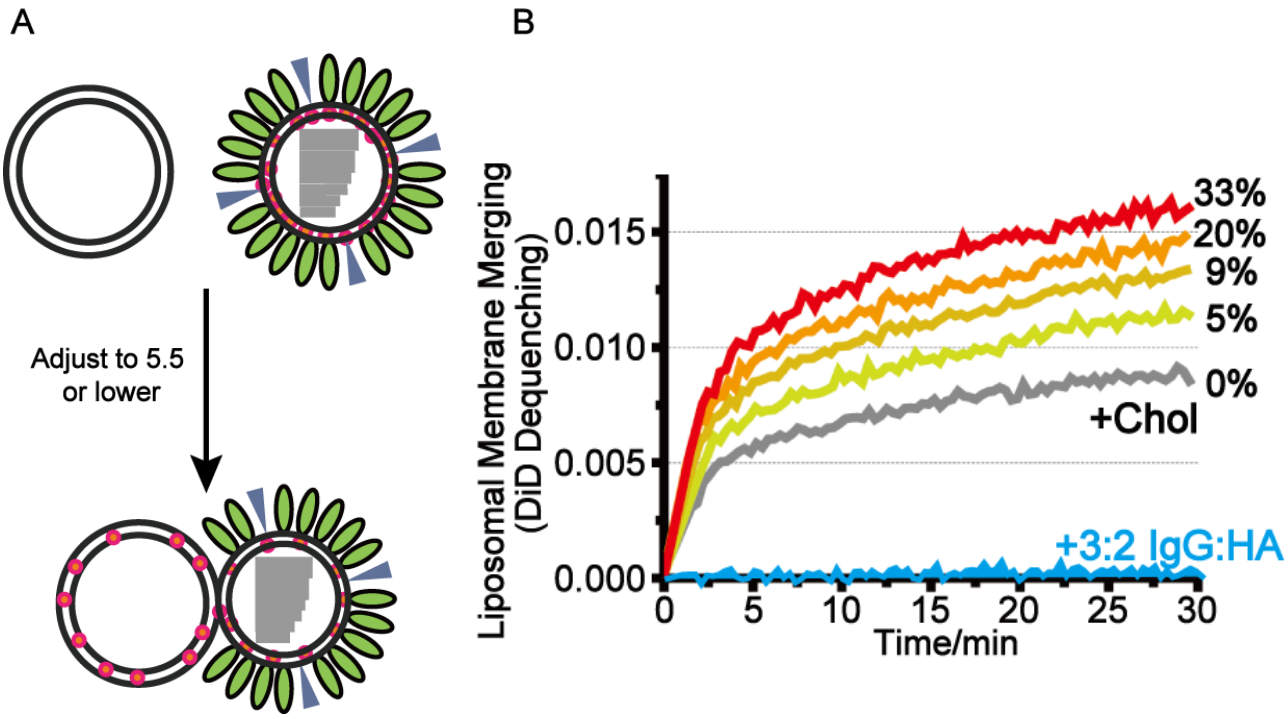

Figure 2.1 Cholesterol on the target membrane enhances membrane lipid mixing (A) When the lipid mixing commences, the dye disperses over a larger membrane area and the fluorescence quenching is relieved. **(B)** The membrane fusion reaction was triggered by lowering pH to 5.5, 37 ˚C, and fluorescence dequenching of DiD, reporting on lipid mixing, was monitored for a series of liposome compositions containing from 0 to 33% molar ratio cholesterol in DOPC. A control experiment was also performed in which fusion of 80% DOPC: 20% cholesterol liposomes and viruses was inhibited by the HA-stem targeted neutralizing antibody, FI6v3 (blue trace),

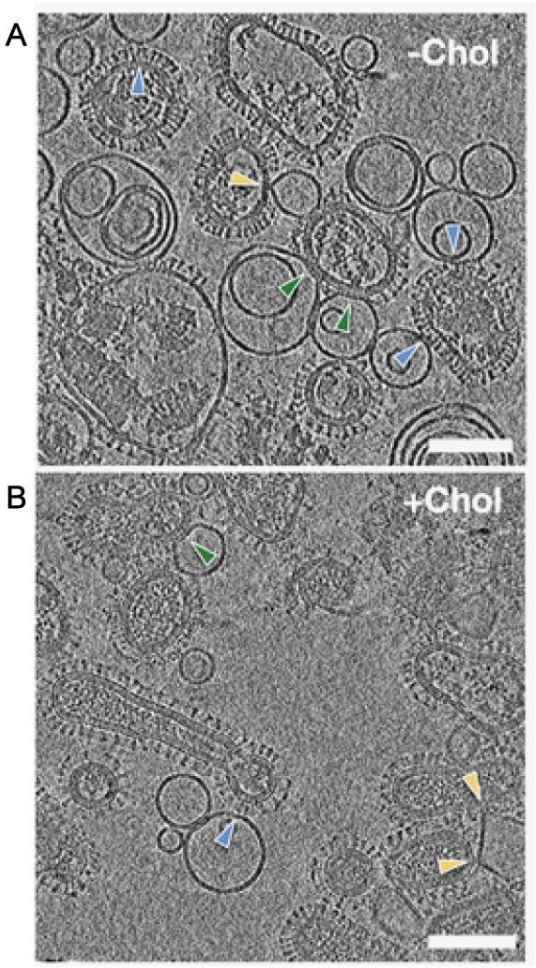

Figure 2.2 Influenza virus-liposome contacts imaged by cryo-electron tomography. 3.2 nm-thick computational slice through reconstructed tomographic density. Influenza virus was mixed with pure DOPC **(A)** or 80% DOPC:20% Chol liposomes **(B)** and incubated at pH 5.5 for 10 min. Blue arrows indicate HA-mediated Type I bridging contacts between virus and liposomes. Yellow arrows indicate Type II localized dimpling interactions. Liposomes also form Type III extended, tightly docked interfaces with viral envelope (green arrows). Scale bars 100 nm.

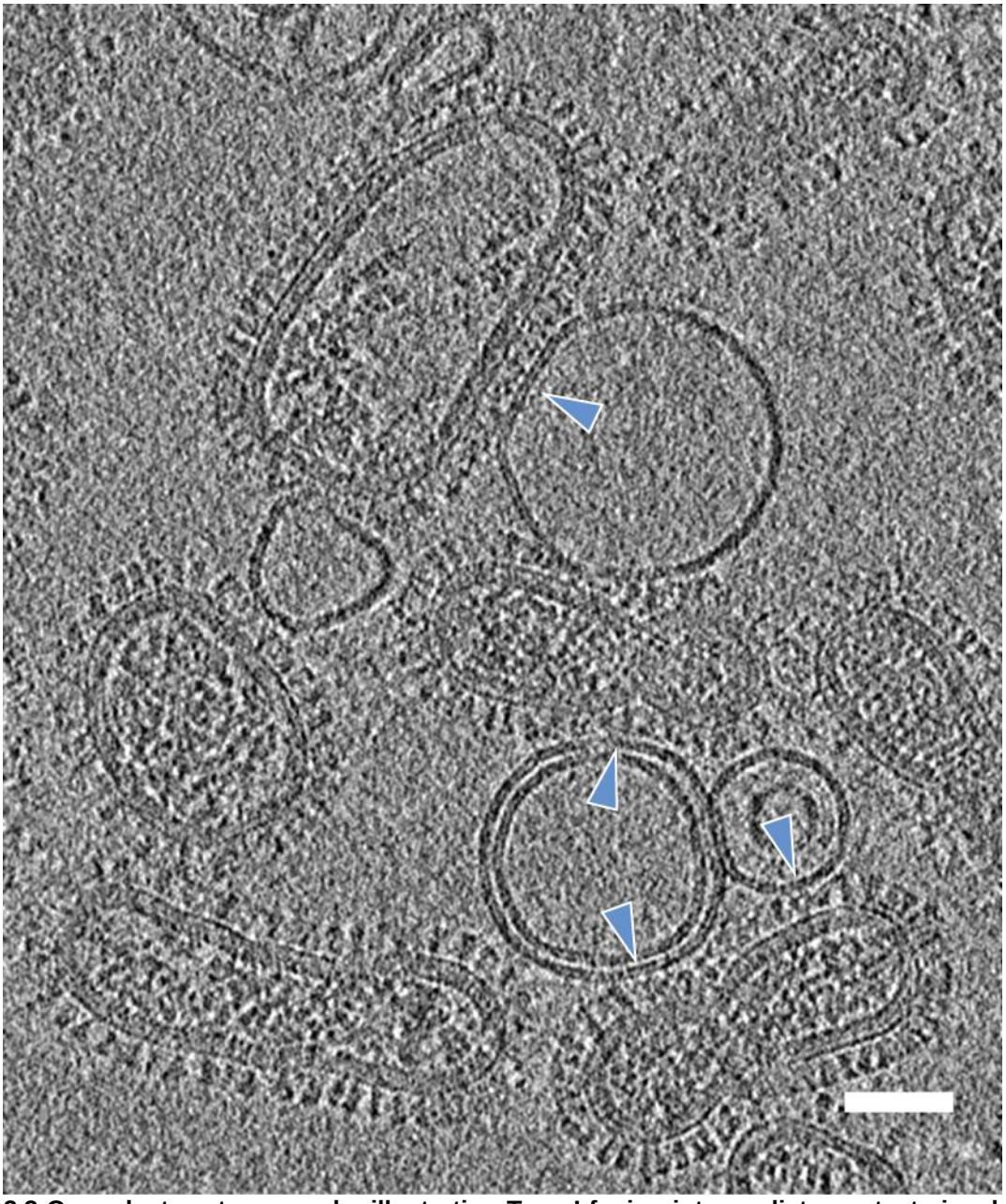

Figure 2.3 Cryo-electron tomography illustrating Type I fusion intermediate contacts in which HA spikes bridge the viral envelope and target membrane. A 3.2 nm-thick computational slice through a reconstructed cryo-electron tomogram shows several examples of HA bridging (blue arrows) between virus particles and 80% DOPC:20% Chol liposomes after 30 seconds incubation at pH 5.5. Scale bar 50 nm.

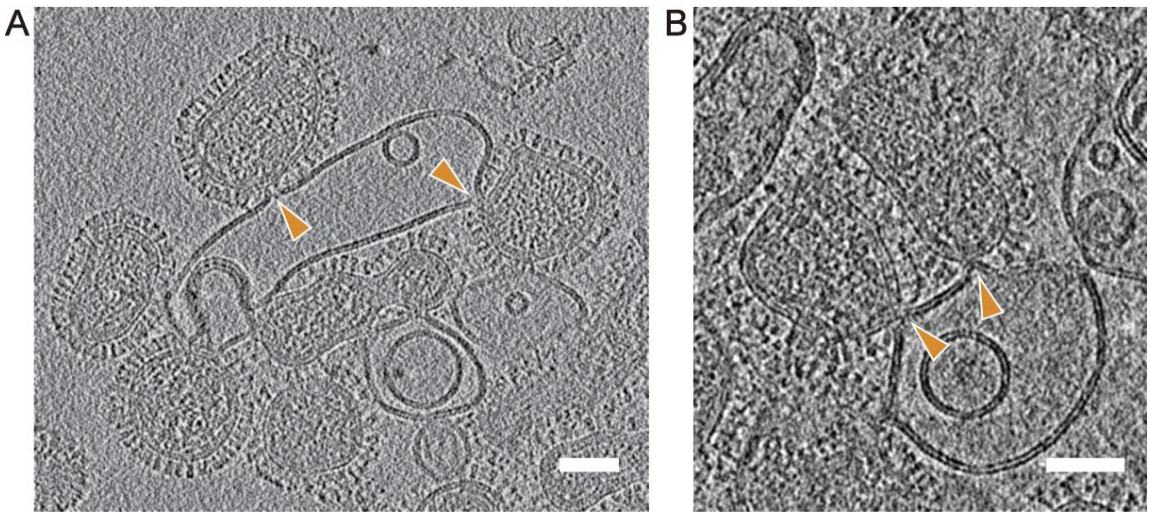

Figure 2.4 Localized membrane deformation at early stages of fusion imaged by cryo-electron tomography. Yellow arrows point to Type II target membrane pinching at liposome-virus contact sites. **(A)** A 3.2 nm-thick computational slice of influenza virus interacting with 80% DOPC:20% Chol liposome at pH 5.5 for 30 minutes. **(B)** A 4.8 nm-thick computational slice of liposomal membrane dimpling between influenza virus and 80% DOPC:20% Chol liposome at pH 5.5 for 30 seconds. Scale bars 50 nm.

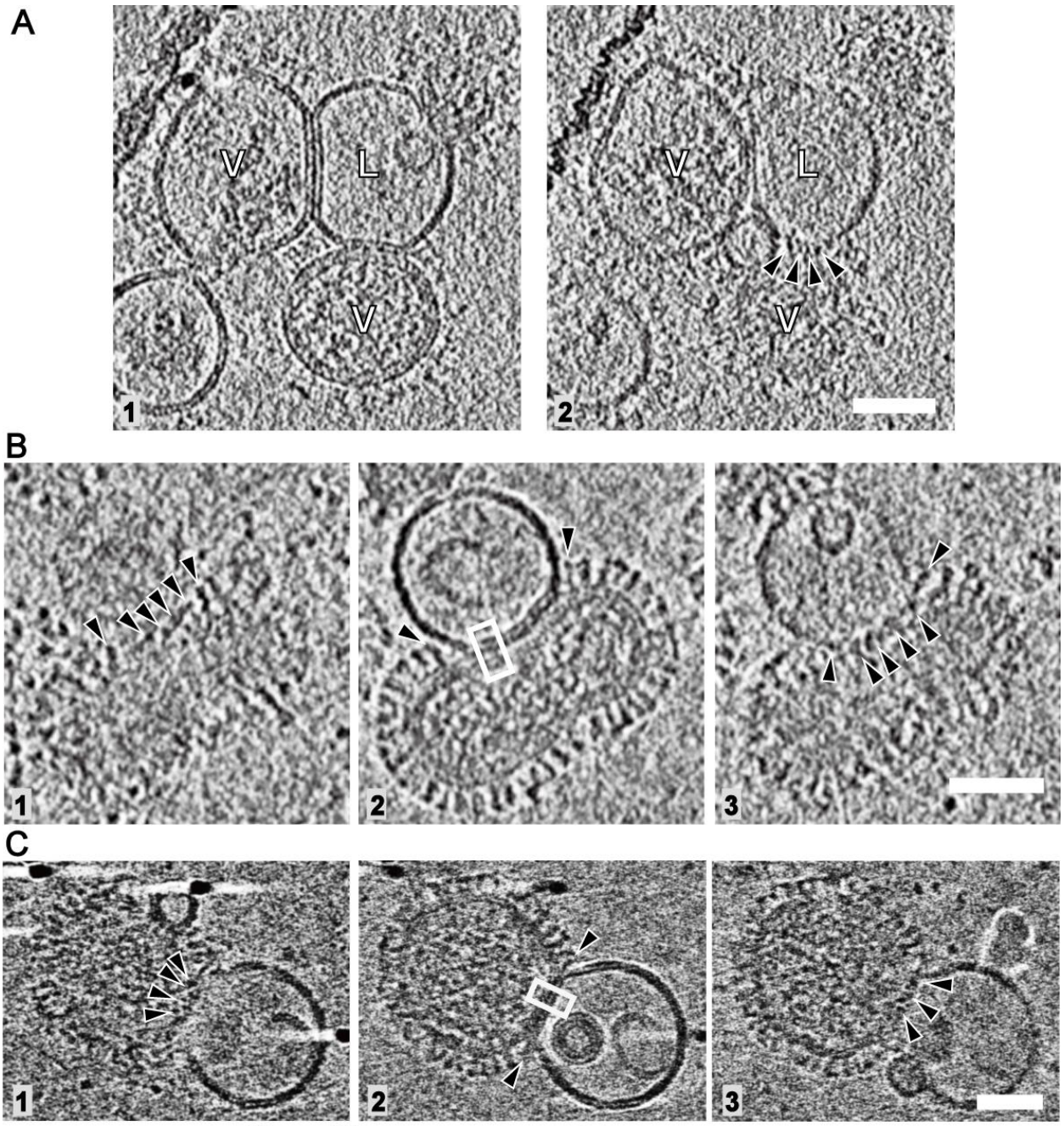
A
V
L
V
1
V
L
V
2
B
1
2
3
C
1
2
3
D
Virus and Liposome
Outer Leaflets
Liposome Inner
Leaflet
Matrix Layer
Virus Inner
Leaflet
Grey Density Value
100
80
60
40
20
0
0
5
10
15
20
Distance/nm
E
Virus and Liposome
Outer Leaflets
Virus Inner
Leaflet
Liposome Inner
Leaflet
Grey Density Value
100
80
60
40
20
0
0
5
10
15
20
Distance/nm

Figure 2.5 Type III Extended, tightly docked virus-liposome complexes. (A) Right: Examples of extended contact zones between virus particles (V) and a liposome (L). The virus on the left lacks an M1 matrix layer, while the one on the bottom exhibits a characteristic thick envelope with M1 matrix layer associated with the inner surface of the viral membrane. **Left:** Density corresponding to HA spikes could be found at the top (Z+7.2 nm) of the extended interface (highlighted by white arrows). **(B)** Serial 4.8 nm-thick computational slices through a reconstructed virus-liposome complex. Liposomes are tightly docked with the viral envelope, forming an interface in which the outer leaflets of liposomes and virus are virtually indistinguishable but the inner leaflets remain separate. Density corresponding to HA spikes is visible at the top and bottom of extended interfaces (white arrows), but glycoproteins appear to be excluded from the interface itself. Scale bars 50 nm. **(C)** Extended interface between a liposome and a matrix-free virus particle. Glycoprotein density is excluded from the contact zone but observed at the periphery of the membrane interface (white arrows). Scale bars 50 nm. **(D)** Electron density plot across the boxed region of the extended interface in B. **(E)** Electron density plot across the boxed region of the extended interface in C.

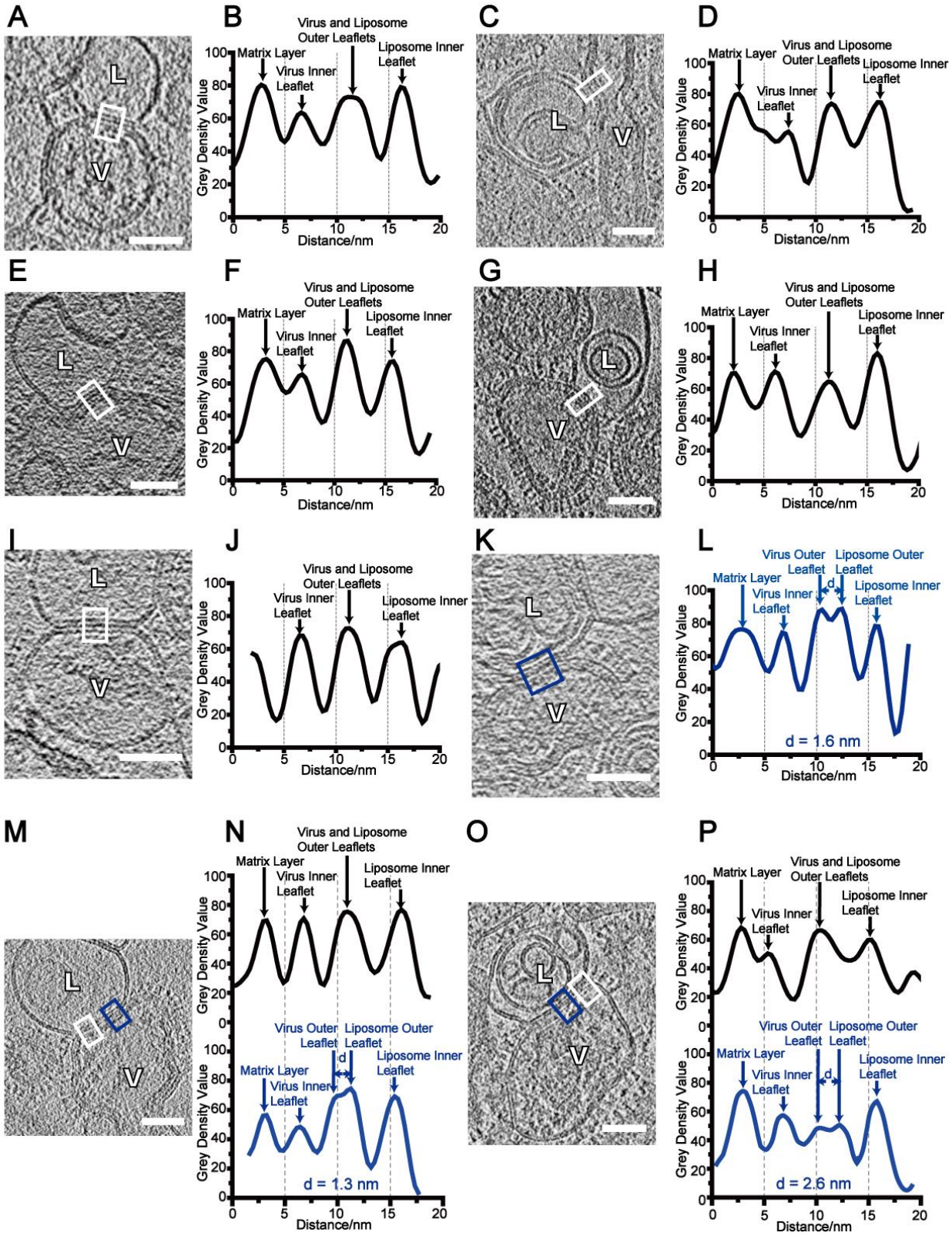

Figure 2.6 Additional examples of Type III extended interfaces in which the two proximal membrane leaflets are closely docked over broad areas. 3.2 nm-thick computational slices through the

reconstructed tomograms are shown. Electron density plot across the box region of each tomographic slices are presented adjacent to each image. **(A-J)** Virus and liposome outer leaflets were tightly docked together and they display as a merged peak. **(K-P)** In certain cases, a narrow distance of 1.3 – 2.6 nm was observed between two proximal membrane leaflets. Influenza viruses were labeled as “V” and target liposomes were labeled as “L”. Scale bars 50 nm.

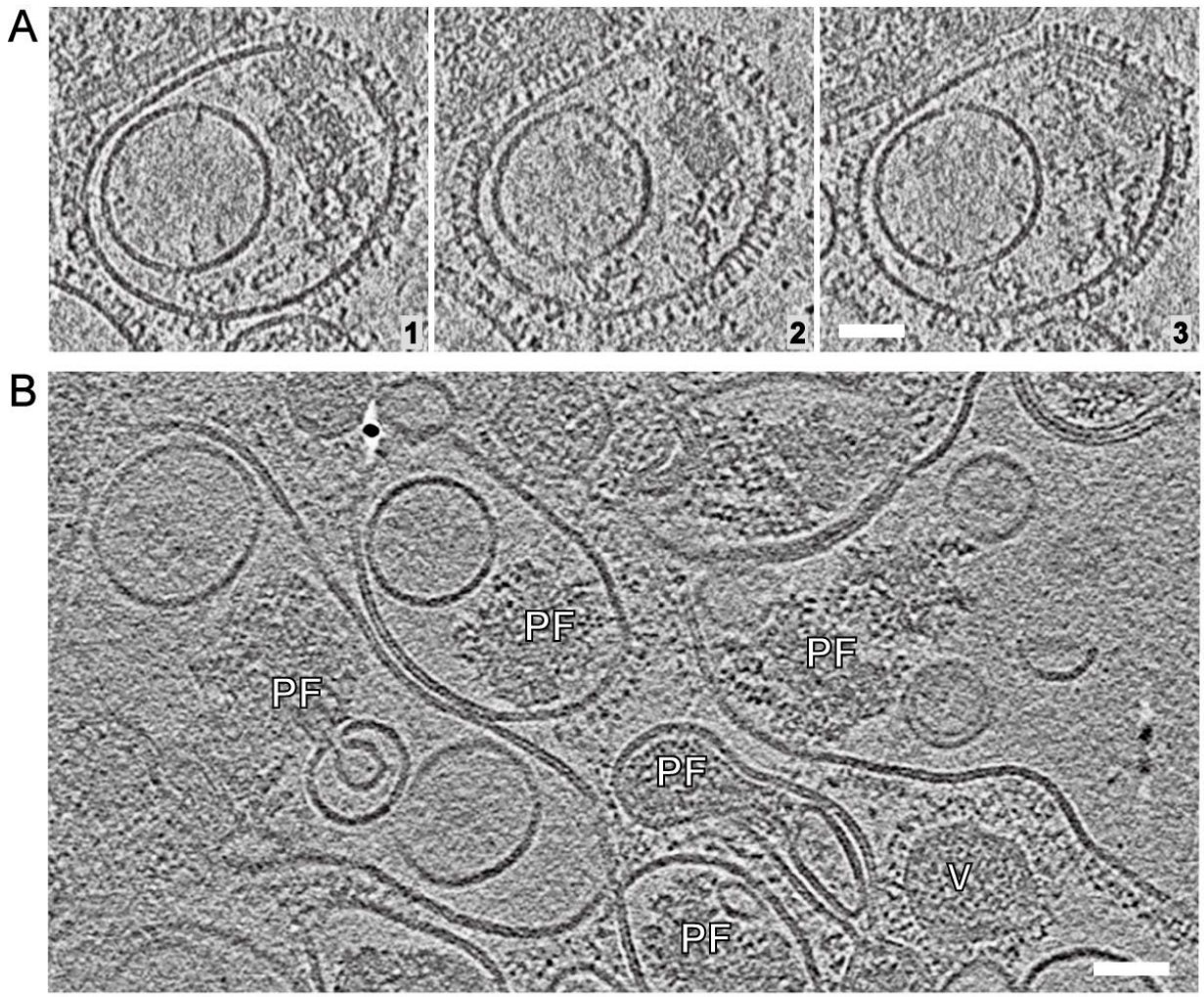

Figure 2.7 Post-fusion influenza-liposome complexes (Type IV fusion contact) imaged by cryo-electron tomography. (A) Computational slices (3.2 nm thick) through a post-fusion complex between virus and 80% DOPC:20% Chol liposome at pH 5.5 for 10 minutes. As is generally the case for post-fusion complexes, this complex displays glycoprotein on its surface and lacks a matrix layer beneath its membrane. Small vesicles encapsulated inside the complex likely originate from inner layers of multi-lamemllar liposomes where the outermost layer fused with the virus membrane. A dense core is observed as well, corresponding to the ribonucleoprotein segments associated with matrix protein. **(B)** 4.8 nm-thick computational slice through a tomogram showing influenza virus fused with 80% DOPC:20% Chol liposomes at pH 5.25 for 30 min. The unfused influenza virus particles (marked “V”) exhibit matrix layer that is still associated with the viral envelope. Post-fusion complexes (marked “PF”) are recognizable by the presence of additional vesicles encapsulated inside the outer merged membrane. Scale bar 50 nm.

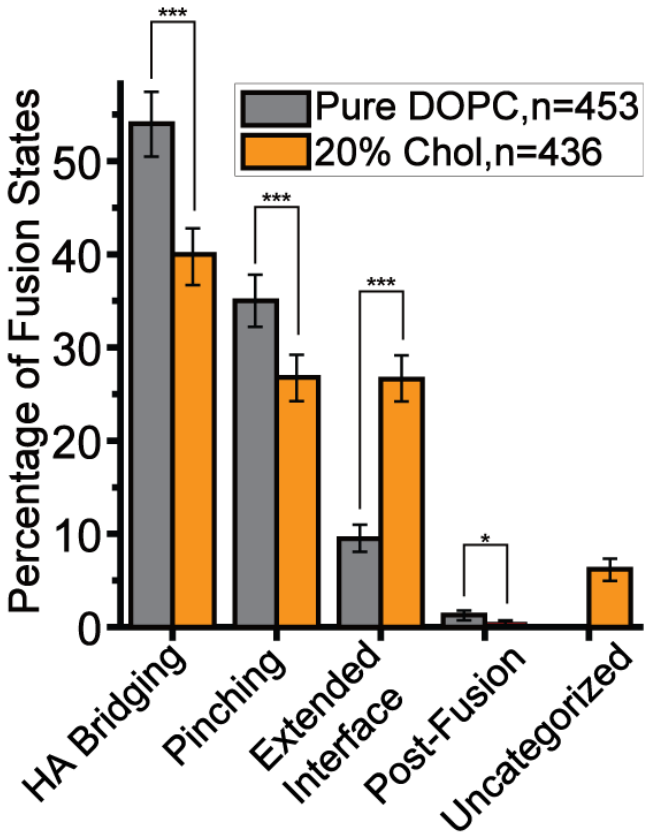

Figure 2.8 Population distribution of four fusion classes imaged by cryo-ET where influenza virus is fusing with 80% DOPC:20% Chol or 100% DOPC liposomes. For pure DOPC liposomes, a total *n* of 453 virus-liposome contacts were assessed; for liposomes containing 20% cholesterol, 436 contacts were analyzed. Individual population counts for each category are provided in Table 2.1. Error bars are calculated as the square root of the number of complexes per state at each given condition and time point, assuming Poisson counting statistics. Statistical significance was assessed via the p-value test ("ns=p>0.05,*=p≤0.05,**=p≤0.01,***=p≤0.001"). Inclusion of cholesterol on target membranes leads to an increase in tightly docked virus-liposome interfaces.

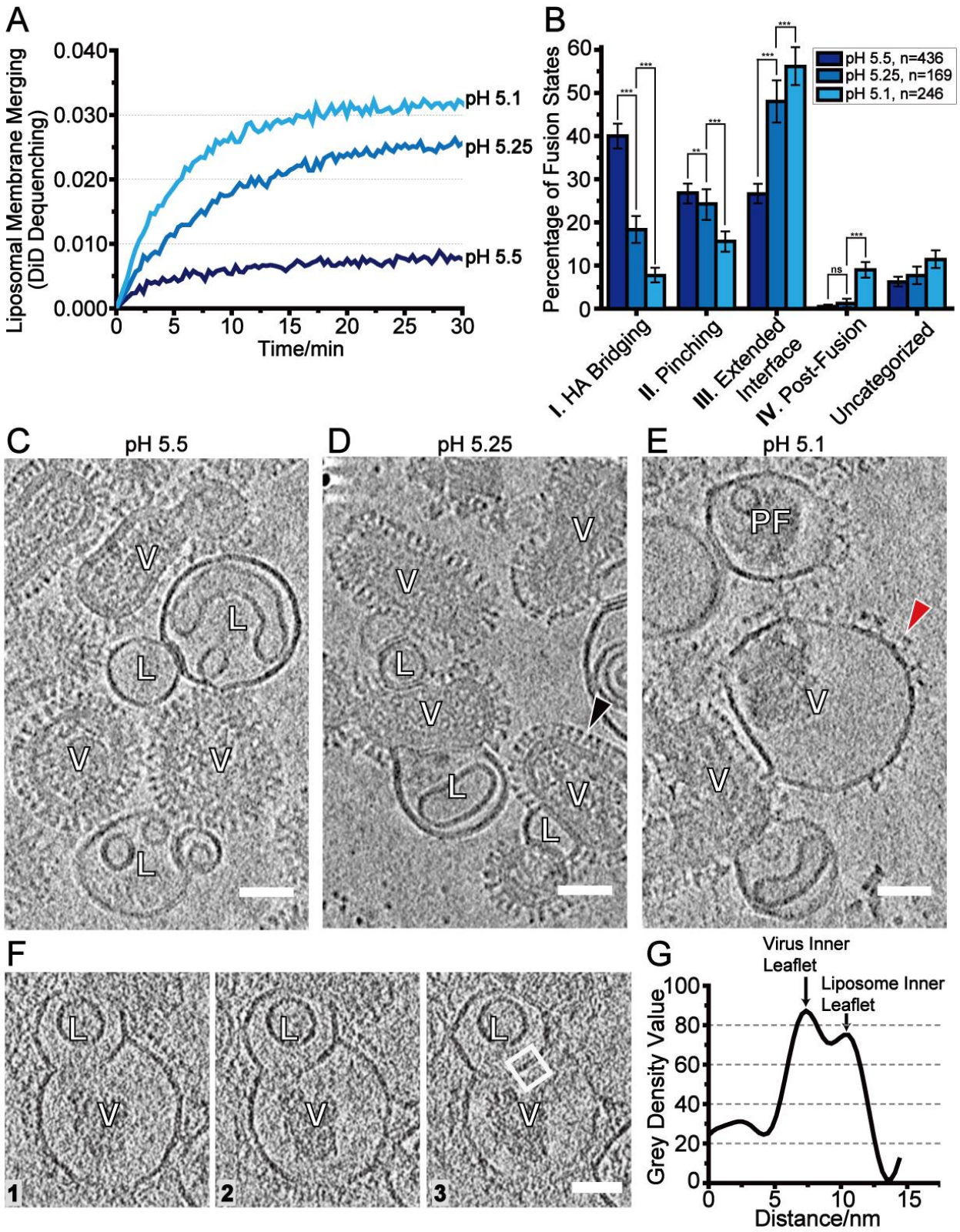

Figure 2.9. pH-dependence of membrane fusion and fusion-complex formation between influenza virus and cholesterol-containing liposomes. (A) In fluorescence-monitored fusion assays, liposomes with 80% DOPC:20% Chol were mixed with DiD-labeled influenza virus at 37 °C and then acidified to final

pH of 5.5, 5.25 or 5.1. **(B)** Comparison of distributions of fusion states at 5.5, 5.25 and 5.1 by cryo-ET. Percentages are given out of a total *n* of 436 virus-liposome contacts at pH 5.5, 169 at pH 5.25, and 246 at pH 5.1. Individual population counts are provided in Table 2.1. Error bars show the standard deviation that is calculated as the square root of the number of complexes per state at each given condition and time point, assuming Poisson counting statistics. Statistical significance was assessed via the p-value test. **(C-E)** 4.8 nm-thick computational slices through cryo-electron tomograms of influenza virus particles (marked "V") and liposomes (marked "L") at pH 5.5, 5.25 and 5.1. **(C)** At pH 5.5, HA spikes retain a structure and organization similar to the pre-fusion conformations and the viral M1 matrix layer remains intact and membrane-associated. Localized dimpling of membranes (Type II contacts) is observed but few instances of post-fusion complexes are seen. **(D)** In the pH 5.25 tomogram, numerous examples of extended interfaces are identifiable, most HA spikes retain a highly organized, ordered form of HA (black arrow). **(E)** At pH 5.1, HA spikes have largely undergone the refolding to a more disorganized post-fusion state (red arrow) and the layer of matrix protein has dissociated from the viral envelope. Examples of post-fusion complex (marked "PF") could also be observed. Scale bar 50 nm. **(F)** Cryo-electron tomogram of hemifusion**.** A rare hemifusion complex between 80% DOPC:20% Chol liposome and virus at pH 5.1 is shown as serial 2.0 nm-thick computational slices through the reconstructed density. Scale bar 50 nm. **(G)** In contrast to the 3-layered density that dominates in the tightly docked, extended interfaces, electron density plot across the hemifused diaphragm shows that only two inner leaflets persist between the virus and liposome.

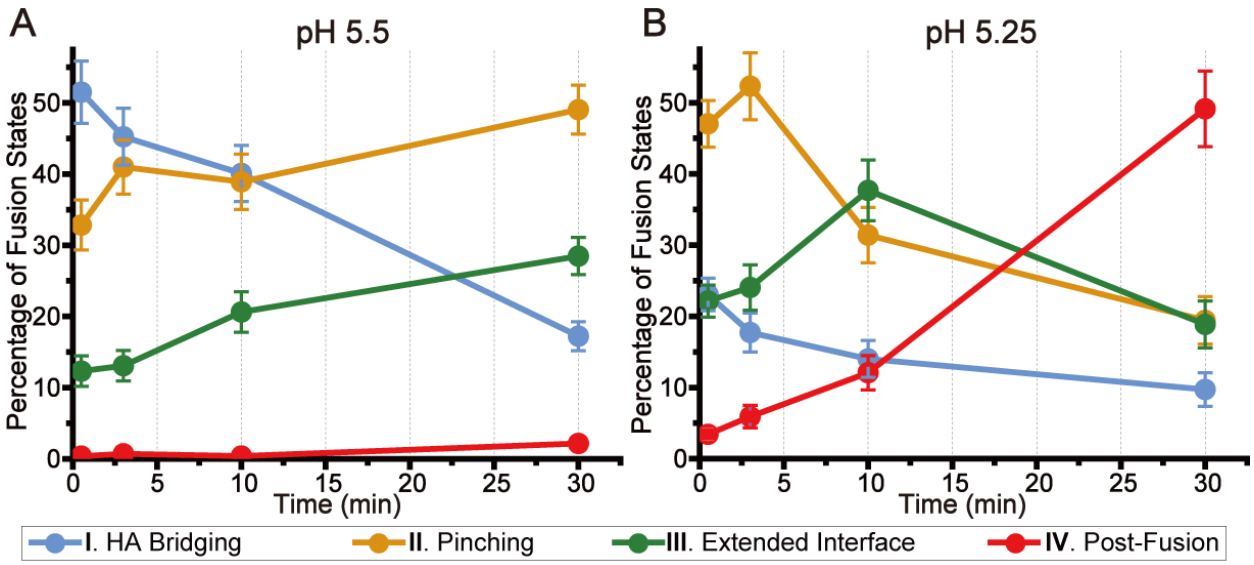

Figure 2.10 Kinetics of fusion state populations for influenza virus fusing with 80% DOPC:20% Chol liposomes at pH 5.5 **(A)** and pH 5.25 **(B)** after 30 s, 3 min, 10 min and 30 min following acidification. The total number of contacts, *n*, examined at pH 5.5 were 268, 283, 257, and 418 for 30 s, 3 min, 10 min, and 30 min datasets. The number of contacts, *n,* examined at pH 5.25 were 438, 237, 207, and 175 for 30 s, 3 min, 10 min, and 30 min datasets. Percentages were calculated as a function of these totals. Individual population counts are provided in Table 2.1. Error bars are calculated as the square root of the number of complexes per state at each given condition and time point, assuming Poisson counting statistics.

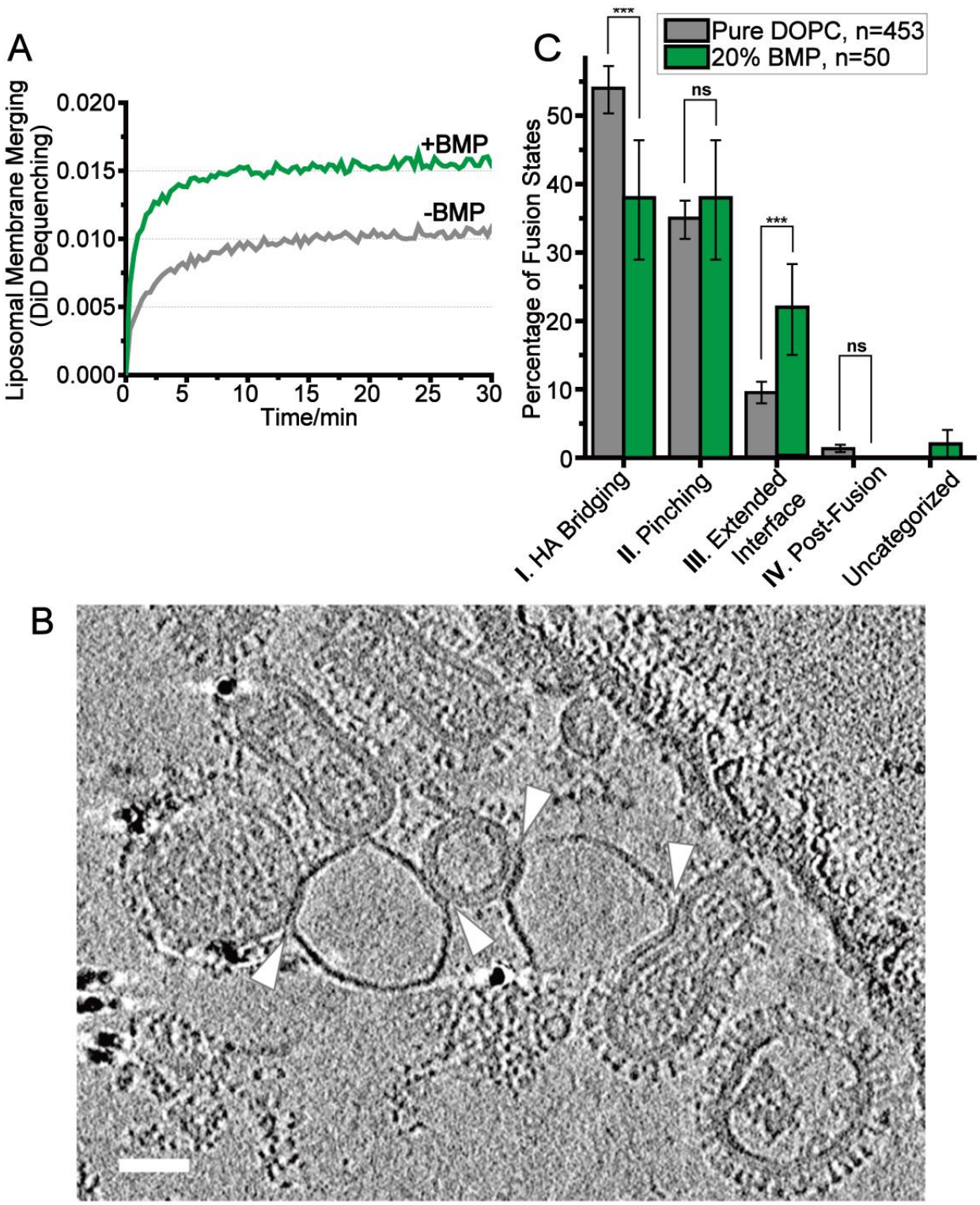

Figure 2.11 BMP enhances lipid mixing and readily forms Type III tightly docked extended interfaces. (A) Fluorescence-monitored fusion assays demonstrated that BMP increases lipid mixing in a similar manner to cholesterol. **(B)** A 4.8 nm-thick computational slice through a reconstructed cryo-electron tomogram shows several examples of extended interfaces (white arrows) between virus particles and BMP-

containing liposomes after 10 min incubation at pH 5.5. Scale bar 50 nm. **(C)** Population distribution of virus-liposome fusion complexes for the cases of 20% BMP:80% DOPC or 100% DOPC liposomes shows that the abundance of extended interfaces significantly increased in the presence of BMP. For analysis of virus and BMP-containing liposomes a total of 50 contacts were characterized. Individual population counts are provided in Table 2.1. Error bars show the standard deviation calculated as the square root of the number of complexes per state at each given condition and time point, assuming Poisson counting statistics. Statistical significance was assessed via the p-value test.

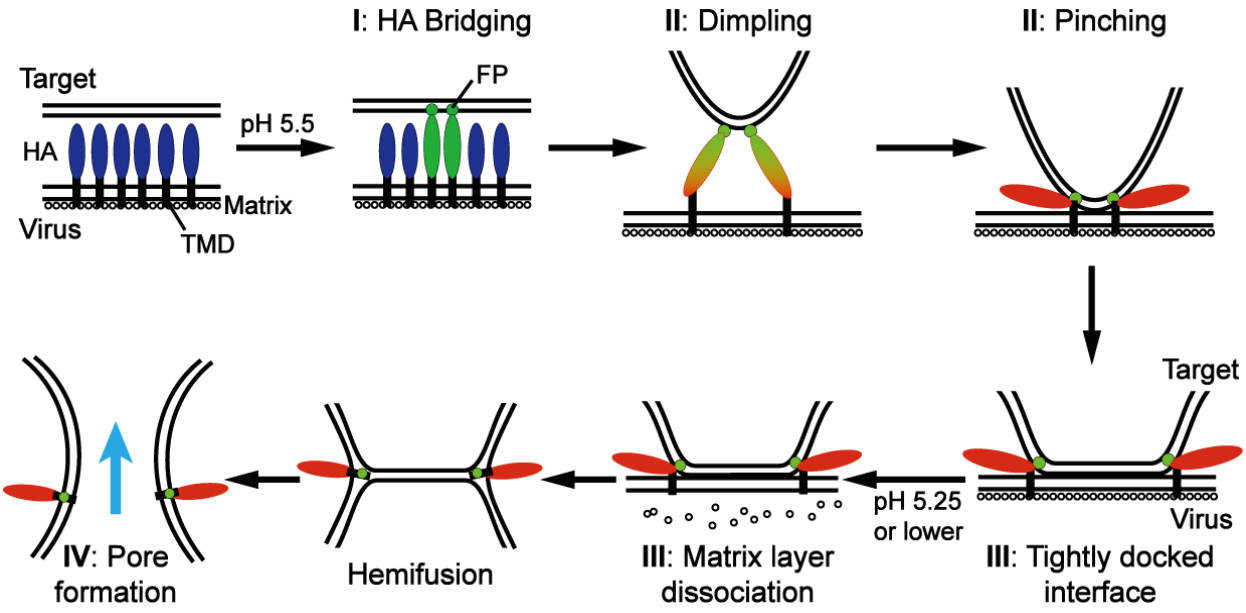

Figure 2.12 Pathway of HA-mediated membrane remodeling during influenza virus fusion based on the combined tomography and fluorescence spectroscopy observations. Key steps involve activation of HA with fusion peptide deployment and insertion into the target membrane, dimpling and membrane apposition, formation of the tightly docked, extended interface, matrix layer dissociation leading to release of matrix-related restraints on the cytoplasmic tail and transmembrane domain, hemifusion, and finally dilation of the fusion pore.

Table 2.1 Population counts for fusion intermediates from cryo-ET analysis.

Liposome Sample (with X31 flu virus)	HA Bridging	Pinching	Extended Interface	Post-fusion	Uncategorized	Total Number (n)
Figure 2.8						
Pure DOPC (10 mins, pH 5.5)	245	159	43	6	0	453
20% Chol (10 mins, pH 5.5)	174	117	116	2	27	436
Figure 2.9B						
20% Chol (10 mins, pH 5.5)	174	117	116	2	27	436
20% Chol (10 mins, pH 5.25)	31	41	81	3	13	169
20% Chol (10 mins, pH 5.1)	19	39	138	22	28	246
Figure 2.10A						
20% Chol (0.5 min, pH 5.5)	138	88	33	1	8	268
20% Chol (3 mins, pH 5.5)	128	116	37	2	0	283
20% Chol (10 mins, pH 5.5)	103	100	53	1	0	257
20% Chol (30 mins, pH 5.5)	72	205	119	9	13	418
Figure 2.10B						
20% Chol (0.5 min, pH 5.25)	101	206	97	15	19	438
20% Chol (3 mins, pH 5.25)	42	124	57	14	0	237
20% Chol (10 mins, pH 5.25)	29	65	78	25	10	207
20% Chol (30 mins, pH 5.5)	17	34	33	86	5	175
Figure 2.11C						
Pure DOPC (10 mins, pH 5.5)	245	159	43	6	0	453
20% BMP (10 mins, pH 5.5)	19	19	11	0	1	50

Number of influenza-liposome interactions observed by cryo-ET for each contact category.

Chapter 3. Cholesterol-dependent Membrane Deformation Induced by Influenza Hemagglutinin at low pH

3.1 Introduction

During the entry of enveloped viruses into host cells, viral fusion proteins mediate membrane remodeling necessary for inducing their fusion (Jahn *et al*, 2003; Harrison, 2008; 2015; White *et al*, 2008; Kielian, 2014). Research on Class I viral fusion proteins has emphasized the functional importance of their relatively short amphipathic domains, referred to as fusion peptides (Harter *et al*, 1989; Epand & Epand, 1994; Epand, 2003; Cross *et al*, 2009). These subdomains are responsible for tethering the viral fusion protein to the host membrane once the fusion machinery is activated and inducing some degree of membrane reorganization that may be important for promoting different stages of fusion as well.

In influenza HA, the amphipathic fusion peptides are generated by proteolytic cleavage of the HA_0 polypeptide, which results from translation of the HA gene, into HA_1 and HA_2. The first 23 residues of the newly formed N-terminus of the fusion subunit, HA_2 form the fusion peptide (Wilson *et al*, 1981; Steinhauer, 1999; Cross *et al*, 2009). The HA fusion peptide sequence is highly conserved across HA serotypes, highlighting the critical functional role played by the HA fusion peptide during membrane fusion. Substitution of the first amino terminal Gly of the fusion peptide with any other amino acid has been shown to significantly alter the protein's fusion activity (Steinhauer *et al*, 1995; Cross *et al*, 2009). Structures of HA fusion peptide fragments in lipid environments at neutral and low pH have been solved by NMR, but the results have shown surprising variability (Han *et al*, 2001; Lai & Tamm, 2007; Lorieau *et al*, 2010; Lorieau & Louis, 2012). A truncated form of the HA fusion peptide of subtype H3 was reported to adopt an open boomerang-shaped kinked helix structure based on ^{1}H-NMR spectroscopy (Han *et al*, 2001; Lai & Tamm, 2007). Alternatively, the 23-residue HA fusion peptide of subtype H1 was found to adopt a tight helical hairpin arrangement at pH 7 and predominantly maintains this structure at pH 4

(Lorieau *et al*, 2010). Given the sequence conservation the differences that were observed may reflect differences in experimental and sample conditions.

Upon activation, conformational rearrangements of fusion proteins lead to exposure of the fusion peptides, which allows them to insert into the target membrane (White *et al*, 2008). This stage of fusion peptide insertion is the first critical step that can lead to target membrane remodeling. Electron-spin resonance studies of the HA fusion peptide in membranes demonstrated that at acidic, fusogenic pH conditions the fusion peptide increased ordering of the acyl chain segments close to the phospholipid head group but not deeper into the apolar regions of the membrane (Ge & Freed, 2009). This effect was found to be dependent upon to two highly conserved residues in the peptide (Ge & Freed, 2009). Solid-state NMR results examining the interaction between lipid bilayers and fusion peptides of parinfluenza virus 5 (PIV5) F protein, which also is a class I fusion protein, indicated that the insertion of the PIV5 fusion peptides into the target membrane resulted in curvature change (Yao & Hong, 2013). Recent molecular dynamics simulations showed that the wild-type HA fusion peptide induced a positive curvature of lipid bilayer and decreases the thickness of the lipid bilayer surrounding the wild-type fusion peptide (Li *et al*, 2010; Légaré & Lagüe, 2012).

The previous studies suggest that the insertion of fusion peptide into target membrane can alter membrane structure and lipid organization, but so far they have not provided definitive experimental of the membrane structures and spatial remodeling that results from fusion peptide insertion. Cryo-electron tomography (cryo-ET) offers the opportunity to image the complex, asymmetric and heterogeneous fusion complex. In the studies described in this chapter we sought to use structural and biophysical approaches to characterize the influence of fusion peptide and activated fusion protein interaction with membranes. By directly imaging the consequences of HA fusion peptide-induced membrane deformation, we hope to obtain valuable information into this still poorly understood process. We also wanted to investigate the influence of membrane composition on the fusion protein-membrane interaction and membrane remodeling. One of the

lipid components we have chosen to focus on, cholesterol, is of special interest. Cholesterol is found in high concentrations (typically 20-30 mol%) of animal cell membranes and has numerous functions in membranes ranging from reducing passive permeability to increasing membrane rigidity, and to controlling neuronal exocytosis and enveloped viral entry. (Róg *et al*, 2009; Mouritsen & Zuckermann, 2004; Huang *et al*, 2006; Linetti *et al*, 2010) Previous experiments that investigated cholesterol's effects on the membrane fusion have been reported (Hambleton *et al*, 2007; Huang *et al*, 2006; Sun & Whittaker, 2003; Domanska *et al*, 2013). For instance, depletion of cholesterol on the viral envelope or target cell membrane inhibits viral membrane fusion(Hambleton *et al*, 2007; Huang *et al*, 2006). Another biophysical study indicated that cholesterol tends to be enriched in the high curvature regions of the membrane fusion process and promotes membrane fusion (Wang *et al*, 2007). In the case of influenza virus, low levels of cholesterol on the viral envelope or cell membrane have been reported to inhibit membrane fusion (Sun & Whittaker, 2003). By monitoring lipid mixing between influenza virus and liposomes, Domanska *et al.* found that cholesterol on the viral envelope plays different roles in the fusion kinetics compared with cholesterol on the target membrane. Their results showed that the presence of cholesterol on the target membrane promoted membrane fusion. Meanwhile, decreasing cholesterol on the viral membrane (~75% cholesterol removal) enhanced membrane fusion but even more severe depletion of cholesterol on the viral membrane (~ 90% cholesterol removal) decreased the rate of membrane fusion. Most of the experiments mentioned above were conducted by indirect measurements from which changes in membrane behavior were inferred. Direct imaging of membrane deformation under different concentration of cholesterol is still needed in order to help provide a better understanding of the influence of lipid composition on membrane remodeling and fusion peptide-induced membrane structural changes.

In the previous chapter, the effect of target membrane composition on the fusion process with whole influenza viruses was examined. In this chapter, my work primarily focuses on the simpler system of soluble HA fusion proteins and seeks to understand how their interaction with

lipid bilayers influences membrane reorganization that may relate to fusion. We hypothesize that the HA fusion peptide is capable of inducing membrane deformation of target membrane and the membrane remodeling is highly sensitive to the amount of cholesterol due to cholesterol's effect on membrane elasticity and spontaneous monolayer curvature. To test our hypothesis, I have employed cryo-electron tomography and fluorescence spectroscopy to investigate cholesterol-dependent membrane deformation induced by HA ectodomain and to compare those effects with what is observed with HA on whole intact virus particles. Fluorescence lipid mixing assays of whole influenza virus particles with liposomes composed of different molar ratios of cholesterol will be performed. Next, membrane deformation will be imaged using cryo-ET. The experiments will compare the extent of membrane deformation when the target liposome membranes are composed of pure DOPC or including 20% molar ratio of cholesterol in DOPC. Most critically, using cryo-ET, I will determine whether the HA ectodomain alone (lacking transmembrane anchor) induces different degrees of membrane remodeling when bound to liposomes under fusion-active conditions. From these studies a much clearer understanding of the range of membrane changes induced by activated fusion proteins (via their fusion peptide insertion) can be obtained. The majority parts of this chapter are not published and the manuscript is still in preparation.

3.2 MATERIALS AND METHODS

3.2.1 BHA preparation

Bromelain-released HA (BHA) was generated by digestion of 30 mg (total protein) of whole virus with 20 mg of bromelain (Sigma-Aldrich) in 150 mM NaCl, 10 mM HEPES pH 7.8, 1 mM EDTA, 25 mM β-mercaptoethanol and 0.02% NaN_3 at 37 °C for 3 hours. The particles were recovered by ultracentrifugation, and additional digestions were performed twice thereafter. Soluble BHA was purified via size exclusion column (GE-Superdex 200) in 150 mM NaCl, 10 mM HEPES pH 7.4 and 0.02% NaN_3, and concentrated via spin filtration using a Centriprep YM-30 and an Amicon Ultra, Ultracel-30 membrane (30 kDa NMWLMWCO) (Millipore, Billerica,

MA)(Garcia *et al*, 2015). BHA purity was assessed by SDS-PAGE and native PAGE gel and its concentration was determined via spectrometer A280.

3.2.2 Liposome preparation

Cholesterol sulfate and cholesteryl phosphocholine were purchased from Avanti Polar Lipids and the liposomes were prepared as described in Chapter 2. The fluorescence spectroscopy of SRB-containing liposomes composed of 20% cholesterol sulfate or 20% cholesteryl phosphocholine were measured at acidic pH in the absence of influenza virus or BHA. No signal of dye dequenching was reported, suggesting the liposomes composed of cholesterol-derivatives are stable at fusogenic pH.

3.2.3 Fluorescence spectroscopy, Cryo-EM and tomography processing

The fluorescence spectroscopy, Cryo-EM and tomography processing were carried out as previously described in Chapter 2.

3.3 RESULTS

3.3.1 Cholesterol-dependence of virus-liposome fusion probed by fluorescence spectroscopy

In order to examine the effect of cholesterol in target membranes on influenza virus membrane fusion, a series of synthetic liposomes composed of 1,2-dioleoyl-sn-glycero-3-phosphatidylcholine (DOPC) and 0%, 5%, 9%, 20%, and 33% molar fraction of cholesterol were prepared by freeze-thaw and extrusion methods (Lee, 2010). The liposomes contained the hydrophilic fluorophore sulforhodamine-B (SRB) at self-quenching concentrations, while the membrane of X31 H3N2 influenza virus was labeled with a lipophilic fluorophore, DiD, also to a self-quenching concentration (Figure 3.1A). Both dyes exhibit pH-independent fluorescence over the range of pH (5.0-7.5) examined in these studies.

When the SRB-labeled liposomes were mixed with DiD-labeled influenza virus at pH 5.5, increases in fluorescence intensity as a result of dequenching for both SRB and DiD could be detected (Figures 3.1B, C). At pH 5.5, the magnitude of the DiD signal increase, reporting on lipid mixing, correlated with the increase in cholesterol concentration, roughly doubling when the cholesterol molar fraction was increased from 0 to 33%. Conversely, SRB dequenching, reporting on liposomal content leakage and transfer, decreased when cholesterol was present in the target liposomal membrane. These results indicate that at pH 5.5, cholesterol in the target membrane has a potent effect on the fusion process, enhancing lipid mixing but reducing content leakage.

3.3.2 Cholesterol-dependent membrane scission imaged by cryo-ET

Our fluorescence assays suggested that cholesterol on the target membrane decreased the content leakage and possibly affected the early stage of membrane remodeling. In order to image the 3-dimensional organization of influenza virus undergoing membrane fusion with liposomes, cryo-ET was applied and influenza X31 virus particles were combined with liposomes composed purely of DOPC or including 20% molar ratio cholesterol with 80% DOPC. In each case, the virus-liposome mixture was plunge frozen in liquid ethane after 10 minutes incubation at pH 5.5, 37 ˚C. As mentioned in Chapter 2, similar types of virus-liposome contact organizations were observed for the two types of liposomes. However, we observed that localized pinching contacts (Type-II interaction) was sensitive to cholesterol on the target membrane and target membrane at 20% cholesterol preferred to form closed, sealed membrane deformation rather than opened membrane rupture.

Of the 159 membrane-pinching events observed between X31 virus and pure DOPC liposomes, 109 out of 159 (69%) exhibited an open-mouthed funnel-shaped deformation of the target liposomal membrane characteristic of the pre-fusion contacts observed previously between influenza particles and pure DOPC liposomes at pH 5.5 (Figures 3.2A-C). By contrast, here with 20% chol: 80% DOPC liposomes, a minority (26%, 31 of 117) exhibited an open-mouthed funnel

at the site of dimpling while the majority did not exhibit membrane scission. (Figures 3.2C-E). The fact that cholesterol facilitates dimpling without loss of target membrane integrity is consistent with the fluorescence observations that liposomes with cholesterol show less liposomal content leakage (Figure 3.1B).

3.3.3 Cholesterol-dependence of HA ectodomain-induced membrane permeabilization

Since our fluorescence experiments and cryo-ET experiments monitoring fusion between influenza virus and liposomes with different levels of cholesterol demonstrated that cholesterol has a significant effect on membrane permeability and lipid mixing as well as affecting characteristics of membrane remodeling, we also sought to determine whether the HA ectodomain alone would induce different degrees of membrane remodeling when bound to liposomes under fusion-active conditions. Influenza X31 HA ectodomain (i.e. bromelain-released HA, BHA) was mixed with liposomes containing a range of cholesterol concentrations and SRB encapsulated inside. Liposomes with cholesterol molar ratios of 0, 5, 9, 20, and 33% in DOPC were examined. SRB leakage at pH 5.25 was detected by a time-dependent increase in fluorescence (Figure 3.3). The BHA-induced liposome leakage monitored by fluorescence plotted in Figure 3.3 followed a similar but more exaggerated cholesterol-dependence trend compared with the virus-liposome case; higher cholesterol concentration in the target membrane reduced SRB leakage. SRB dequenching nearly disappeared when the cholesterol was 20% or higher, suggesting that at this level, BHA-induced membrane deformation leading to leakage was suppressed. We also note that the content leakage induced by BHA showed quite different kinetics with the whole virus. It is quite likely due to lack of HA cooperativity in the BHA group. Previous fluorescence assays and computational simulations have suggested that an average of three neighboring HA molecules are required to fuse the endosomal and viral membranes, and the fusion rate largely depends on the probability of assembling a group of HA neighbors inserted into the target membranes (Danieli *et al*, 1996; Ivanovic *et al*, 2013). The concerted action of the

HA spikes on the whole virus proceeded at higher probability on the viral envelope while the individual BHA molecule was far more dispersed in the cuvette volume.

Cryo-ET was used to image BHA-induced liposome membrane remodeling at pH 5.25 for liposomes with DOPC alone and including 20% cholesterol (Figure 3.4). BHA spikes were frequently found to cover the majority of the liposome surface. For liposomes with DOPC alone, BHA binding results in large-scale membrane deformation (Figures 3.4A&B). In certain regions of the liposomes, the membrane appears to have lost its integrity and acute protrusions or pinched features are observed. In contrast, when BHA inserts into the liposomal membrane containing cholesterol, the membrane shows far less perturbation (Figure 3.4C). For the liposomes composed purely of DOPC, 74% (217/292) exhibited membrane deformation due to BHA binding at pH 5.25 (Figure 3.5). The fraction of deformed liposomes falls to 33% (54/165) and 27% (51/186) in the liposomes containing 20% and 33% molar fraction of cholesterol respectively. The cholesterol-dependent membrane-altering effects resulting from the BHA ectodomain under acidic conditions thus recapitulate the trends observed with whole virus, confirming the moderating effect of cholesterol on membrane permeability and deformation.

3.3.4 Cholesterol derivatives also affect HA-mediated membrane fusion

What properties of cholesterol stabilize the target membrane against fusion peptide-induced membrane deformation? We hypothesized that the flip-flop propensity of cholesterol due to its relatively low polarity hydroxyl head group most likely releases the strain from the insertion of fusion peptide (Wang *et al*, 2007; Biswas *et al*, 2008). To test this hypothesis, we included liposomes containing cholesterol derivatives with different size of headgroups, namely cholesterol sulfate and cholesteryl phosphocholine (CholPC), in our fluorescence assays. These cholesterol derivatives (cholesterol sulfate and CholPC) contain similar structures of rigid hydrophobic body, but the charged headgroups (negatively charged in cholesterol sulfate and zwitterionic in CholPC) are expected to slow the flipping rate, owing to the increased energy required to dehydrate and

transfer it through the hydrophobic interior of the lipid bilayers (Rodrigueza et al, 1995). A series of SRB-containing liposomes were prepared that consisted of DOPC with 20% molar fraction of cholesterol, 20% cholesterol sulfate, or 20% CholPC (Figure 3.6A). SRB leakage induced by whole influenza virus particles or BHA at fusogenic pH was detected by a time-dependent increase in fluorescence. The fluorescence results follow a previous trend that cholesterol on the target membrane reduces liposomal content leakage. Cholesterol sulfate, with a slightly larger polar head group and slower rate of flip-flop, is able to moderately suppress the BHA-induced SRB leakage but to a lesser extent than cholesterol (Figure 3.6B). Surprisingly, SRB leakage was enhanced when CholPC was incorporated into the target membrane (Figure 3.6C).

The reason why CholPC in the target membrane increase liposomal content leakage is not entirely clear. Previous studies by Lonnfors and co-workers indicate that CholPC induces a dramatic destabilization of the gel phases of saturated phosphatidylcholine (PC) and this disruption of the gel phase is most likely explained by mismatch in the volumes of the headgroup versus the hydrophobic part of CholPC and saturated PC. The volume of the phosphocholine group is similar for both molecules, but the volume of the sterol body is much less than the volume of the hydrophobic tails of saturated PC (Lonnfors et al, 2015). We note that in our assays, the liposomal membrane is mainly composed of unsaturated DOPC (two double bonds, Tm = -17^{o}C) and the membrane is in the liquid phase instead of the gel phase. But the size mismatch between CholPC and DOPC still exists. It may be that the cholesterol part of CholPC is unable to fill the intermolecular void created when it is mixed with DOPC, thus resulting in a similar destabilization of lipid bilayers as with DOPC alone. This destabilized membrane, if disturbed by HA fusion peptide, would be more likely to form open and leaky membrane deformation. In addition, CholPC is reported to fail in forming a liquid ordered phase unlike cholesterol with saturated phosphatidylcholine (PC) because the large headgroup in CholPC has been speculated to prevent it from interacting closely with PC (Lonnfors et al, 2015). More experiments such as CholPC in liposomes composed of saturated PC may shed further light on this unexpected result.

3.4 DISCUSSION

Here we used fluorescence spectroscopy and cryo-electron tomography to characterize the changes in membrane permeability and the three-dimensional nature of membrane deformation induced by HA on whole influenza virus particles or BHA ectodomains at different ratios of cholesterol concentration on the target membrane. In contrast to Chapter 2 in which we focused on the entire pathway of membrane remodeling leading to the efficient membrane fusion, the focus here was on determining the influence of target membrane composition on differences in membrane deformation induced by HA at early stages of fusion. Understanding the nature of membrane remodeling that underlies the lipid-specific enhancement of the fusion process was of central interest in our study.

Previous experimental and theoretical models support that membrane fusion begins with a “hemifusion stalk” that is hourglass-shaped with local merger of only the proximal leaflets of the two membranes (see Figure 1.1B). The stalk has a high degree of negative curvature along one axis and positive curvature along the other. In support of this model, several mechanism of HA fusion peptide interacting with lipids have been proposed. For instance, Fuhrmans and Marrink concluded that the HA fusion peptide promotes positive membrane curvature based on molecular dynamics simulations (Fuhrmans and Marrink, 2013). NMR and X-ray diffraction studies revealed that negatively induced curvature and fusion activity were significantly induced by the presence of the HA fusion peptide (Smrt et al, 2015; Tenchov et al, 2013). However, previous approaches have been largely limited: molecular dynamics could not predict the exact membrane deformation due to time limitation and NMR studies focused on membrane remodeling in small membrane systems such as bicelles (diameter < 1 nm). In addition, monomeric fusion peptides instead of full trimeric fusion proteins were applied but some reports suggested that trimeric fusion peptides changed the biophysical properties of fusion peptide in membranes and such oligomerization promoted membrane fusion. Thus, a direct imaging method towards the full-length, trimeric fusion

proteins interacting with large-scale membrane is required to fulfill the blank of our understanding of membrane fusion. Our tomographic reconstructions directly imaged the HA spikes and related membrane curvature changes. We observed that fusion peptide insertion by HA resulted in a positive membrane curvature on the target membrane characterized by buckling and scission of the bilayer. Finger-like protrusions and regions of positive curvature were observed with protein density that we attribute to membrane-inserted HA at the zenith of these curved regions (Figure 3.4B). These observations are also consistent with solid-state NMR studies examining human parainfluenza virus 5 fusion peptides in negatively curved phosphoethanolamine membranes, which reported that human parainfluenza virus 5 fusion peptides strongly alter the bias of membrane curvature from negative to positive (Yao & Hong, 2013).

The detailed mechanism of fusion peptide-induce membrane deformation has still remained exclusive. We posit that the disruptive effect results from confinement of the membrane-inserted fusion peptide to the proximal leaflet due to its amphipathic character (Longo *et al*, 1997; Han *et al*, 2001), which leads to asymmetric packing of the leaflets and a positive change in membrane curvature (Campelo *et al*, 2008). As a result it is likely that the membranes increase in permeability, giving rise to increased leakage and local rupture. With cholesterol present in the liposome membrane, a dramatic reduction in membranes with open funnel pinching (with HA on whole virus) or significant buckling (with the BHA ectodomain) was observed by cryo-ET. We rationalize that dramatic reduction in membrane deformation in cholesterol-containing liposomes most likely results from cholesterol's propensity to flip-flop between leaflets due to its relatively low polarity hydroxyl head group. When fusion peptides insert into one leaflet, cholesterol may migrate to the opposing leaflet to mitigate the stresses on the asymmetrically packed leaflets seen with pure DOPC liposomal membranes, resulting in reduced strain and curvature. Indeed, Bruckner et al. used Förster resonance energy transfer to demonstrate the transbilayer movement of cholesterol induced under membrane deformation (Bruckner *et al*, 2009). Our observations are also consistent with computational modeling that has determined that inclusion of cholesterol

reduces a membrane's propensity to leak and become permeabilized during membrane fusion (Risselada *et al*, 2014).

To further test the hypothesis that cholesterol flip-flop was responsible for moderating the curvature-inducing influence of HA fusion peptide insertion into target membranes, we examined cholesterol derivatives that we considered would be less likely to flip-flop due to the polar and bulky nature of their headgroups. While cholesterol sulfate with its polar headgroup as opposed to a simple hydroxyl group in cholesterol indeed showed an intermediate level of content leakage and membrane permeability relative to pure DOPC and 80% DOPC: 20% cholesterol membranes under the influence of BHA ectodomain binding, the bulkier, zwitterionic cholesterol phosphatidylcholine compound showed surprisingly high levels of membrane permeabilization once activated HA was introduced. Future experiments with additional cholesterol derivatives may help to clarify the influence of the head group moiety on HA-induced membrane deformation and fusion.

We also note that the moderating effect of cholesterol on membrane bending and deformation would seem to run contrary to the hypothesis that cholesterol facilitates formation of the high-energy, high-curvature intermediates that have been envisioned to form during membrane fusion (Chen & Rand, 1997; Wang *et al*, 2007; Sun & Whittaker, 2003; Domanska *et al*, 2013). We argue that most of their experiments were conducted at pH 5.0 or lower, focusing on the late fusion stages such as formation and expansion of open fusion pores. In our studies, we are more interested in the nascent fusion steps such as fusion peptide interactions with target membrane and how viral envelope and target membranes are bought together, thus our investigation was focused on conditions around pH 5.5. In addition, we note that while it has been suggested that cholesterol promotes membrane curvature, in the present study, we did not for example observe an increase in localized dimple formation when cholesterol was present in the target membrane, suggesting it did not make the membranes more prone to form regions of high curvature, at least at the early stages of HA-mediated membrane fusion.

In summary, we have demonstrated that even the HA ectodomain in isolation, out of the context of whole influenza virus particles can induce significant membrane remodeling once activated by acidic pH. We have gained a detailed structural perspective on the nature of those membrane reorganizations as well as the effect that additional lipidic components have on HA-membrane remodeling.

References:

Biswas S, Yin SR, Blank PS & Zimmerberg J (2008) Cholesterol promotes hemifusion and pore widening in membrane fusion induced by influenza hemagglutinin. *J. Gen. Physiol.* **131:** 503–513

Bruckner RJ, Mansy SS, Ricardo A, Mahadevan L & Szostak JW (2009) Flip-flop-induced relaxation of bending energy: implications for membrane remodeling. *Biophys. J.* **97:** 3113–3122

Campelo F, McMahon HT & Kozlov MM (2008) The hydrophobic insertion mechanism of membrane curvature generation by proteins. *Biophys. J.* **95:** 2325–2339

Chen Z & Rand RP (1997) The influence of cholesterol on phospholipid membrane curvature and bending elasticity. *Biophys. J.* **73:** 267–276

Cross KJ, Langley WA, Russell RJ, Skehel JJ & Steinhauer DA (2009) Composition and functions of the influenza fusion peptide. *Protein Pept. Lett.* **16:** 766–778

Danieli T, Pelletier SL, Henis YI & White JM (1996) Membrane fusion mediated by the influenza virus hemagglutinin requires the concerted action of at least three hemagglutinin trimers. *J. Cell Biol.* **133:** 559–569

Domanska MK, Wrona D & Kasson PM (2013) Multiphasic Effects of Cholesterol on Influenza Fusion Kinetics ReflectMultiple Mechanistic Roles. *Biophys. J.* **105:** 1383–1387

Epand RM (2003) Fusion peptides and the mechanism of viral fusion. *Biochimica et Biophysica Acta (BBA) - Biomembranes* **1614:** 116–121

Epand RM & Epand RF (1994) Relationship between the infectivity of influenza virus and the ability of its fusion peptide to perturb bilayers. *Biochem and Biophys Res. Commun.* **202**:1420-5.

Garcia NK, Guttman M, Ebner JL & Lee KK (2015) Dynamic changes during acid-Induced activation of influenza hemagglutinin. *Structure* **23:** 665–676

Ge M & Freed JH (2009) Fusion peptide from influenza hemagglutinin increases membrane surface order: an electron-spin resonance study. *Biophys. J.* **96:** 4925–4934

Hambleton S, Steinberg SP, Gershon MD & Gershon AA (2007) Cholesterol dependence of varicella-zoster virion entry into target cells. *J. Virol.* **81:** 7548–7558

Han X, Bushweller JH, Cafiso DS & Tamm LK (2001) Membrane structure and fusion-triggering conformational change of the fusion domain from influenza hemagglutinin. *Nat. Struct. Biol.* **8:** 715–720

Harrison SC (2008) Viral membrane fusion. *Nat. Struct. Mol. Biol.* **15:** 690–698

Harrison SC (2015) Viral membrane fusion. *Virology* **479-480:** 498–507

Harter C, James P, Bächi T & Semenza G (1989) Hydrophobic binding of the ectodomain of

influenza hemagglutinin to membranes occurs through the" fusion peptide". *J. Biol. Chem.* 264(11):6459-64.

Huang H, Li Y, Sadaoka T, Tang H, Yamamoto T, Yamanishi K & Mori Y (2006) Human herpesvirus 6 envelope cholesterol is required for virus entry. *J. Gen. Virol.* **87:** 277–285

Ivanovic T, Choi JL, Whelan SP, van Oijen AM & Harrison SC (2013) Influenza-virus membrane fusion by cooperative fold-back of stochastically induced hemagglutinin intermediates. *eLife* **2:** e00333

Jahn R, Lang T & Südhof TC (2003) Membrane fusion. *Cell* **112:** 519–533

Kielian M (2014) Mechanisms of Virus Membrane Fusion Proteins. *Annu. Rev. Virol.* **1:** 171–189

Lai AL & Tamm LK (2007) Locking the kink in the influenza hemagglutinin fusion domain structure. *J. Biol. Chem.* **282:** 23946–23956

Lee KK (2010) Architecture of a nascent viral fusion pore. *EMBO J.* **29:** 1299–1311

Légaré S & Lagüe P (2012) The Influenza Fusion Peptide Adopts a Flexible Flat V Conformation in Membranes. *Biophys. J.***102:** 2270–2278

Li J, Das P & Zhou R (2010) Single Mutation Effects on Conformational Change and Membrane Deformation of Influenza Hemagglutinin Fusion Peptides. *J. Phys. Chem. B* **114:** 8799–8806

Linetti A, Fratangeli A, Taverna E, Valnegri P, Francolini M, Cappello V, Matteoli M, Passafaro M & Rosa P (2010) Cholesterol reduction impairs exocytosis of synaptic vesicles. *J. Cell. Sci.* **123:** 595–605

Longo ML, Waring AJ & Hammer DA (1997) Interaction of the influenza hemagglutinin fusion peptide with lipid bilayers: area expansion and permeation. *Biophys. J.* **73:** 1430–1439

Lorieau JL & Louis JM (2012) pH-triggered, activated-state conformations of the influenza hemagglutinin fusion peptide revealed by NMR. *Proc. Natl. Acad. Sci. USA* **109:** E1609–18

Lorieau JL, Louis JM & Bax A (2010) The complete influenza hemagglutinin fusion domain adopts a tight helical hairpin arrangement at the lipid: water interface. *Proc. Natl. Acad. Sci. USA* **107**:11341-6

Mouritsen OG & Zuckermann MJ (2004) What's so special about cholesterol? *Lipids.* **39**:1101-13.

Risselada HJ, Bubnis G & Grubmüller H (2014) Expansion of the fusion stalk and its implication for biological membrane fusion. *Proc. Natl. Acad. Sci. USA* **111:** 11043–11048

Róg T, Pasenkiewicz-Gierula M, Vattulainen I & Karttunen M (2009) Ordering effects of cholesterol and its analogues. *BBA - Biomembranes* **1788:** 97–121

Steinhauer DA (1999) Role of hemagglutinin cleavage for the pathogenicity of influenza virus. *Virology* **258:** 1–20

Steinhauer DA, Wharton SA, Skehel JJ & Wiley DC (1995) Studies of the membrane fusion activities of fusion peptide mutants of influenza virus hemagglutinin. *J. Virol.* **69:** 6643–6651

Sun X & Whittaker GR (2003) Role for Influenza Virus Envelope Cholesterol in Virus Entry and Infection. *J. Virol.* **77:** 12543–12551

Wang W, Yang L & Huang HW (2007) Evidence of Cholesterol Accumulated in High Curvature Regions: Implication to the Curvature Elastic Energy for Lipid Mixtures. *Biophys. J.* **92:** 2819–2830

White JM, Delos SE, Brecher M, Schornberg K (2008) Structures and mechanisms of viral membrane fusion proteins: multiple variations on a common theme. *Crit. Rev. Biochem. Mol. Biol.* **43**: 189-219

Wilson IA, Skehel JJ & Wiley DC (1981) Structure of the haemagglutinin membrane glycoprotein of influenza virus at 3 A resolution. *Nature* **289:** 366–373

Yao H & Hong M (2013) Membrane-Dependent Conformation, Dynamics, and Lipid Interactions of the Fusion Peptide of the Paramyxovirus PIV5 from Solid-State NMR. *J. Mol. Biol.* **425:** 563–576

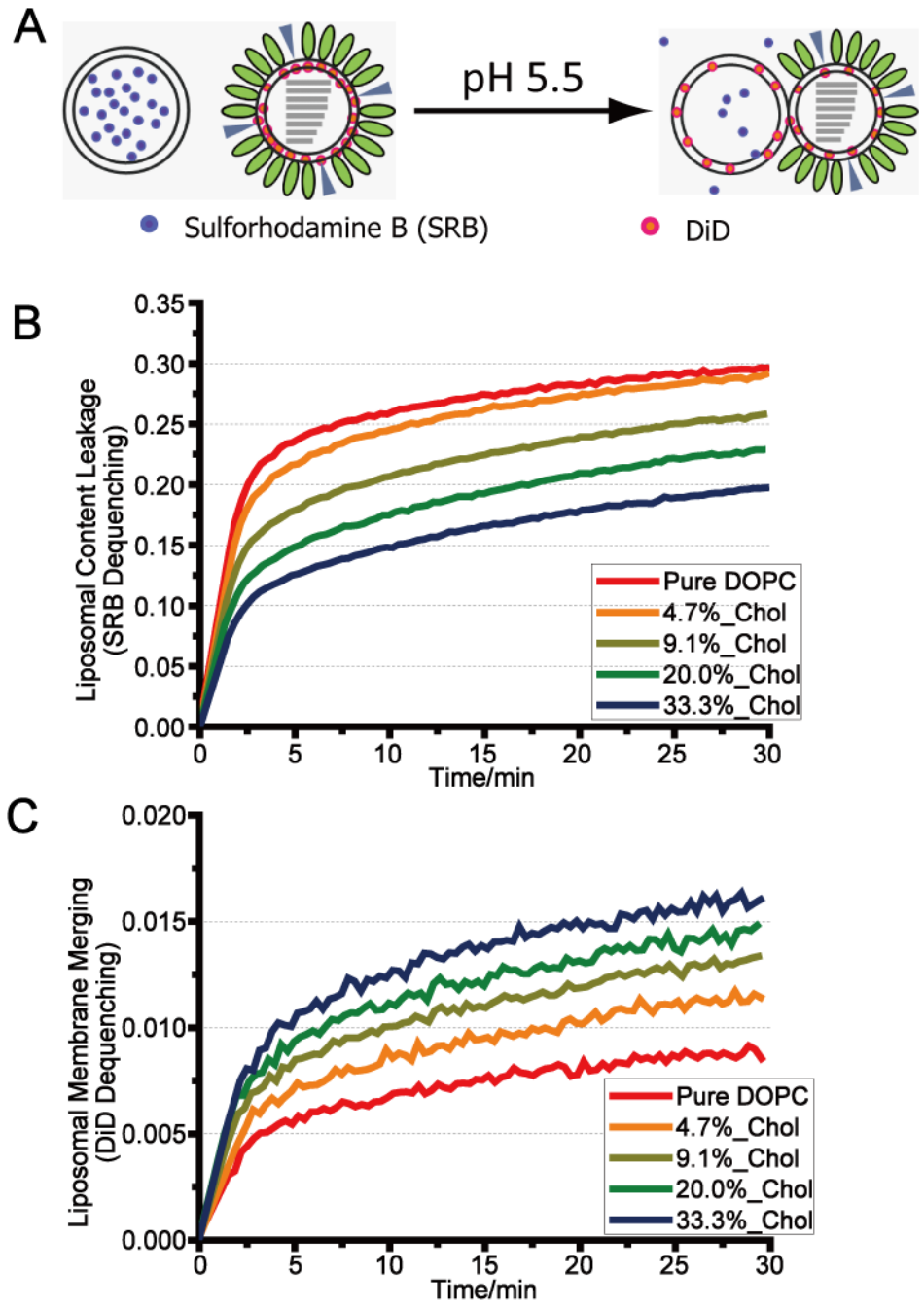

Figure 3.1 Cholesterol on the target membrane enhances membrane lipid mixing but reduces liposomal content leakage as monitored by fluorescence spectroscopy. (A) Schematic diagram shows fluorescence lipids mixing assays. **(B, C)** When the membrane fusion is triggered by lowering pH to 5.5, 37 ˚C, both the dye disperses over a larger membrane area and the fluorescence quenching is relieved. Fluorescence dequenching of SRB, reporting liposome content leakage **(B)**, and DiD, reporting lipid mixing **(C),** were monitored.

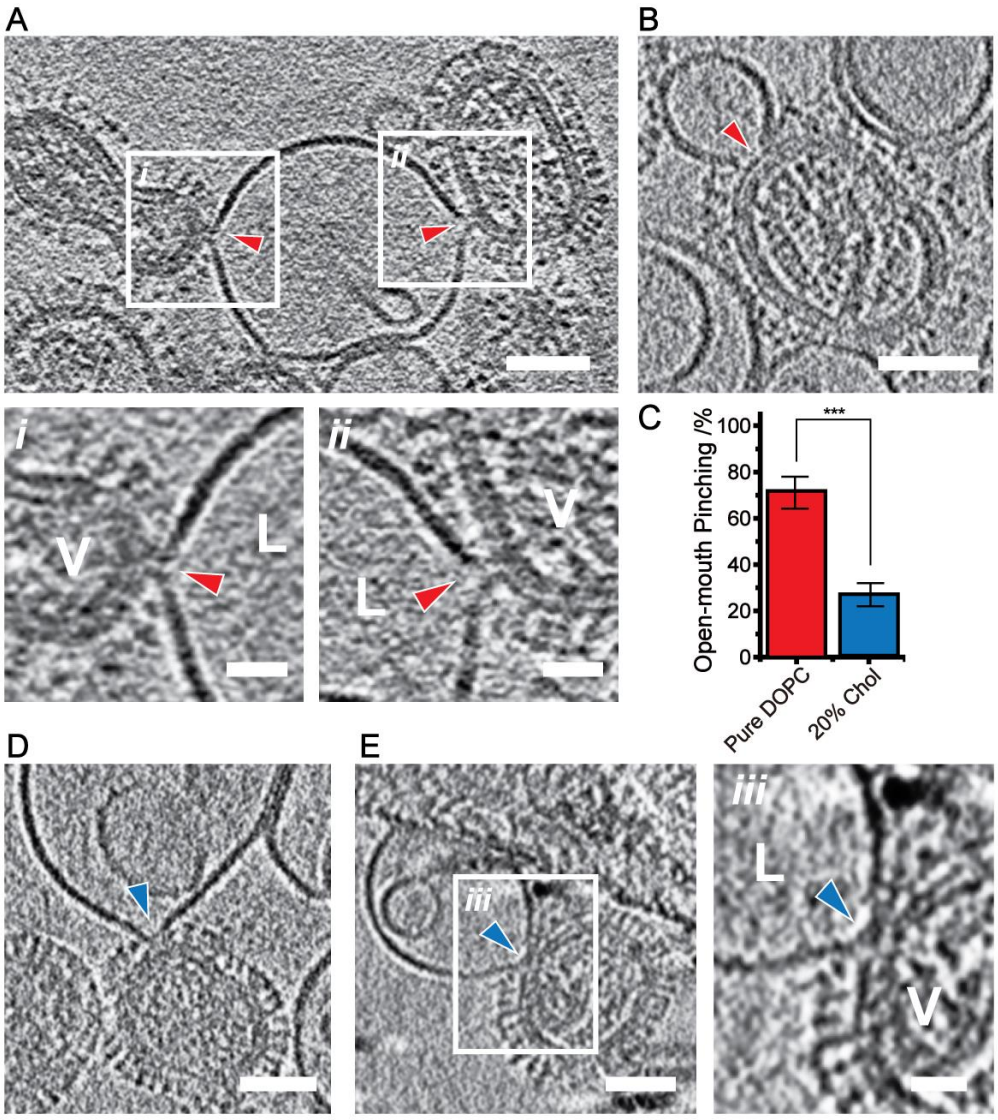

Figure 3.2 Inclusion of cholesterol on target membranes reduces membrane scission in regions of localized membrane deformation. **(A,B)** Cryo-electron tomograms of open-mouthed liposomal contacts between 100% DOPC liposomes and virus at pH 5.5. Red arrows point to open-mouthed funnels at liposome-virus contact sites. Scale bar 50 nm. (i,ii) close-up view of boxed regions of interest in **(A);** inset scale bar 20 nm. **(C)** Abundance of open-mouthed and closed target membrane dimples. Error bars are calculated as the square root of the number of complexes per state at each given condition and time point, assuming Poisson counting statistics. Statistical significance was assessed via the *p*-value test ("ns=p>0.05,∗=p⩽0.05,∗∗=p⩽0.01,∗∗∗=p⩽0.001"). **(D,E)** Cryo-electron tomograms of 20% Chol:80% DOPC interacting with influenza particles showing apposition of the pinched liposomal membranes to the virus surface without membrane scission (blue arrows). (iii) Close-up view of boxed regions of interest in **(E)** in which the membrane leaflets are resolved; inset scale bar 20 nm. Scale bars 50 nm.

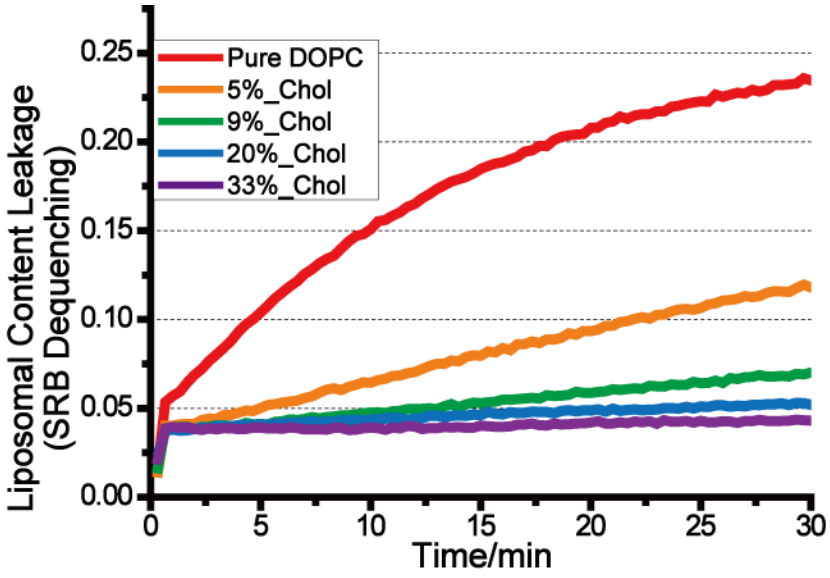

Figure 3.3 Cholesterol-dependent liposomal content leakage induced by HA ectodomain. Bromelain-released HA ectodomain (BHA) was incubated with DOPC-based SRB-encapsulating liposomes with 5%, 9%, 20%, 33% Chol at 37 ˚C, pH 5.25. Fluorescence dequenching of SRB was measured, showing cholesterol-dependent liposomal content leakage.

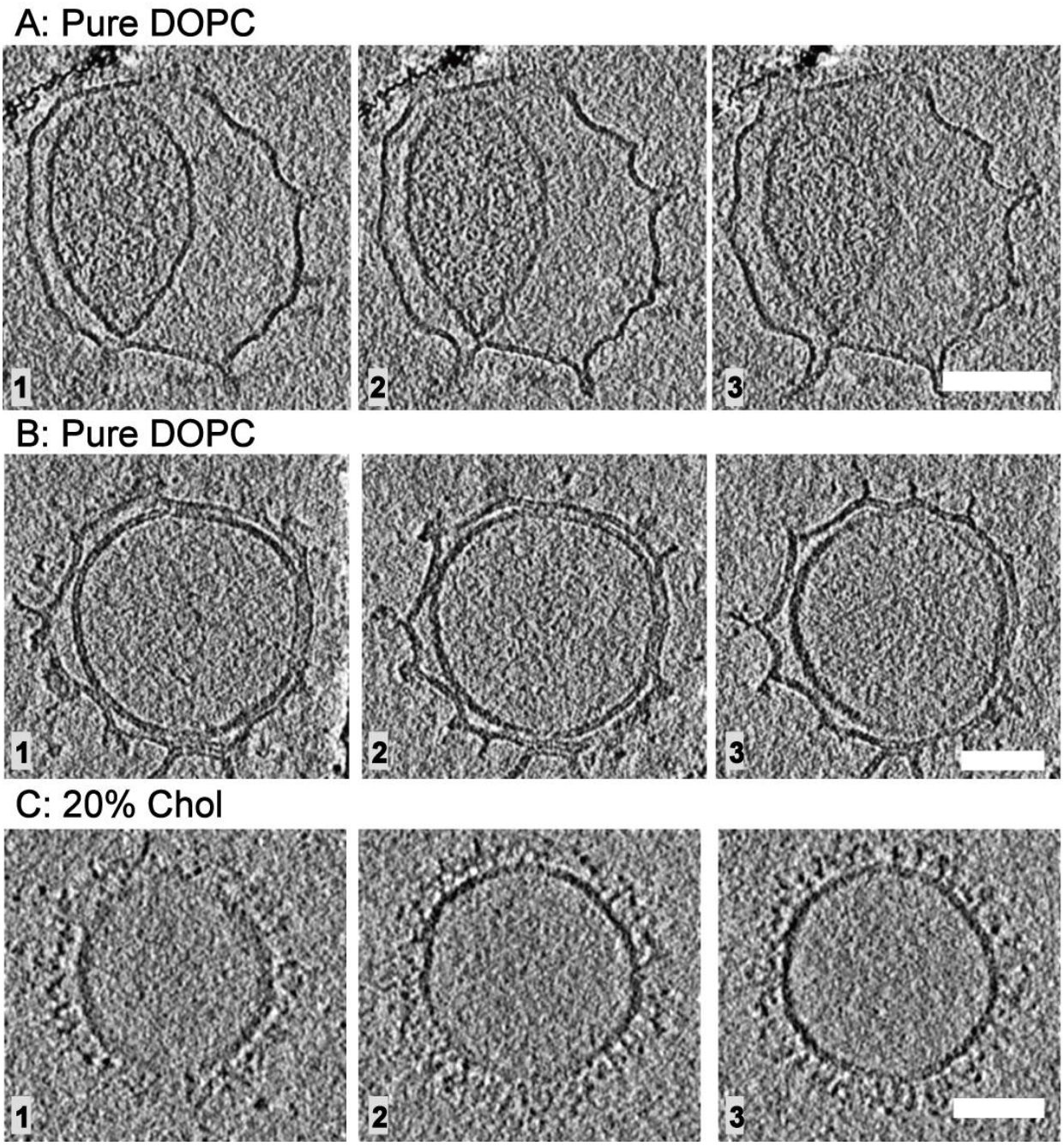

Figure 3.4 Cholesterol-dependent membrane deformation induced by HA ectodomain imaged by cryo-ET. (A, B) 6.6 nm-thick serial sections through the reconstructed tomographic density of a 100% DOPC liposome with BHA bound at 37 ˚C, pH 5.25. Scale bar 50 nm **(C)** A 6.6 nm-thick section through reconstructed tomographic density of a 20% chol:80% DOPC liposome at pH 5.25 bound at high density by activated BHA spikes. Scale bar 50 nm.

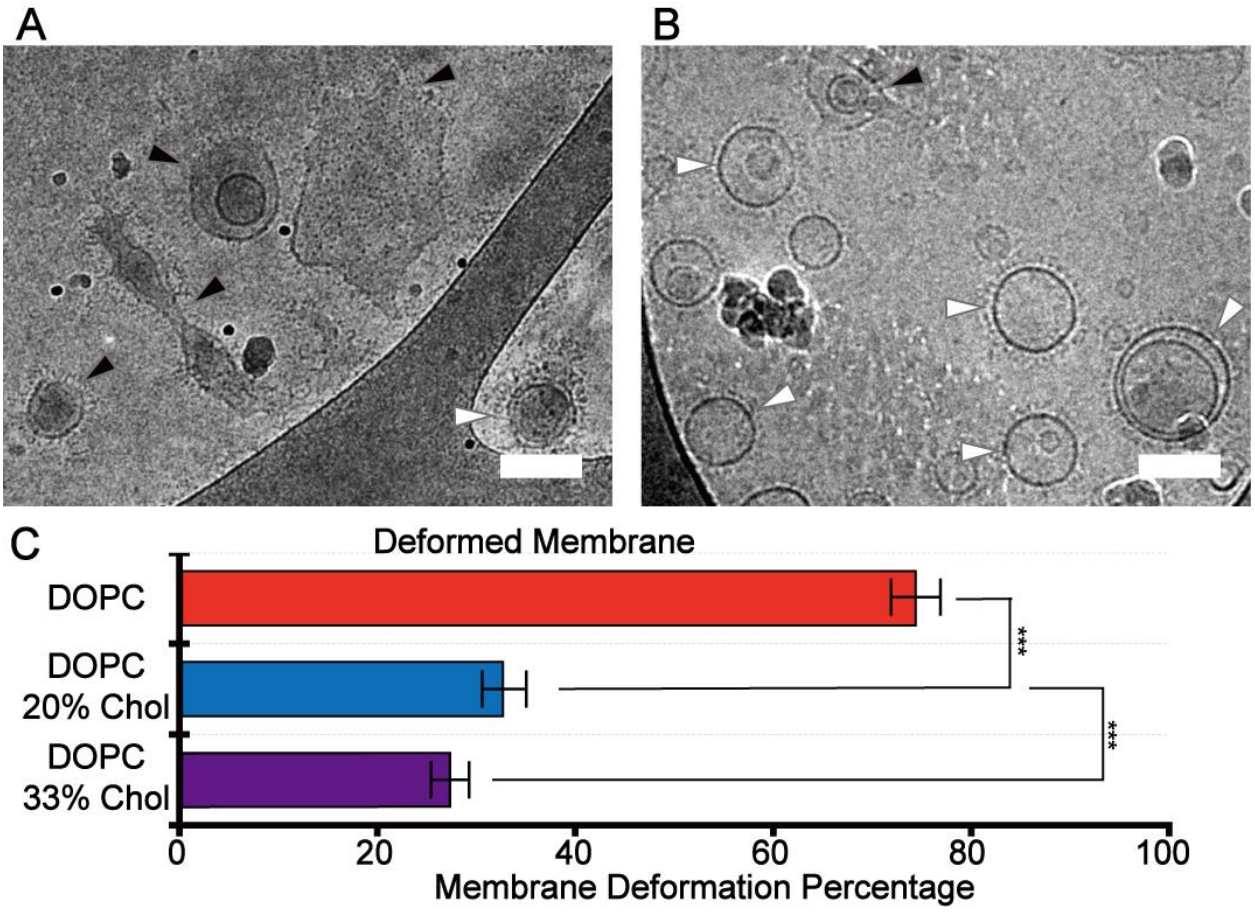

Figure 3.5 Cryo-EM images of **(A)** 100% DOPC liposomes or **(B)** liposomes with 33% chol:67% DOPC with activated BHA bound at pH 5.25 following 10 min, 37 ˚C incubation. Black arrows highlight liposomes exhibiting membrane pinching and deformation. White arrows highlight liposomes whose membranes remain visually unperturbed with BHA bound. Scale bars 100 nm. **(C)** Bar graph showing the percentage of liposomes exhibiting BHA-induced membrane deformation as imaged by cryo-EM. Error bars are calculated as the square root of the number of complexes per state at each given condition and time point, assuming Poisson counting statistics. Statistical significance was assessed via the *p*-value test.

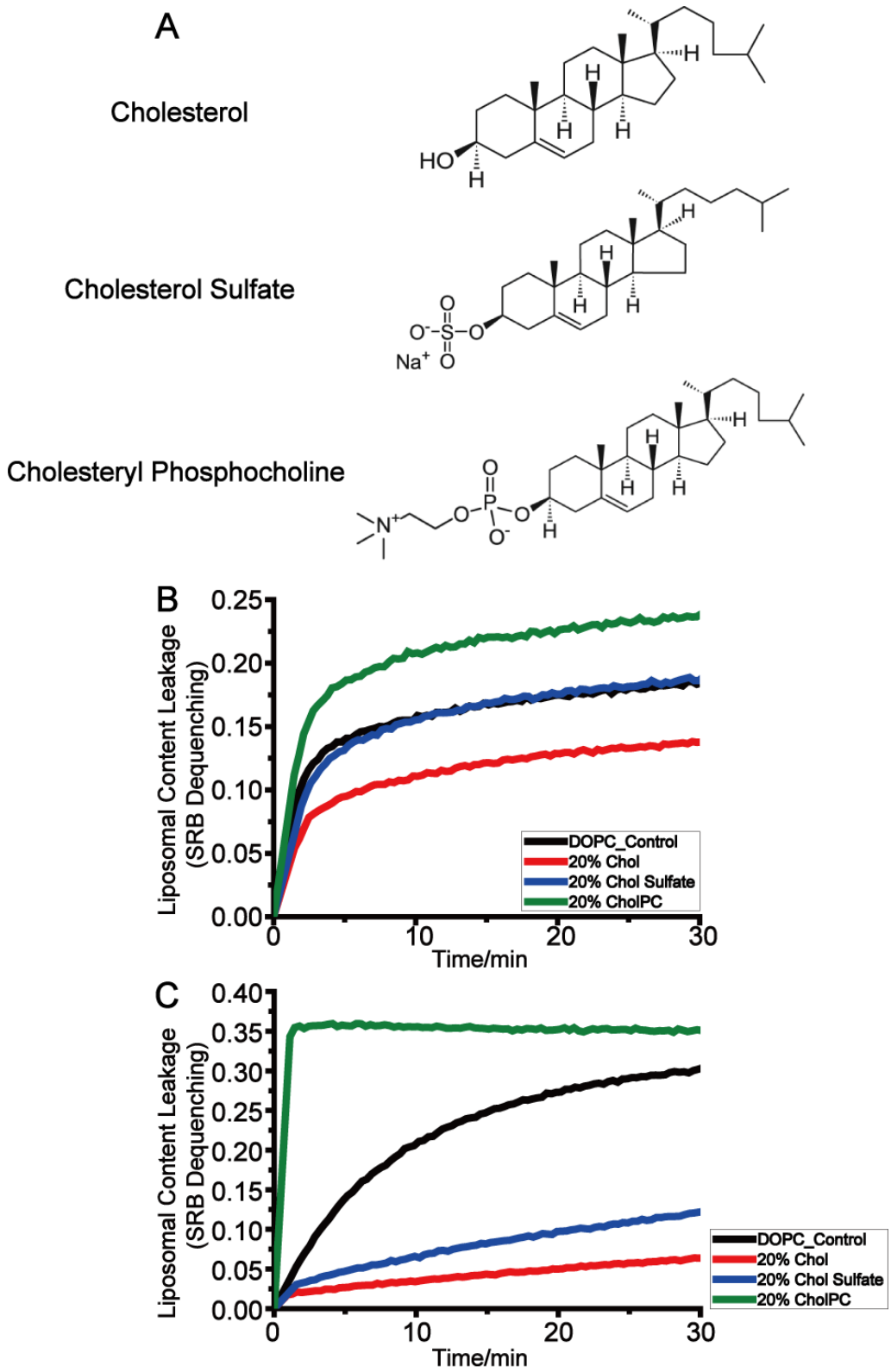

Figure 3.6 Liposomal content leakage was monitored in the presence of cholesterol derivatives on the target membrane. (A) Cholesterol sulfate and cholesteryl phophocholine (CholPC) are modified from

cholesterol with larger polar head, resulting different rate in flip-flop between the lipid bilayers. **(B, C)** In fluorescence-monitored fusion assays, SRB-containing liposomes with 20% cholesterol, 20% cholesterol sulfate, or 20% CholPC were mixed with whole influenza virus particles **(B)** or Bromelain-released HA ectodomain **(C)** at 37 ˚C, pH 5.5.

Chapter 4. Glycoprotein organization on the surface of human parainfluenza virus 3 imaged by electron tomography

4.1 Introduction

The enveloped RNA viruses of the Paramyxovirus family, in most cases, employ two surface glycoproteins to carry out the entry stage of the viral life cycle (Jardetzky & Lamb, 2014; Plattet & Plemper, 2013). A receptor binding protein --hemagglutinin-neuraminidase (HN) for HPIV3 or H or G depending on virus -- binds to the viral receptor on the host cell plasma membrane, and a separate membrane fusion (F) protein, once activated by the receptor binding protein, mediates the fusion of virus and host membranes in order to deliver the viral ribonucleoprotein into the host cell. Paramyxovirus F proteins convert from a metastable prefusion form to a highly stable postfusion form when the appropriate biological trigger is sensed, or in some cases when exposed to extremes of temperature (Ludwig *et al*, 2008; White *et al*, 2008). Our observation that active participation of receptor-engaged HN is required for the F-mediated fusion process (Moscona & Peluso, 1991; Moscona & Peluso, 1993; Porotto *et al*, 2003), is consistent with subsequent studies showing that the HN interaction is necessary in order to activate the fusion machinery, and that engagement of the HN (or H or G) with the respective receptor is critical for fusion (Chang & Dutch, 2012; Iorio *et al*, 2009; Mateo *et al*, 2014; Navaratnarajah *et al*, 2012; Steffen *et al*, 2012; Vigant & Lee, 2011).

Current models of paramyxovirus surface glycoprotein interaction during fusion activation and viral entry posit that either (a) the HN-F interaction occurs in the absence of a receptor and “clamps” the two proteins together until the proper time, when F is released to proceed towards fusion, or (b) the HN-F interaction occurs only upon receptor binding and the receptor-binding protein provides the “trigger” after which F proceeds to fusion (Also see Chaptor 1, Figure 1.5) (Chang & Dutch, 2012; Corey & Iorio, 2007; Harrison, 2008; Iorio *et al*, 2009; Lamb *et al*, 2006; Li *et al*, 2004; Mirza *et al*, 2011; Plemper *et al*, 2011; Porotto *et al*, 2012a; Smith *et al*, 2009). For

morbilliviruses, the fusion protein is stable in its prefusion configuration even without associated receptor binding protein (H); as for HPIV3 HN, H decreases the activation energy hurdle for fusion triggering (Ader *et al*, 2013).

In previous studies of human parainfluenza virus type 3 (HPIV3), an important respiratory pathogen, we have shown that HPIV3 hemagglutinin-neuraminidase (HN) receptor binding protein and F protein interact before and during fusion activation (Porotto *et al*, 2011). We have proposed that HN contributes to maintaining F in its pre-triggered state until the correct time and place for entry, at which time receptor binding switches HN to an active role with respect to activating F, and "triggers" F (Porotto *et al*, 2011). To address the role of receptor engagement and to elucidate how HN and F interact during fusion, we previously observed the sequence of events leading up to HN/F mediated membrane fusion in real time, in live cells using bimolecular fluorescent complementation (BiFC), a technique that allows HN-F interactions to be studied under minimally perturbing conditions (Porotto, Palmer *et al*, 2012). We determined when and where HN and F interact on the surface of cells prior to and during cell-cell fusion, and identified the role of specific sites in HN in mediating the interaction (Porotto *et al*, 2012b). These BiFC results, in combination with other studies of events preceding viral entry, led us to propose a model of how paramyxovirus HN and F mediate fusion during infection (Farzan *et al*, 2011; Palmer *et al*, 2012; Porotto *et al*, 2011; Porotto *et al*, 2012b; Porotto *et al*, 2010; Porotto *et al*, 2012a). In this model, HN-F association prior to receptor binding helps stabilize F, preventing its premature activation (Porotto *et al*, 2012b; Porotto *et al*, 2012c). HN's engagement of receptor molecules drives the formation of HN/F clusters at the site of fusion and a putative second sialic acid receptor binding site positioned in the dimer interface of HPIV3 HN directly modulates F-activation and interaction with F in living cells (Xu *et al*, 2013; Palmer *et al*, 2012a; Porotto *et al*, 2006; Porotto *et al*, 2003; Porotto *et al*, 2012b). After initial activation of F, HN and F remain associated and HN acts on F even beyond the step of fusion peptide insertion into the target. As fusion progresses

further, either HN and F dissociate or the clusters of HN-F complexes disperse (Porotto *et al*, 2012b).

To evaluate viral surface glycoprotein events of early entry in the context of the virus, we previously conducted a preliminary negative-stain electron tomography analysis of HPIV3 viral particles that were prepared in the absence of receptors for the virus. The majority of viral particles showed fairly continuous coats of glycoprotein spikes with two layers of density that we interpreted to reflect staggered HN and F spikes, in which HN was present in association with prefusion F. Surface density on a sub-population of small viral particles showed clusters of glycoprotein spikes resembling the crystal structure for postfusion HPIV3 F trimers (Yin *et al*, 2006) and the moderate-resolution cryo-negative-stain EM reconstruction reported for paramyxovirus SV5 (PIV5) F (Ludwig, Schade *et al*, 2008). These observations supported the idea that HN and F are associated on the virion surface prior to receptor engagement.

While a number of other studies have explored paramyxovirus ultrastructure by electron microscopy (Battisti *et al*, 2012; Kiss *et al*, 2014; Liljeroos *et al*, 2011; Liljeroos *et al*, 2013; Loney *et al*, 2009; Terrier *et al*, 2009), the resolution of surface features has eluded detailed characterization until recently; specifically, the relative distribution, conformation and interaction of the receptor-binding and fusion surface proteins. In a recent advance the use of an engineered measles receptor binding protein (H) with an elongated stalk permitted visualization of the envelope glycoproteins on a virion surface, and provided evidence that direct contact between F and the head domain of H may not be required for activation of measles virus fusion(Brindley *et al*, 2013).

Challenges of characterizing the surface glycoprotein organization in paramyxoviruses include the multiplicity of conformations HN and F can adopt and the potential for varied interactions between the proteins in different states.

The F protein is generated as a single precursor polypeptide chain that, to be functional, must be cleaved by host proteases into two subunits (F1 and F2), which remain associated

(Thompson-Wicking *et al*, 2012; Welch *et al*, 2012). The F monomers oligomerize into a squat trimer with a central cavity, giving it a rounded, donut-like appearance from the side and a triangular shape viewed from above (McLellan *et al*, 2013; Yin *et al*, 2006). The ectodomain sits on top of a short tether formed by portions of the C-terminal heptad repeat (HRC) segments, which are anchored via the transmembrane domain to the viral membrane. The fusion peptide that corresponds to the N-terminal ~20 residues of the F2 subunit only becomes available to insert into the target membrane once the appropriate trigger for fusion activation is encountered. Once triggered or destabilized, the trimer converts to a more elongated, narrow structure characterized by a stable helical bundle formed by N and C terminal heptad repeats (HRN, HRC). This reorganization co-localizes the two membrane interactive domains, the fusion peptide and transmembrane anchor. The 3-dimensional structure of the F fusion trimer from multiple paramyxoviruses including HPIV3 has been described in postfusion forms (McLellan *et al*, 2011; Swanson *et al*, 2010; Wen *et al*, 2012; Yin, Paterson *et al*, 2005).

The several activities of HN – receptor binding, receptor cleaving, fusion activation, and possibly F protein stabilization -- are regulated within a type II membrane protein consisting of a cytoplasmic domain, a membrane-spanning region, a stalk region, and a globular head. The stalk confers specificity for the homologous F in the fusion activation process (Bose *et al*, 2011; Deng *et al*, 1995; Porotto *et al*, 2003; Sergel *et al*, 1993; Tanabayashi & Compans, 1996; Yuan *et al*, 2011; Yuasa *et al*, 1995). Crystal structures of the avian paramyxovirus Newcastle disease virus (NDV) HN (Crennell *et al*, 2000; Zaitsev *et al*, 2004) and later of the HPIV3 HN (Lawrence *et al*, 2004) and PIV5 HN (Yuan *et al*, 2005) led to identification of the locations of the primary binding/neuraminidase active site residues on the globular head. For NDV, HPIV1, and HPIV3, a secondary sialic acid binding site on HN play distinct roles in binding or promoting fusion (Bousse and Takimoto, 2006; Palmer *et al*, 2012; Porotto *et al*, 2006; Porotto *et al*, 2003; Porotto *et al*, 2012b; Zaitsev, von Itzstein *et al*, 2004). The relation of the head and stalk domains in functional paramyxovirus receptor binding proteins remains a critical feature to elucidate because of: (1) the

role identified for the stalk region in triggering F (Ader *et al*, 2012; Bishop *et al*, 2008; Bose *et al*, 2014; Maar *et al*, 2012; Navaratnarajah, Negi *et al*, 2012; Porotto *et al*, 2003; Talekar *et al*, 2013a); and (2) the proposed function of the head of the receptor binding protein in both receptor binding and transmitting the activation signal to F (Ader *et al*, 2012; Bishop *et al*, 2008; Bose *et al*, 2014; Maar *et al*, 2012; Navaratnarajah *et al*, 2012; Porotto *et al*, 2003; Talekar *et al*, 2013b). Receptor binding proteins from various paramyxoviruses have been characterized by crystallography in several conformations and oligomeric forms (Lawrence *et al*, 2004; Welch *et al*, 2013; Xu *et al*, 2013; Yuan *et al*, 2012; Yuan *et al*, 2011; Yuan *et al*, 2005). The evidence suggests that these proteins can adopt at least three arrangements including a “heads-down” tetramer in which two dimers of HN are organized around a 4 helix stalk (Yuan *et al*, 2011), a “heads-up” form (Yuan *et al*, 2005), and a two “heads-up” two “heads-down” form that has been proposed to represent an intermediate conformation (Welch *et al*, 2013). It has been suggested that the head domains of HN in the “heads-down” configuration are responsible for masking the triggering residues on the stalk region (Bose *et al*, 2011; Yuan *et al*, 2011).

In order to better define the relationship between HN and F on whole infectious virions prior to receptor engagement, and to begin to test models of activation that have emerged from experimental data (Chang & Dutch, 2012; Iorio *et al*, 2009; Jardetzky & Lamb, 2014; Mateo, Navaratnarajah *et al*, 2014; Navaratnarajah, Negi *et al*, 2012; Plattet & Plemper, 2013; Porotto *et al*, 2011; Porotto *et al*, 2012b; Steffen *et al*, 2012; Vigant & Lee, 2011; Xu *et al*, 2013), we used a combination of negative-stain and cryo-electron tomography (cryo-ET) here to image HPIV3 ultrastructure. We observed that many of the observed surface features are interpretable in terms of known structures for F and HN that have been determined by crystallography, and provide information about how the two proteins relate to each other on the surface of virions. The observations of HPIV3 are consistent with a model for fusion in which prefusion F and HN in a “heads-up” conformation interact prior to receptor engagement, without activating F. The majority of this chapter is adapted from our previous publication titled “Electron tomography imaging of

surface glycoproteins on human parainfluenza virus 3: association of receptor binding and fusion proteins before receptor engagement" (Gui *et al*, 2015).

4.2 Methods and Materials

4.2.1 Virus growth and purification

CV-1 cells (in 70–90% confluent monolayers) in T175 flasks were infected with HPIV3 411 (multiplicity of infection 0.1) in 10 mL Opti-MEM (L-glutamine and HEPES) for 90 min in a 37 °C humidified, 5% CO2 incubator. During the 90 minutes of incubation, flasks were gently shaken every 15 minutes. Viral inocula were replaced with 20 mL of complete medium, and cultures were placed in a 37°C humidified, 5% CO2 incubator. After 48 h, the cell culture supernatant fluid was collected and clarified by centrifugation (3,000 rpm, 10 min, 4 °C, Eppendorf 5810R). The clarified supernatant fluid was centrifuged (25,000 rpm, 120 min, 4°C, SW28 rotor, Beckman L8-80M ultracentrifuge) through an 8 mL 20% (wt/vol) sucrose cushion in PBS (pH 7.4) or in PBS containing 1mM zanamivir (pH 7.4) to prevent receptor engagement by HN. Pellets were resuspended in 200 µL of PBS (4°C, pH 7.4) for each T175 flask. Virus stocks were stored at −80 °C or kept at 4°C before analysis. HPIV3 stocks were titered by a plaque assay performed as described before (Palmer *et al*, 2013). Titers for purified viruses after storage at -80 °C were $1.00x10^7$ pfu/ml.

4.2.2 Negative Staining and Cryo-electron tomography

Purified HPVI3 produced as described above was mixed with 10-nm colloidal gold and prepared for cryo-electron tomography by adding 3-µl samples onto holey carbon-coated grids (C-flat, 200 mesh; Electron Microscopy Sceinces) and plunge freezing the samples in liquid ethane using a Vitrobot (Mark V, FEI Co.). Negative staining grids were prepared similarly by loading 3-µl samples onto carbon-coated electron microscope grids (300 mesh; Electron

Microscopy Sciences) and stained with nano-W (2% methylaminetungstate, NanoProbes). Vitrified grids were imaged at liquid nitrogen temperature in a FEI Tecnai F20 transmission electron microscope equipped with a Gatan Ultrascan 4000 CCD Camera. Images were captured at a nominal magnification of 50,000 x and binned by a factor of 2, corresponding to a pixel size of 4.4 Å per pixel calibrated from the 0.463 µm distance grating grids (Electron Microscopy Sciences). Images were acquired at 2-4 µm underfocus and specimens were tilted in 2° steps from approximately 58° to -58° by using Leginon software package (Suloway *et al*, 2009). Total electron dosage for the entire tilt series is estimated at ~100 e/Å2 per tilt series. Tomograms were reconstructed using weighed back-projection method in IMOD package (Kremer *et al*, 1996). Images are visualized in ImageJ and denoised as previously described (Lee, 2010).

Crystal structures for prefusion F trimer (4GIP.pdb [Welch *et al*, 2012]), postfusion F trimer (1ZTM.pdb [Yin *et al*, 2006]), "heads-down" tetrameric HN from NDV (3T1E.pdb [Yuan *et al,* 2011]) and the globular head domain from HPIV3 HN (1V2I.pdb [Lawrence *et al,* 2004]) were docked into 3-dimensional reconstructed EM density maps that had been denoised by Gaussian filtering and using the "Hide Dust" function in Chimera (Pettersen *et al*, 2004). The automated "Fit to Map" function was used following initial manual placement of the PDB model into the EM density map.

4.3 Results

4.3.1 HPIV3 particle morphology

As in previously described ultrastructural studies of paramyxoviruses, a high degree of pleomorphy is observed in the population of HPVI3 particles as examined by both negative stain and cryo-electron microscopy (Figure 4.1) (Battisti *et al*, 2012; Liljeroos *et al*, 2011; Liljeroos *et al*, 2013; Loney *et al*, 2009; Terrier *et al*, 2009). Particles range from 100-500 nm in diameter and are generally rounded in morphology. Filamentous virions were rarely observed in the virus preparations.

In projection images, a complex cloak of surface density was observed on the particles, and in many cases, regularly ordered grid-like patterns of density in the projection images could be discerned (Figures 4.1B&C). To obtain a more detailed understanding of virus ultrastructure and to be able to distinguish surface from internal features, we carried out tomographic reconstruction of both negatively stained and cryo-EM specimens (Figures 4.2&4.3). These reveal that the grid-like density is located on the virus exterior rather than forming an internal layer such as matrix. In many cryo-electron tomographic reconstructions, the lipid bilayer is clearly resolved. In contrast to for example influenza virus where the majority of particles bear a thick membrane-associated matrix layer (Lee, 2010), the vast majority of particles we observed appeared to lack a membrane-associated matrix layer; less than 10% of particles appeared to exhibit an organized matrix layer (Figure 4.3D). The particles that did exhibit thicker envelopes were generally small that lack encapsulated RNP. The small particles were observed to bear some discernable post-fusion F proteins on their surface (Figure 4.3C) (Ludwig *et al*, 2008; Porotto *et al*, 2012c). In a previous study of RSV, membrane-associated matrix protein was primarily observed in filamentous particles, while round particles appeared to lack an intact membrane-associated matrix layer (Liljeroos *et al*, 2013). Our observations are consistent with those for RSV, as most of the particles we observe are round and appear to lack internal matrix layers. In a study of NDV, a similar ratio of 90% of particles appeared to lack an intact matrix layer, while 10% exhibited a pseudo-tetrameric array of internal, membrane-associated density attributed to matrix (Battisti *et al*, 2012).

Significant ribonucleoprotein density is observed within the majority of particles over 100 nm in diameter, both by negative-stain, in cases where stain was able to penetrate into the virions (Figure 4.2), and by cryo-ET (Figure 4.3). The number of RNPs packaged appears to vary substantially across the population. These helical tubes exhibit a left-handed twist with an average pitch of ~5.5 nm. They are composed of slanted rings where each ring segment exhibits an outer diameter of 20 nm and an inner wall of diameter ~7nm. Overall the HPVI3 RNP appear to be

similar to the 20 nm diameter, matrix-lacking nucleocapsid tubes reported for measles virus (Liljeroos *et al*, 2011).

In addition to the internal RNP density, the particles appear to encapsulate a significant amount of additional material, most likely cytoplasmic proteins. In some cases what appear to be actin filaments are evident (Figure 4.3B); these become more apparent when particles break open and the encapsulated material can spread out.

4.3.2 HN tetramers in "heads-down" conformation are found in large ordered arrays

In projection images, a variety of complex surface density features were observed on the particles (Figure 4.1). In many cases, regularly ordered grid-like patterns of density in the projection images were apparent. Tomographic reconstructions of particles examined by negative-stain and cryo-ET revealed that the grid-like density was located on the virus exterior rather than forming an internal layer such as matrix (Figure 4.2A&4.3A). The arrays covered significant areas on the virus surfaces; however, we noted that a high degree of variability in the amount of surface area covered by the arrays was observed; some particles even appeared devoid of the grid-like arrays (Figure 4.2B), while others had a majority of their surface covered. The ratio of particles that show the grid-like surface arrays versus those that do not was approximately 2:1; for example, in cryo-electron micrographs, 90 particles showed arrays, while 47 exhibited surfaces without prominent lateral ordering of density. We also observed that multiple arrays with different relative orientations coexisted on different patches of the surface. The arrays were found on both small and large particles, suggesting that surface curvature and overall particle size are not major determinants of array formation (see, for example, Figure 4.3C). The ordered, grid-like arrays evident in both negative-stain (Figures 4.2 and 4.4) and cryo-EM (Figures 4.3&4.4) images were composed of repeating units of density consistent with the known high-resolution structure for a tetramer, or dimer of dimers, of NDV HN in the heads-down conformation (Figure 4.4) (Yuan *et al*, 2011). In the negative-stain reconstruction shown in Figure 4.4A,

sequential slices through the density revealed that the basic unit of the array viewed from above had the form of a slanted “H,” which was positioned above punctate dots of density that are consistent with the density for a helical bundle stalk (Figure 4.4A). The tetrameric NDV HN structure (3T1E.pdb) could be docked into the EM density, which shows excellent agreement with the “heads-down” HN conformation (Figures 4.4 B&C) (Yuan *et al*, 2011).

Viewed laterally at the edge of a virus particle (Figure 4.4C), the HN arrays were observed to flow into repeating rows of Y-shaped density features that correspond to the view of the HN array along the red line shown in Figure 4.4B. In other orientations (Figure 4.4D), the arrays can be viewed down a different line of sight, as indicated by the blue dashed line in Figure 4.4B.

We note that the patches of HN arrays appeared to be composed exclusively of HN in the heads-down conformation; they did not contain density recognizable as F in either postfusion or prefusion conformations.

The HN array density distribution peaks at ~10 nm above the viral membrane (measured from the distance at half-maximum density of the outer leaflet to the peak intensity distal to the membrane) (Figure 4.5). This peak density likely corresponds to the neck junction of the HN tetramer, where 3 layers of density from 2 HN head subunit dimers and the tip of the stalk converge (Yuan *et al*, 2011). The stalk height of 10 nm is the expected height if the complete stalk exists in a helical conformation. Observed from above, the stalks appeared as puncta that are ~4-nm in diameter, consistent with the dimensions expected for a bundle of 4 helices in cross section, as seen in the NDV HN tetramer and stalk domain crystal structures (Figure 4.4A) (Yuan *et al*, 2011; Bose *et al*, 2011). The arms of the Y feature extended ~12 nm above the outer leaflet (Figure 4.5 [measured between distances of half-maximum density at membrane outer leaflet and the distal density peak]) of the viral membrane. The spacings of HN tetramers, measured between stalks center to center, are ~9 nm along one axis of the array and ~14 nm along the other axis. Viewed from above where the dimer of dimers slanted H motif was clearly visible, the edges were 5 nm across and 9 nm long and the distance across the bar of the H was ~11 nm; again

corresponding to the NDV heads-down tetramer structure (Yuan *et al*, 2011). As seen in Figure 4.4, tetramers were also staggered row by row rather than being organized in a simple square grid.

4.3.3 In areas without HN arrays, prefusion F is often intermingled with density that may correspond to HN with a heads-up conformation

In most particles, in addition to presenting HN heads-down arrays, large portions of the surfaces were covered in a cloak of density that exhibited significant complexity and appeared to be composed of two primary layers of density (Figures 4.5&4.6). The double surface layer extended ~16 nm above the virus membrane (Figure 4.5). As seen by tomography, the glycoproteins in these complex double layers did not appear to exhibit lateral organization into ordered arrays (Figures 4.2B and 4.6).

The complex double-layered density reflected mixtures of protein types, and while individual glycoproteins were not always discernible, in many instances, prefusion F could be clearly distinguished as the more membrane proximal of the 2 prominent layers of density (Figure 4.6). Indeed, in edge views of central slices through tomograms, the prefusion F trimers were recognized by their squat, rounded shapes with a diameter of ~8.5 nm and central cavities, in excellent agreement with the available crystal structures for prefusion F (e.g., 4GIP.pdb from the related PIV5 [Welch *et al*, 2012]), which could readily be docked into the EM density (Figure 4.6C) (Welch *et al*, 2012; McLellan *et al*, 2013; Yin *et al*, 2006). The F trimer squats above the membrane, while a discontinuous canopy of density was often observed at higher elevation. In some regions (for example, blue arrows in Figure 4.6A), the canopy density was resolved into punctate ~4- to 5-nm-diameter dots that are consistent in size with a globular HN head domain (5 by 4 by 6 nm); the radial density distribution also reflected this distinct 4- to 5 nm-wide feature as the outer density layer (Figure 4.5). These outermost globular features themselves were placed atop tethers ~10 to 12 nm above the virus surface. The taller height of these canopy features

compared to the shorter heads-down HN tetramer is likely due to the relative positioning of the head and stalk domains in a heads-up configuration. In rare circumstances, what appeared to be individual HN in a heads-up state extending to a height of ~16 nm above the membrane could be seen (Figure 4.6I, blue arrow).

In views of top and bottom slices of the reconstructed tomograms for the double surface layer, no evidence was found that suggests other tetrameric organizations of HN, such as the "four-heads-up" state that has been proposed (Yuan *et al*, 2005; Welch *et al*, 2013). Instead it appeared that the canopy density of HN proximal to F may have been comprised of monomers or dimers of HN. This oligomeric state for HN was not unprecedented as the NDV HN ectodomain, including the stalk domains, yields primarily monomers and dimers in solution, even though dimers of dimers were observed when the constructs were crystallized (Yuan *et al*, 2011).

Viewed from above by negative-stain ET elevations close to the viral membrane, triangular features with edges ~8.5 nm long that have stain-penetrable central cavities were observed, scattered in an irregular fashion (Figure 4.6E, "Lower"). These features are consistent with crystal structures of prefusion F trimers, which are shown docked into the EM density (4GIP.pdb) (orange ribbon diagram in Figure 4.6E). In slices of density positioned a few nanometers above these layers (Figure 4.6E, "Upper"), we found scattered density, some of which appeared to consist of ~4- to 5-nm dots, sometimes loosely paired; these were similar in dimension and distribution to the globular density features observed in the lateral views of the envelope glycoprotein canopy. Other features seen from this vantage appeared to correspond to F in its postfusion helical bundle state, which appeared as a smaller-dimension triangular feature, with edges ~7 nm long and a spot of stain in its center. The crystal structure for HPIV3 postfusion F could be precisely docked into these density features (1ZTM.pdb) (red ribbon diagram in Figure 4.6E) (Yin *et al*, 2005). Many of these smaller triangles had electron-dense stalks beneath them that were ~2.5 nm in diameter, consistent in dimension with the helical bundles formed by the HRN and HRC domains in postfusion F (Yin *et al*, 2005). Prefusion F trimers are also observed in clusters adjacent to each

other, in some cases without clear signs of associated HN (Figure 4.6I). In lateral views at the edge of particles observed in central slices, the distinction of prefusion and postfusion F, as well as the double-layered surface density, were clearly evident.

In cryo-EM reconstructions, due to the need to work at higher defocus values and because the particles were more rounded rather than flattened in the negative-stain case, views of trimers down their axis of symmetry were rare. However, in lateral views seen in central tomographic slices, the regions of the virus surface with two layers of external density were evident just as with the negative-stained samples (Figures 4.6F to I). In addition, the positioning and radial density distribution of surface density features were found to be similar by cryo- and negative-stain EM (Figure 4.5). Thus, the overall surface glycoprotein organizations analyzed by cryo- and negative-stain EM are in good agreement.

The EM observations and comparison with crystal structures suggest that prefusion F is present in fields interspersed with copies of what we infer to be HN in a nonarrayed, heads-up form that gives rise to the canopy of density.

4.4 DISCUSSION

4.4.1 HN in its heads-down conformation is not associated with F

The electron tomography studies reported here shed light on the diversity of glycoprotein organization that can exist on the surface of HPIV3. Much of the observed surface features are interpretable in terms of known structures for F and HN that have been determined by crystallography, however we now gain a significantly clearer sense of how the two types of proteins relate to each other and are distributed on the virus surface.

Perhaps the most immediately striking features we observed are the arrays of HN in a tetrameric, “heads-down” form. The arrays may be stabilized by interactions between the HN tetramers involving the two outermost head domains in each tetramer; conversely packing in the arrays may help to maintain the HN tetramers in the “heads-down” conformation. These data

demonstrate that the structure observed by crystallography of the isolated NDV HN ectodomain, “heads-down” tetramer can exist on the surface at least of some paramyxoviruses. The linkage of this conformational state to HN biological function, receptor binding and neuraminidase activity, remains to be more fully characterized, but the ultrastructural observations provide steric considerations for HN and its receptor binding sites. In the “heads-down” conformation, none of the sialic acid binding site are directly oriented to face the target membrane, and only two out of the four HN head domains would be proximal to the target membrane while the other two are apparently engaged in interactions with the HN stalk and sequestered from interacting with the receptors on the target membrane (Yuan *et al*, 2011). It was previously suggested that during interaction with sialic acid receptors on the target cell membrane, the head domains may reorient to further expose the other head domains and, in the case of NDV at least, a secondary sialic acid binding site on each subunit (Yuan *et al*, 2011).

Interestingly, in the regions of the virus surface that exhibit double layers of density, we observe a tall canopy of density above prefusion F trimers that we infer to be HN in a different, conformation than the “heads-down” tetramer. This canopy density appears to be attributable to HN dimers with loosely associated head domains or possibly even monomers in a “heads-up” configuration atop an extended stalk. We do not observe clearly ordered density that would be consistent with HN in a “heads-up” tetramer, a conformation that was proposed based on a crystal structure for the SV5 HN head domain (Yuan *et al*, 2005). Is it unexpected to not find HN in a “heads-up” tetrameric form? In fact, HN head domains, lacking the stalk regions, from various paramyxoviruses rarely form tetramers in solution. HPVI3 HN head domains crystallized as a dimer (Lawrence *et al*, 2004; Xu *et al*, 2013). Likewise, the head domain of some paramyxoviruses such as NDV and PIV5 are monomeric in solution, while the introduction of the stalk domain can facilitate tetramerization (Yuan *et al*, 2008). Indeed the helical stalk region in some paramyxoviruses such as PIV5 has a propensity to form 4 helix bundles (Bose *et al*, 2011; Yuan *et al*, 2008). In another case, Lamb and coworker have noted that HN from NDV has a lower

propensity to form a tetramer (Bose *et al*, 2011). They proposed that a specific complement of residues that are positioned to face the helical bundle's hydrophobic core in PIV5 are substituted by polar residues in NDV, possibly hindering its stalk-driven receptor binding protein tetramerization (Yuan *et al*, 2008). Interestingly HPIV3 HN has polar glutamine residues in those same positions, and we postulate, like NDV, may have a lower intrinsic propensity to tetramerize than PIV5 HN.

One question that lies at the heart of dispute between models of F activation by HN is whether F requires constraining interactions with HN to maintain its metastable prefusion conformation (Paterson *et al*, 1997; Porotto *et al*, 2012a). The observation of clusters of prefusion F trimers on the virus surface shown in Figure 4.6, without any detectable glycoprotein "chaperone" such as HN in close contact reinforces the view that prefusion F does not necessarily require close association or coordination with HN to hold it in the metastable prefusion form. The present results thus appear to run contrary to the strictest interpretation of the "clamp" model for HN/F triggering. This would be consistent with previously reported data that suggests that HN and F in HPVI3 may not associate tightly prior to fusion activiation (Paterson *et al*, 1997).

In a previous study, lower resolution images suggested that HN and F colocalized formed the double layers and were interpreted as being consistent with the model that HN-F exhibit substantial interactions prior to triggering (Porotto *et al*, 2012b). The new, higher resolution and more comprehensive data here suggest a more nuanced relation of interspersed HN and F on the surface of HPIV3. Our results reveal that prefusion F and HN in an apparently "heads-up" state can intermingle and combine to form the double layers of density on the virus surface, with prefusion F trimers situated beneath the canopy formed by mostly monomeric or dimeric HN. However it is not clear from the available data whether in the colocalized state, HN and F strongly interact and are specifically associated, or whether they are simply clustered in the same vicinity. Prefusion F trimers mingled with HN do not appear to adopt a regular organization, and we do

not see evidence that every F trimer is for example coordinated by 3 adjacent copies of HN; thus if there is an interaction it does not appear to exhibit a specific stoichiometry.

4.4.2 Oligomerization and implications for activation

Most biochemical data reported thus far suggests an important role for HN in triggering the F protein's fusion activation (reviewed in [Iorio *et al*, 2009]). In light of our observations, we hypothesize that conversion of HN to the F-activatable form may be mediated by receptor binding avidity that encourages oligomerization of HN monomers (or possibly dimers) into functional dimers or perhaps tetramers (Figure 4.7). Specific residues on the stalk domain have been implicated in triggering F protein activation in related paramyxoviruses such as PIV5 (Bose *et al*, 2011). The analogous residues in HPIV3 HN in extended conformations would likely be exposed and available to interact with nearby F trimers, yet the presentation of these residues on the monomeric or loosely dimerized "heads up" HN do not appear sufficient to efficiently trigger F fusion. Perhaps it is necessary for the stalk domains to oligomerize such as into helical bundles in order to present the proper quaternary spatial organization of residues for binding and triggering F (Figure 4.7B). It was recently shown that mutations in HPIV3 that affect HN dimerization also impact F activation and fusion efficiency (Xu *et al*, 2013). Thus it seems plausible that a dimerization or oligomerization stage is required for HPIV3 F protein activation. This oligomerization may be facilitated by interaction with multivalent receptors on the host cell surface. With Sendai virus, it has been observed that the tetrasialylated GQ1b ganglioside induces fusion far more efficiently than the disialylated GD1a (Markwell *et al*, 1981). In HPVI3, oligomerization could be driven by multivalent interactions with cell surface receptors that help to cluster HN head domains together and overcome the HPVI3 stalk domain's apparent reluctance to form a tetrameric or higher order helical bundle. Models involving changes in HN oligomerization have been proposed before (McGinnes *et al*, 2002). And in studies of fusion activation by headless

forms of measles virus H protein, while the head was shown to be dispensable, a tetramerization motif was required for the stalk in order to produce efficient F activation (Brindley *et al*, 2013).

It should be noted that little evidence exists to indicate that the head domains themselves adopt a tightly organized “heads-up” tetramer in addition to the tetramerized stalk domain. The hypothetical tetrameric, “heads-up” model was based upon a crystal structure for heads only, lacking the tethers (Yuan *et al*, 2005), and may not necessarily represent the physiological assembly of HN that triggers F. What does appear to be key is some degree of oligomerization of the HN stalk, which interacts with the F protein.

An alternative and not necessarily mutually exclusive mechanism is found in the provocateur model. It has been proposed that receptor engagement triggers HN to undergo a switch from “heads-down” to “heads-up” configuration, leading to exposure of an F-interactive motif on the HN stalk region. If this mechanism is at play, the arrays of HN with “heads-down” would need to be disrupted in order to transition to the proposed HN “heads-up” conformation that can interact with and activate F. In the model that has been proposed before, HN adopts a tetrameric, “heads-up” organization upon receptor binding (Welch *et al*, 2013; Yuan *et al*, 2005). It is not clear whether the HN in the arrays once activated would then diffuse to regions where F trimers are localized or recruit the F trimers, out-competing the HN that are already interspersed with the F trimers in the double layer surface regions.

In summary, the “heads-down” to “heads-up” conversion envisaged in the provocateur model, the proposed receptor avidity-driven oligomerization of HN described above, or both mechanisms operating side-by-side to some degree could conceivably lead to conversion of significant levels of HN to an F-activatable form. Further experiments will determine the relative contributions of each hypothetical mode of activation.

While these data shed light on the organization of F and HN on the surface of virions, and also illustrate the range of configurations and conformations the glycoproteins can adopt *in situ*, they do not yet resolve the question of triggering and sequencing of events. At this stage, we do

not yet have sufficient resolution to determine which parts of F may be interacting with the HN stalk and head domains. Likewise it is not entirely clear how the dual functions of receptor binding and neuraminidase activity are incorporated into a single enzymatic HN subunit or how the functions are regulated. In light of the variety of configurations that HN appears to adopt on the surface of HPVI3 virions, each with different exposures of sialic acid binding active sites and levels of association with prefusion F trimers, it is conceivable that each function performed by HN may be attributable to one or another of the observed HN configurations. In mutagenesis studies that differentially affect these functions, it may be that the conformational and associational equilibrium of HN on the surface of the virus is altered and this may have as significant an effect on function as changes to the individual HN head domains. This study represents a first step forward to revealing the complex interplay of receptor binding and fusion proteins on the surface of parainfluenza viruses.

References:

Ader N, Brindley M, Avila M, Orvell C, Horvat B, Hiltensperger G, Schneider-Schaulies J, Vandevelde M, Zurbriggen A, Plemper RK, Plattet P (2013) Mechanism for active membrane fusion triggering by morbillivirus attachment protein. *J. Virol*. **87**: 314-26

Ader N, Brindley MA, Avila M, Origgi FC, Langedijk JP, Orvell C, Vandevelde M, Zurbriggen A, Plemper RK, Plattet P (2012) Structural rearrangements of the central region of the morbillivirus attachment protein stalk domain trigger F protein refolding for membrane fusion. *J. Biol. Chem.* **287**: 16324-34

Battisti AJ, Meng G, Winkler DC, McGinnes LW, Plevka P, Steven AC, Morrison TG, Rossmann MG (2012) Structure and assembly of a paramyxovirus matrix protein. *Proc. Natl. Acad. Sci. U S A* **109**: 13996-4000

Bishop KA, Hickey AC, Khetawat D, Patch JR, Bossart KN, Zhu Z, Wang LF, Dimitrov DS, Broder CC (2008) Residues in the stalk domain of the hendra virus g glycoprotein modulate conformational changes associated with receptor binding. *J. Virol*. **82**: 11398-409

Bose S, Song AS, Jardetzky TS, Lamb RA (2014) Fusion Activation through Attachment Protein Stalk Domains Indicates a Conserved Core Mechanism of Paramyxovirus Entry into Cells. *J. Virol.* **88**: 3925-41

Bose S, Welch BD, Kors CA, Yuan P, Jardetzky TS, Lamb RA (2011) Structure and mutagenesis of the parainfluenza virus 5 hemagglutinin-neuraminidase stalk domain reveals a four-helix bundle and the role of the stalk in fusion promotion. *J. Virol.* **85**: 12855-66

Bousse T, Takimoto T (2006) Mutation at residue 523 creates a second receptor binding site on human parainfluenza virus type 1 hemagglutinin-neuraminidase protein. *J Virol* **80**: 9009-16

Brindley MA, Suter R, Schestak I, Kiss G, Wright ER, Plemper RK (2013) A stabilized headless measles virus attachment protein stalk efficiently triggers membrane fusion. *J. Virol*.**87**: 11693-703

Chang A, Dutch RE (2012) Paramyxovirus fusion and entry: multiple paths to a common end. *Viruses* **4**: 613-36

Corey EA, Iorio RM (2007) Mutations in the stalk of the measles virus hemagglutinin protein decrease fusion but do not interfere with virus-specific interaction with the homologous fusion protein. *J. Virol*.**81**: 9900-10

Crennell S, Takimoto T, Portner A, Taylor G (2000) Crystal structure of the multifunctional paramyxovirus hemagglutinin- neuraminidase. *Nat Struct Biol* **7**: 1068-74

Deng R, Wang Z, Mirza A, Iorio R (1995) Localization of a domain on the paramyxovirus attachment protein required for the promotion of cellular fusion by its homologous fusion protein spike. *Virology* **209**: 457-469

Farzan SF, Palermo LM, Yokoyama CC, Orefice G, Fornabaio M, Sarkar A, Kellogg GE, Greengard O, Porotto M, Moscona A (2011) Premature Activation of the Paramyxovirus Fusion Protein before Target Cell Attachment with Corruption of the Viral Fusion Machinery. *J. Biol. Chem.* **286**: 37945-54

Fujii T, Iwane AH, Yanagida T, Namba K (2010) Direct visualization of secondary structures of F-actin by electron cryomicroscopy. *Nature* **467**: 724-8

Gui L, Jurgens EM, Ebner JL, Porotto M, Moscona A, Lee KK (2015) Electron tomography imaging of surface glycoproteins on human parainfluenza virus 3: association of receptor binding and fusion proteins before receptor engagement. *mBio* **6**:e02393-14.

Harrison SC (2008) Viral membrane fusion. *Nat Struct Mol Biol* **15**: 690-8

Iorio RM, Melanson VR, Mahon PJ (2009) Glycoprotein interactions in paramyxovirus fusion. *Future Virol*. **4**: 335-351

Jardetzky TS, Lamb RA (2014) Activation of paramyxovirus membrane fusion and virus entry. *Curr Opin Virol* **5**C: 24-33

Kiss G, Holl JM, Williams GM, Alonas E, Vanover D, Lifland AW, Gudheti M, Guerrero-Ferreira RC, Nair V, Yi H, Graham BS, Santangelo PJ, Wright ER (2014) Structural Analysis of Respiratory Syncytial Virus Reveals the Position of M2-1 between the Matrix Protein and the Ribonucleoprotein Complex. *J. Virol*. **88**: 7602-17

Kremer J, Mastronarde D, McIntosh J (1996) Computer visua- lization of three-dimensional image data using IMOD. *J. Struct. Biol.* **116**: 71–76

Lamb RA, Paterson RG, Jardetzky TS (2006) Paramyxovirus membrane fusion: lessons from the F and HN atomic structures. *Virology* **344**: 30-7

Lawrence MC, Borg NA, Streltsov VA, Pilling PA, Epa VC, Varghese JN, McKimm-Breschkin JL, Colman PM (2004) Structure of the Haemagglutinin-neuraminidase from Human Parainfluenza Virus Type III. *J. Mol. Biol.* **335**: 1343-57

Lee KK (2010) Architecture of a nascent viral fusion pore. *EMBO J.* **29**: 1299-311

Li J, Quinlan E, Mirza A, Iorio RM (2004) Mutated form of the Newcastle disease virus hemagglutinin-neuraminidase interacts with the homologous fusion protein despite deficiencies in both receptor recognition and fusion promotion. *J. Virol.* **78**: 5299-310

Liljeroos L, Huiskonen JT, Ora A, Susi P, Butcher SJ (2011) Electron cryotomography of measles virus reveals how matrix protein coats the ribonucleocapsid within intact virions. *Proc Natl Acad Sci U S A* **108**: 18085-90

Liljeroos L, Krzyzaniak MA, Helenius A, Butcher SJ (2013) Architecture of respiratory syncytial virus revealed by electron cryotomography. *Proc Natl Acad Sci U S A* **110**: 11133-8

Loney C, Mottet-Osman G, Roux L, Bhella D (2009) Paramyxovirus ultrastructure and genome packaging: cryo-electron tomography of sendai virus. *J. Virol.* **83**: 8191-7

Ludwig K, Schade B, Bottcher C, Korte T, Ohlwein N, Baljinnyam B, Veit M, Herrmann A (2008) Electron cryomicroscopy reveals different F1+F2 protein States in intact parainfluenza virions. *J. Virol.* **82**: 3775-81

Maar D, Harmon B, Chu D, Schulz B, Aguilar HC, Lee B, Negrete OA (2012) Cysteines in the stalk of the Nipah virus G glycoprotein are located in a distinct subdomain critical for fusion activation. *J. Virol*. **86**:6632-42.

Markwell M, Svennerholm L, Paulson J (1981) Specific gangliosides function as host cell receptors for Sendai virus. *Proc Natl Acad Sci U S A* **78**: 5406-10

Mateo M, Navaratnarajah CK, Cattaneo R (2014) Structural basis of efficient contagion: measles variations on a theme by parainfluenza viruses. Curr. Opin. Virol. **5**: 16-23

McLellan JS, Chen M, Leung S, Graepel KW, Du X, Yang Y, Zhou T, Baxa U, Yasuda E, Beaumont T, Kumar A, Modjarrad K, Zheng Z, Zhao M, Xia N, Kwong PD, Graham BS (2013) Structure of RSV fusion glycoprotein trimer bound to a prefusion-specific neutralizing antibody. *Science* **340**: 1113-7

McLellan JS, Yang Y, Graham BS, Kwong PD (2011) Structure of respiratory syncytial virus fusion glycoprotein in the postfusion conformation reveals preservation of neutralizing epitopes. *J. Virol.* **85**: 7788-96

Mirza AM, Aguilar HC, Zhu Q, Mahon PJ, Rota PA, Lee B, Iorio RM (2011) Triggering of the newcastle disease virus fusion protein by a chimeric attachment protein that binds to Nipah virus receptors. *J. Biol. Chem.* **286**: 17851-60

Moscona A, Peluso RW (1991) Fusion properties of cells persistently infected with human parainfluenza virus type 3: Participation of hemagglutinin-neuraminidase in membrane fusion. *J. Virol.* **65**: 2773-2777

Moscona A, Peluso RW (1993) Relative affinity of the human parainfluenza virus type 3 hemagglutinin-neuraminidase for sialic acid correlates with virus-induced fusion activity. *J. Virol.* **67**: 6463-8

Navaratnarajah CK, Negi S, Braun W, Cattaneo R (2012) Membrane fusion triggering: three modules with different structure and function in the upper half of the measles virus attachment protein stalk. *J. Biol. Chem.* **287**: 38543-51

Palmer SG, DeVito I, Jenkins SG, Niewiesk S, Porotto M, Moscona A (2014) Circulating clinical strains of human parainfluenza virus reveal viral entry requirements for in vivo infection. J. Virol. **88**: 13495-502

Palmer SG, Porotto M, Palermo LM, Cunha LF, Greengard O, Moscona A (2012) Adaptation of human parainfluenza virus to airway epithelium reveals fusion properties required for growth in host tissue. mBio **3**: e00137-12

Paterson RG, Johnson ML, Lamb RA (1997) Paramyxovirus fusion (F) protein and hemagglutinin-neuraminidase (HN) protein interactions: intracellular retention of F and HN does not affect transport of the homotypic HN or F protein. *Virology* **237**: 1-9

Pettersen EF, Goddard TD, Huang CC, Couch GS, Greenblatt DM, Meng EC, Ferrin TE (2004) "UCSF Chimera - A Visualization System for Exploratory Research and Analysis." J. Comput. Chem. **25**: 1605-1612

Plattet P, Plemper RK (2013) Envelope protein dynamics in paramyxovirus entry. *mBio* **4**

Plemper RK, Brindley MA, Iorio RM (2011) Structural and mechanistic studies of measles virus illuminate paramyxovirus entry. PLoS Pathog. **7**: e1002058

Porotto M, Devito I, Palmer SG, Jurgens EM, Yee JL, Yokoyama CC, Pessi A, Moscona A (2011) Spring-loaded model revisited: Paramyxovirus fusion requires engagement of a receptor binding protein beyond initial triggering of the fusion protein. *J. Virol*. **85**: 12867-80

Porotto M, Fornabaio M, Greengard O, Murrell MT, Kellogg GE, Moscona A (2006) Paramyxovirus receptor-binding molecules: engagement of one site on the hemagglutinin-neuraminidase protein modulates activity at the second site. *J. Virol*. **80**: 1204-13

Porotto M, Murrell M, Greengard O, Doctor L, Moscona A (2005) Influence of the human parainfluenza virus 3 attachment protein's neuraminidase activity on its capacity to activate the fusion protein*. J. Virol*. **79**: 2383-2392

Porotto M, Murrell M, Greengard O, Moscona A (2003) Triggering of human parainfluenza virus 3 fusion protein(F) by the hemagglutinin-neuraminidase (HN): an HN mutation diminishing the rate of F activation and fusion. *J. Virol.* **77**: 3647-3654

Porotto M, Rockx B, Yokoyama CC, Talekar A, Devito I, Palermo LM, Liu J, Cortese R, Lu M, Feldmann H, Pessi A, Moscona A (2010) Inhibition of Nipah virus infection in vivo: targeting an early stage of paramyxovirus fusion activation during viral entry. *PLoS Pathog* **6**: e1001168

Porotto M, Salah Z, Devito I, Talekar A, Palmer SG, Xu R, Wilson IA, Moscona A (2012a) The second receptor binding site of the globular head of the Newcastle disease virus (NDV) hemagglutinin-neuraminidase activates the stalk of multiple paramyxovirus receptor binding proteins to trigger fusion. *J. Virol.* **86**: 5730-41

Porotto M, Palmer SG, Palermo LM, Moscona A (2012b) Mechanism of fusion triggering by human parainfluenza virus type III: communication between viral glycoproteins during entry. *J. Biol. Chem.* **287**: 778-93

Porotto M, Salah ZW, Gui L, Devito I, Jurgens EM, Lu H, Yokoyama CC, Palermo LM, Lee KK, Moscona A (2012c) Regulation of paramyxovirus fusion activation: the hemagglutinin-neuraminidase protein stabilizes the fusion protein in a pretriggered state. *J. Virol.* **86**: 12838-48

Sergel T, McGinnes LW, Peeples ME, Morrison TG (1993) The attachment function of the Newcastle disease virus hemagglutinin-neuraminidase protein can be separated from fusion promotion by mutation. *Virology* **193**: 717-726

Smith EC, Popa A, Chang A, Masante C, Dutch RE (2009) Viral entry mechanisms: the increasing diversity of paramyxovirus entry. *Febs J* **276**: 7217-27

Steffen DL, Xu K, Nikolov DB, Broder CC (2012) Henipavirus mediated membrane fusion, virus entry and targeted therapeutics. *Viruses* **4**: 280-309

Suloway C, Shi J, Cheng A, Pulokas J, Carragher B, Potter CS, Zheng SQ, Agard DA, Jensen GJ (2009) Fully automated, sequential tilt-series acquisition with Leginon. Journal of structural biology 167: 11-8

Swanson K, Wen X, Leser GP, Paterson RG, Lamb RA, Jardetzky TS (2010) Structure of the Newcastle disease virus F protein in the post-fusion conformation. *Virology* **402**: 372-9

Talekar A, DeVito I, Salah Z, Palmer SG, Chattopadhyay A, Rose JK, Xu R, Wilson IA, Moscona A, Porotto M (2013a) Identification of a region in the stalk domain of the nipah virus receptor binding protein that is critical for fusion activation. *J. Virol.* **87**: 10980-96

Talekar A, Moscona A, Porotto M (2013b) Measles virus fusion machinery activated by sialic acid binding globular domain. *J. Virol*. **87**: 13619-27

Tanabayashi K, Compans R (1996) Functional interactions of paramyxovirus glycoproteins: Identification of a domain in Sendai virus HN which promotes cell fusion. *J. Virol.* **70**: 6112-6118

Terrier O, Rolland JP, Rosa-Calatrava M, Lina B, Thomas D, Moules V (2009) Parainfluenza virus type 5 (PIV-5) morphology revealed by cryo-electron microscopy. *Virus research* **142**: 200-3

Thompson-Wicking K, Francis RW, Stirnweiss A, Ferrari E, Welch MD, Baker E, Murch AR, Gout AM, Carter KW, Charles AK, Phillips MB, Kees UR, Beesley AH (2012) Novel BRD4-NUT fusion isoforms increase the pathogenic complexity in NUT midline carcinoma. *Oncogene* **32**:4664-74.

Vigant F, Lee B (2011) Hendra and nipah infection: pathology, models and potential therapies. *Infect Disord Drug Targets* **11**: 315-36

Vigant F, Lee J, Hollmann A, Tanner LB, Akyol Ataman Z, Yun T, Shui G, Aguilar HC, Zhang D, Meriwether D, Roman-Sosa G, Robinson LR, Juelich TL, Buczkowski H, Chou S, Castanho MA, Wolf MC, Smith JK, Banyard A, Kielian M *et al* (2013) A mechanistic paradigm for broad-spectrum antivirals that target virus-cell fusion. *PLoS Pathog.* **9**: e1003297

Welch BD, Liu Y, Kors CA, Leser GP, Jardetzky TS, Lamb RA (2012) Structure of the cleavage-activated prefusion form of the parainfluenza virus 5 fusion protein. *Proc Natl Acad Sci U S A* **109**: 16672-7

Welch BD, Yuan P, Bose S, Kors CA, Lamb RA, Jardetzky TS (2013) Structure of the parainfluenza virus 5 (PIV5) hemagglutinin-neuraminidase (HN) ectodomain. *PLoS Pathog.* **9**: e1003534

Wen X, Krause JC, Leser GP, Cox RG, Lamb RA, Williams JV, Crowe JE, Jr., Jardetzky TS (2012) Structure of the human metapneumovirus fusion protein with neutralizing antibody identifies a pneumovirus antigenic site. *Nat Struct Mol Biol* **19**: 461-3

White JM, Delos SE, Brecher M, Schornberg K (2008) Structures and mechanisms of viral membrane fusion proteins: multiple variations on a common theme. *Crit. Rev. Biochem. Mol. Biol.* **43**: 189-219

Xu R, Palmer SG, Porotto M, Palermo LM, Niewiesk S, Wilson IA, Moscona A (2013) Interaction between the hemagglutinin-neuraminidase and fusion glycoproteins of human parainfluenza virus type III regulates viral growth in vivo. *mBio* **4**: e00803-13

Yin HS, Paterson RG, Wen X, Lamb RA, Jardetzky TS (2005) Structure of the uncleaved ectodomain of the paramyxovirus (hPIV3) fusion protein. *Proc Natl Acad Sci U S A* **102**: 9288-93

Yin HS, Wen X, Paterson RG, Lamb RA, Jardetzky TS (2006) Structure of the parainfluenza virus 5 F protein in its metastable, prefusion conformation. *Nature* **439**: 38-44

Yuan P, Leser GP, Demeler B, Lamb RA, Jardetzky TS (2008) Domain architecture and oligomerization properties of the paramyxovirus PIV 5 hemagglutinin-neuraminidase (HN) protein. *Virology* **378**: 282-91

Yuan P, Paterson RG, Leser GP, Lamb RA, Jardetzky TS (2012) Structure of the ulster strain newcastle disease virus hemagglutinin-neuraminidase reveals auto-inhibitory interactions associated with low virulence. *PLoS Pathog* **8**: e1002855

Yuan P, Swanson KA, Leser GP, Paterson RG, Lamb RA, Jardetzky TS (2011) Structure of the Newcastle disease virus hemagglutinin-neuraminidase (HN) ectodomain reveals a four-helix bundle stalk. *Proc Natl Acad Sci U S A* **108**: 14920-5

Yuan P, Thompson TB, Wurzburg BA, Paterson RG, Lamb RA, Jardetzky TS (2005) Structural studies of the parainfluenza virus 5 hemagglutinin-neuraminidase tetramer in complex with its receptor, sialyllactose. *Structure* **13**: 803-15

Yuasa T, Kawano M, Tabata N, Nishio M, Kusagawa S, Komada H, Matsumura H, Ito Y, Tsurudome M (1995) A cell fusion-inhibiting monoclonal antibody binds to the presumed stalk domain of the human parainfluenza type 2 virus hemagglutinin-neuraminidase protein. *Virology* **206**: 1117-25

Zaitsev V, von Itzstein M, Groves D, Kiefel M, Takimoto T, Portner A, Taylor G (2004) Second sialic acid binding site in newcastle disease virus hemagglutinin-neuraminidase: implications for fusion. *J. Virol*. **78**: 3733-41

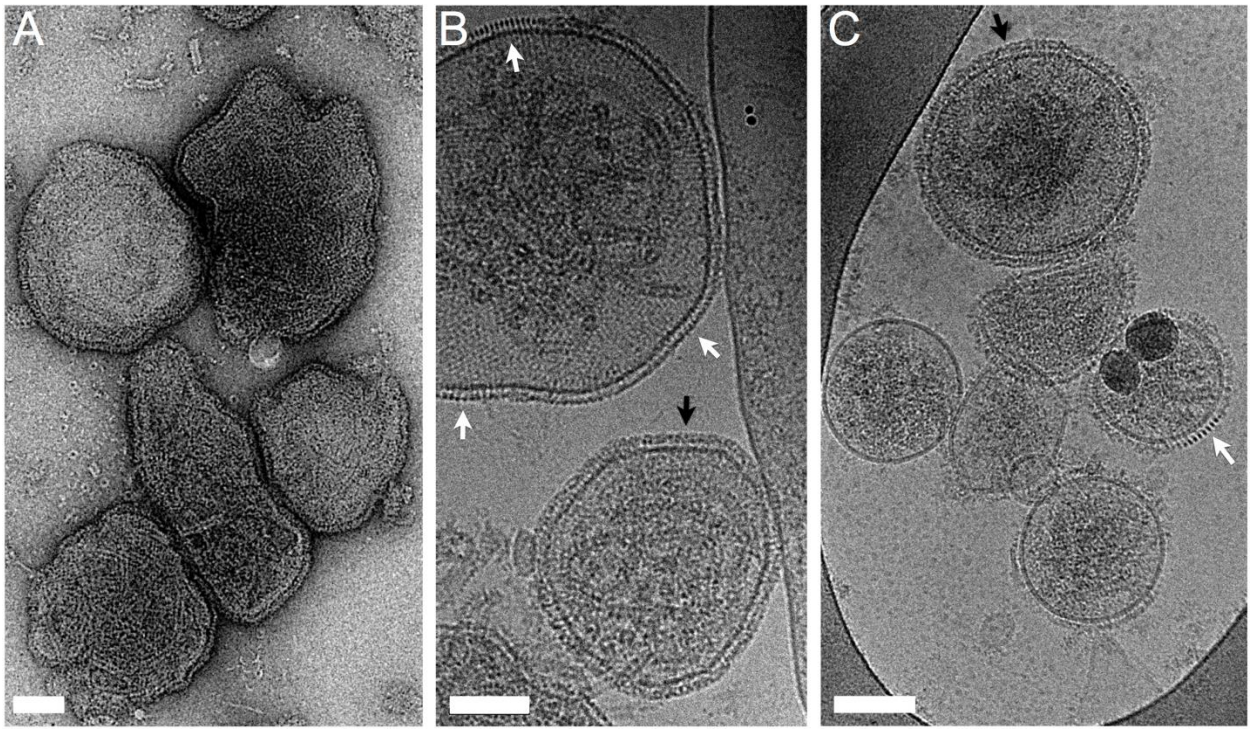

Figure 4.1 HPIV3 imaged by negative-stain (A) and cryo-electron microscopy (B-C). As is particularly evident in cryo-EM micrographs, nearly all particles were rounded rather than filamentous in morphology. In addition to a complex, dense layer of surface density (black arrows), regions of ordered density (white arrows) were evident, both attributed to the viral glycoproteins. Scale bar 100 nm.

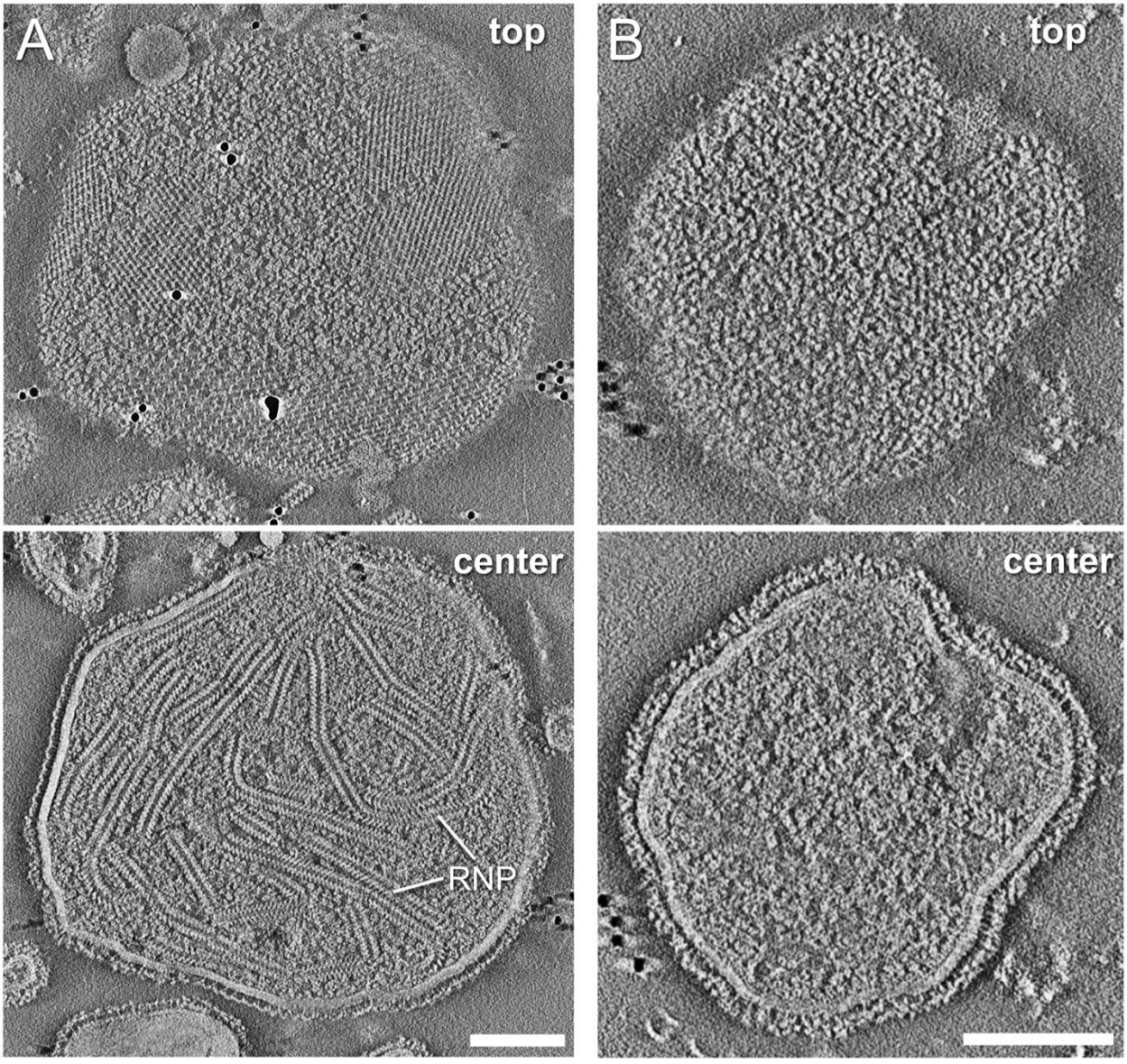

Figure 4.2 Negative-stain tomographic reconstruction of an HPIV3 virion. (A) 4.4 nm thick slices through the reconstructed density reveal a complex organization of surface features including ordered arrays of glycoproteins as well as less regularly ordered proteins, many of which exhibit a triangular shape with stain-penetrable centers. The central slice through the particle reveals significant RNP helical tubes inside as well as lateral views of surface glycoprotein organization. **(B)** 2.2 nm thick slices showing top of particle and central slice through reconstructed particle density shows that some particles do not present the grid-like arrays of surface glycoproteins. Instead in these cases, a more complex, doubled layer surface appears predominant as is evident in the edge views of particle central slices. Scale bars 100 nm.

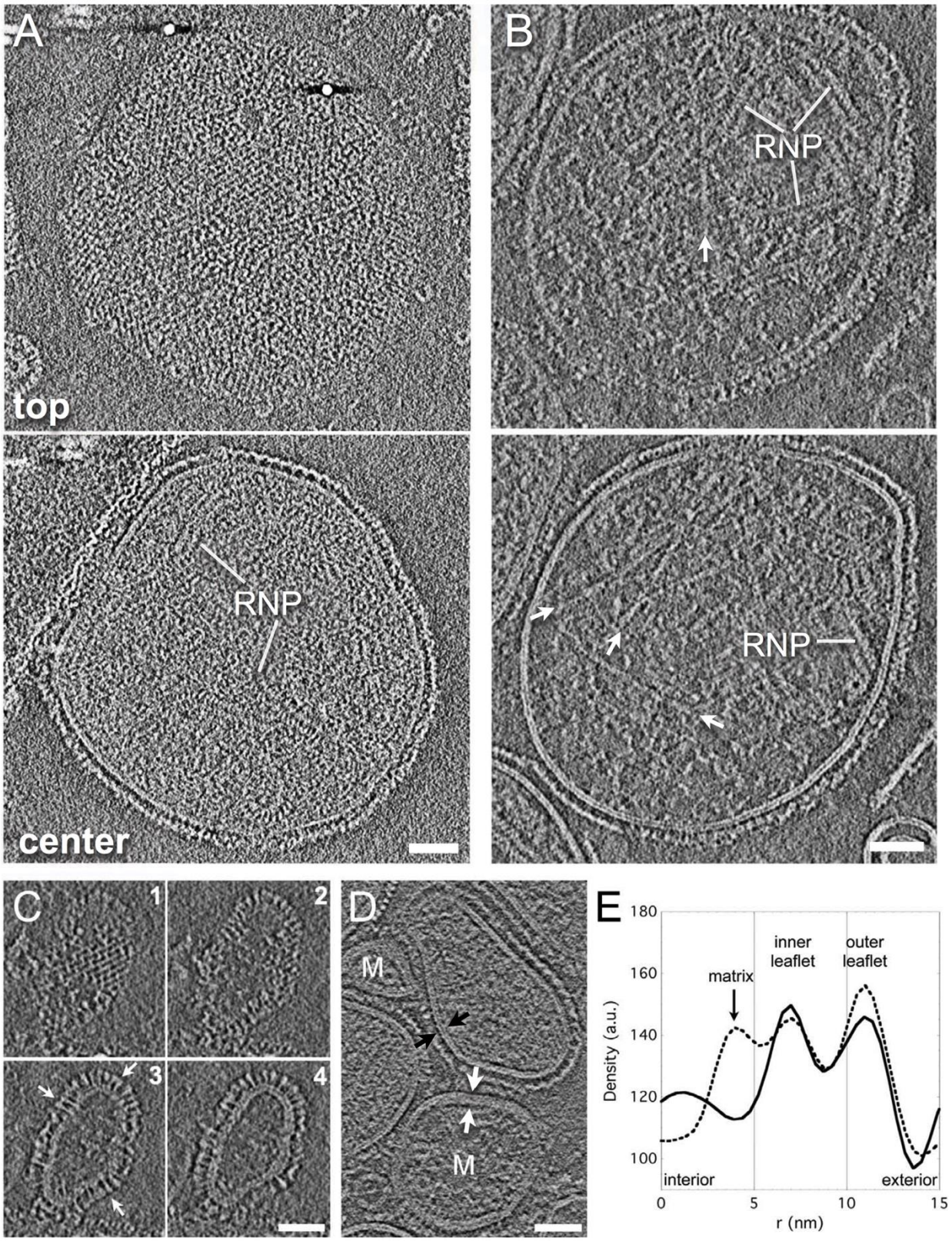

Figure 4.3 HPIV3 particle ultrastructure imaged by cryo-EM tomography. 4.4 nm thick slices showing top and central slices through reconstructed density for two representative HPIV3 particles **(A,B)**. Image

grey scale has been inverted for comparison with negative-stain reconstructions such as in Figure 4.3. As with the negatively stained samples, cryo-ET imaging of particles reveal ordered patterns of density on the virus surface as well as RNP packaged inside **(A)**. In the majority of particles such as in A and B, the envelope consisted of simple lipid bilayers with glycoproteins on the exterior, significant spans of membrane-associated density corresponding to an internal matrix layer were not typically observed. **(B)** In some particles, density consistent with actin filaments are observed inside (white arrows) (Fujii *et al*, 2010). **(C)** A few small particles lacking RNP that bear postfusion F (white arrows, upper and lower right edges) and HN arrays were the primary glycoproteins observed on these small particles. **(D)** Approximately 10% of particles (labeled M) do appear to exhibit matrix layers that contribute to thicker envelopes. **(E)** Electron density plots show solid line across the viral envelope with matrix (white arrows) and dash line across the viral envelope without matrix (black arrows) in D. The internal matrix layer is observed ~3-4 nm separated from the inner bilayer leaflet. Scale bars 50 nm.

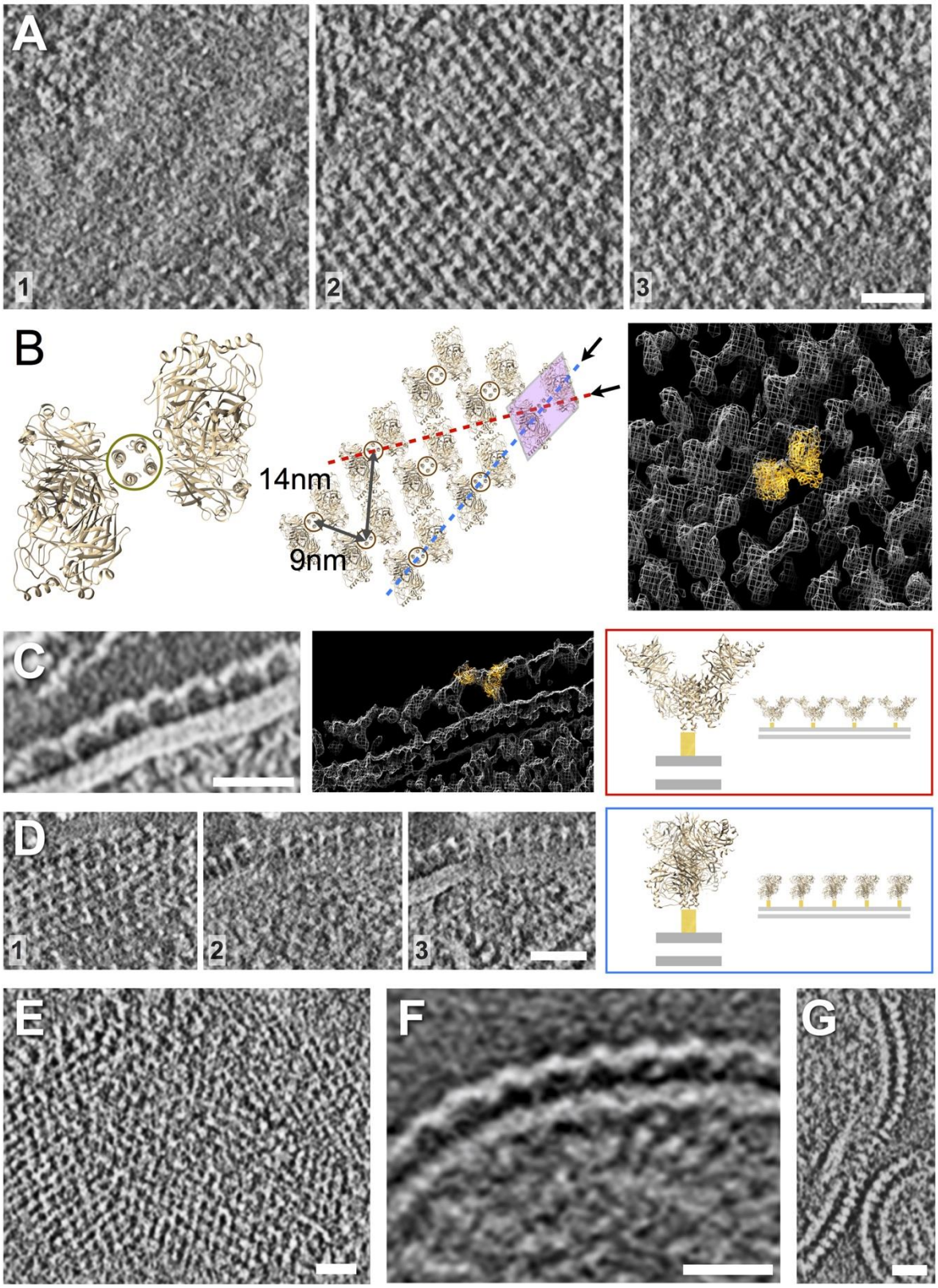

Figure 4.4 HN arrays imaged by negative-stain electron tomography (A-D) and cryo-electron tomography (E-G). (A) Serial 3.2 nm slices of a negative-stain tomographic reconstruction, increasing

in elevation above the virus surface from left to right (numbered 1-3). Viewed from above (slices 2,3), this tetramer has a slanted “H” appearance positioned above punctate dots of density that correspond to the tetramer’s helical bundle stalk (slice 1). The ordered grids of density on the surface of the virions are composed of repeating units of density in excellent agreement with the known structure for a tetramer of HN in the “heads-down” conformation; crystal structure for NDV HN (PDB: 3T1E) shown for comparison. A model of the array organization based on the crystallographic structure for tetrameric, “heads-down” HN is shown in **(B)**, and docked (orange ribbon diagram) into the EM density (white mesh). **(C)** Viewed laterally at the edge of a virus particle, the arrays are observed to flow into repeating rows of Y-shaped density features that correspond to the view of the HN array along the red line shown in (B). PDB 3T1E is shown docked into the EM density. **(D)** In other orientations, the arrays can be viewed down a different axis indicated by the blue line in (A); serial slices ordered from left to right (numbered 1-4). Scale bars 25 nm. **(E)** Cryo-electron tomographic slice of virion surface shows similar arrays of density as seen from the top of a particle; note image grey scale has been inverted for comparison with negative-stain reconstructions above. **(F)** Y-shaped features are also observed at the edge of particles in central slices. **(G)** Additional views of the arrays from a different orientation also reveal the regular ordering of surface density. Scale bars 25 nm.

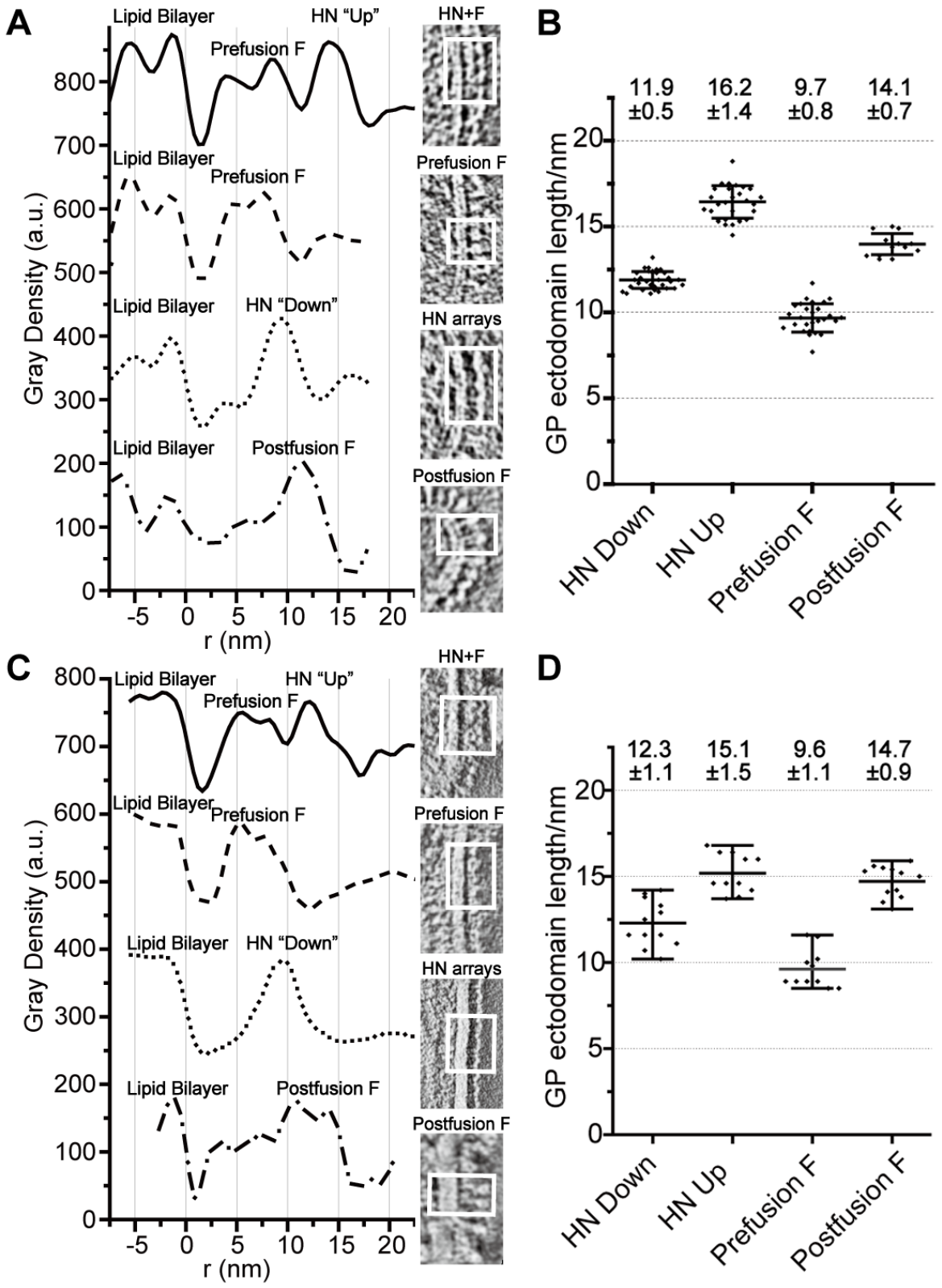

Figure 4.5 Radial density distribution of surface glycoproteins in different organizations through cryo- and negative-stain electron tomography. **(A)** Cryo-electron tomography clearly shows the viral

lipid bilayer, and distinct layers of surface glycoprotein density above the membrane including double layered surfaces composed of HN molecules inferred to be in a “heads-up” configuration adjacent to prefusion F molecules, occasional prefusion F molecules, arrays of HN in “heads-down” configuration, and postfusion F protein. **(B)** Measurements of the height of surface glycoproteins from the viral envelope in cryo-ET reconstructions (distances measured from positions of half-maximum density). Numbers indicate average heights ± standard deviations **(C,D)** Negative-stain electron tomography and height measurements show very similar organizations and good agreement with cryo-ET observations.

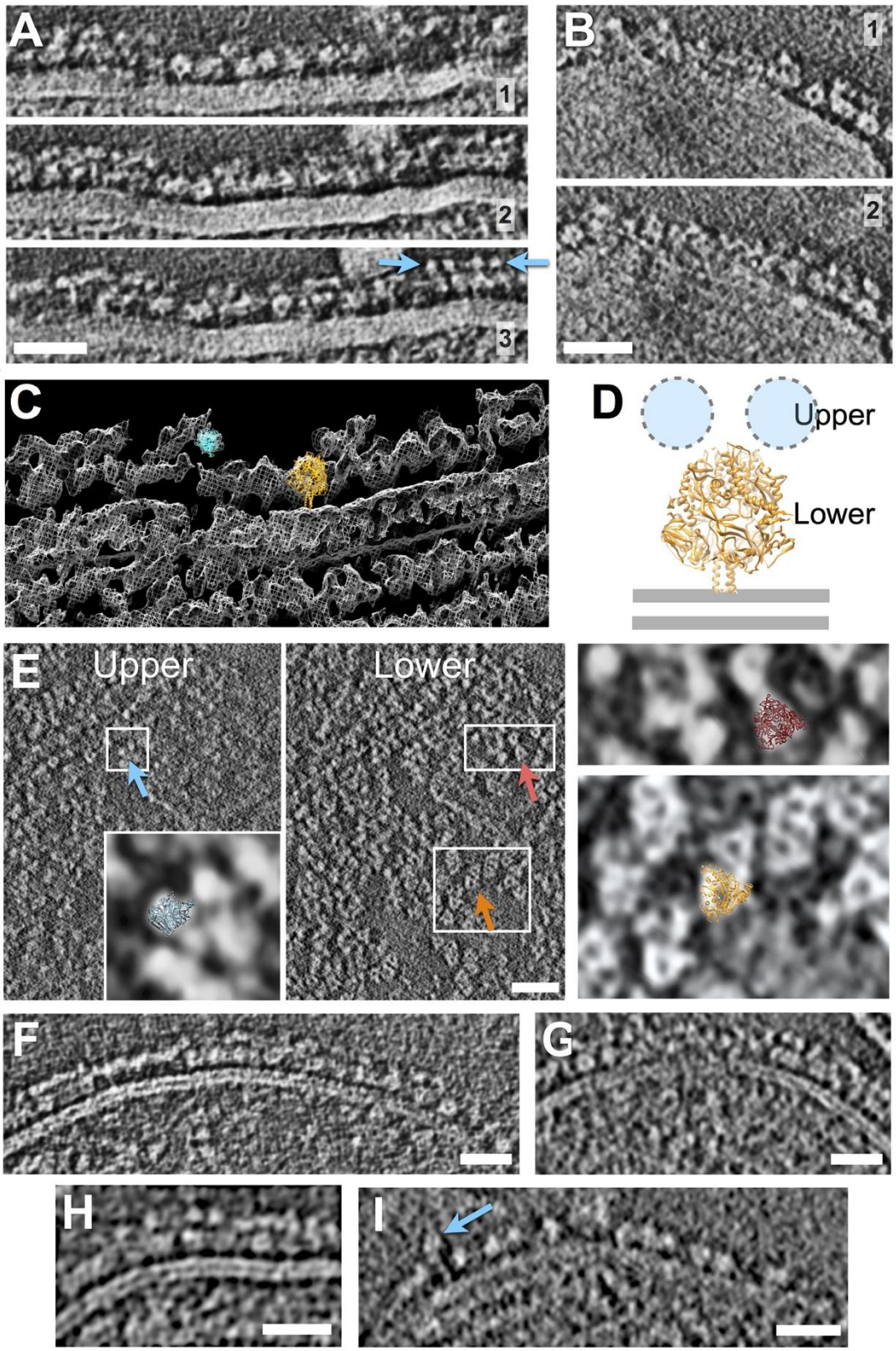

Figure 4.6 Location of prefusion F trimers on the virus surface. Negative-stain **(A-C,E)** and cryo-electron tomography **(F-I)** Note for cryo-electron tomograms (panels F-I) image grey scale has been

inverted to facilitate comparison with negative-stain reconstructions. 4.4 nm thick serial slices showing lateral views of glycoprotein spikes show prefusion F trimers clustered close to the membrane with additional density features at higher elevations forming a canopy above the F trimers **(A,B)** interpreted as HN monomers. In some cases, the canopy density is resolved into discrete 4-5 nm diameter punctae (blue arrows in A). **(C)** Crystal structures for prefusion F (orange ribbon diagram; prefusion F from PIV5 4GIP.pdb [Welch *et al*, 2012]) docked into the EM density for the globular, donut-like membrane-proximal features, show excellent agreement with EM density, suggesting the organization shown in **(D)**, with globular HN positioned in the upper layer of density and prefusion F in the lower layer beneath the canopy. **(E)** The canopy density (4.4 nm thick "upper" slice) viewed from above show that at high elevation, punctate globular density features are observed (blue arrow for example; inset shows one HPIV3 HN monomer from 1V2I.pdb (Lawrence *et al*, 2004), blue ribbon diagram, docked into the EM density); by contrast, tightly associated tetramers as observed in crystal structures of HN head domains from PIV5 (SV5) (1Z4X; [Yuan *et al*, 2005]) were not clearly identifiable. At lower elevations, closer to the virus surface triangular features consistent with primarily prefusion F are observed (orange arrow; lower panel on right shows 4GIP.pdb prefusion F crystal structure docked into EM density (Welch *et al*, 2012); some instances of smaller diameter postfusion F trimers are also distinguishable from the prefusion trimers (red arrow; upper panel on right shows HPIV3 postfusion F trimer, 1ZTM.pdb docked into EM density [Yin *et al*, 2006]). **(F-I)** Central slices of cryo-electron tomography showing lateral views of F protein distribution on the virus surface. In some cases isolated prefusion F trimers are observed **(I)**, while in other cases **(F-H)** prefusion F is found in regions of double layer surface density, positioned beneath a discontinuous canopy of density we infer to be HN. Scale bars 25 nm.

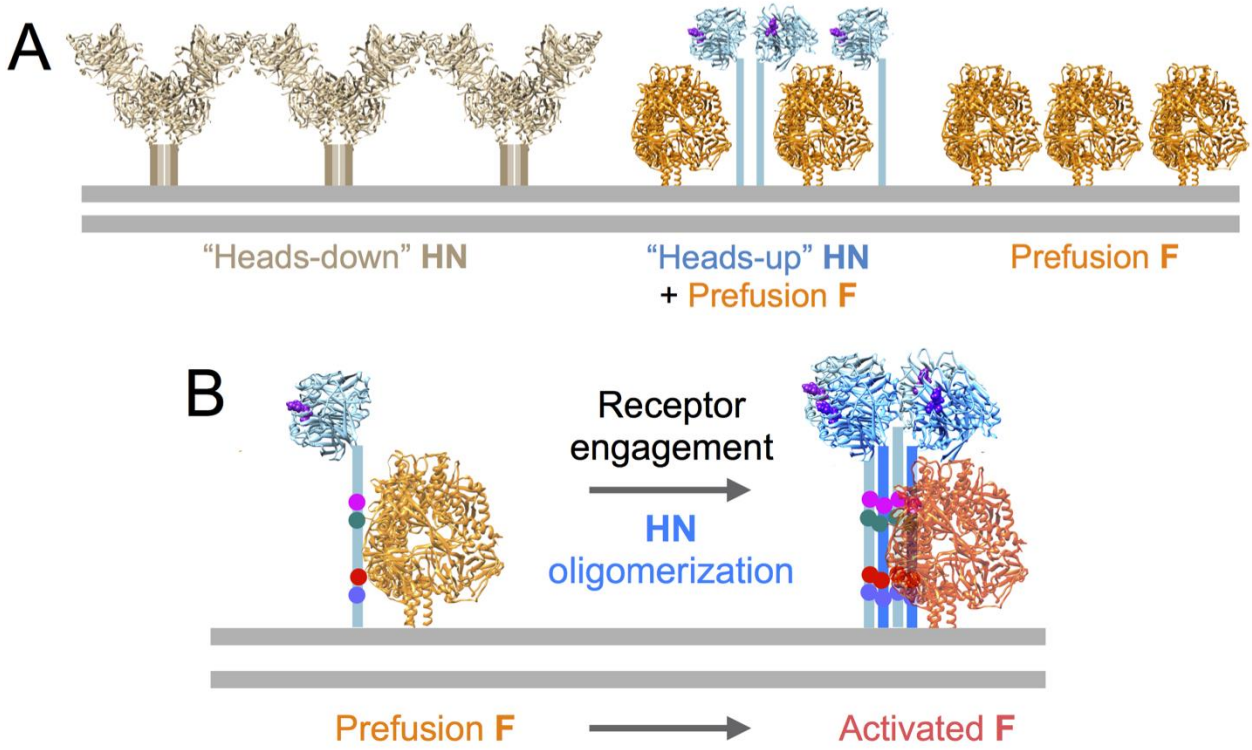

Figure 4.7 Implications for fusion triggering and HN/F interactions. Observation of viral surfaces in the absence of receptor engagement include HN tetramers in "heads-down" configuration in arrays on the virus surface. These "heads-down" tetramers were not observed in association with F. **(A)** On these virions without receptor engagement, some prefusion F is interspersed with HN in an extended configuration with the globular heads towering above the level of the F, consistent with a "heads-up" but monomeric or dimeric form. F alone is also observed both prefusion and postfusion form. The data support the notion that F and HN are clustered with each other prior to receptor engagement by HN, and that the presence of a "heads-up" form of HN in proximity to prefusion F is not sufficient to induce F activation. **(B)** Since tetrameric, "heads-up" HN was not observed either alone or in association with F, the possibility exists that oligomerization induced by receptor engagement (not studied here) is important for triggering F.

Chapter 5. Summary and Future Directions

Protein-mediated membrane fusion is an essential step in the life cycle of enveloped virus, such as influenza, human parainfluenza viruses and HIV (Chan & Kim, 1998; Harrison, 2008; White *et al*, 2008; Harrison, 2015). It also is a ubiquitous and key event that underlies many fundamental cellular processes (Jahn *et al*, 2003; Martens & McMahon, 2008). Despite its biological significance, the states that drive the fusion process have been refractory to classical structure determination, and the interplay of fusion proteins and membranes remains exclusive. Much of currently available information has been inferred from low-resolution, indirect approaches such as fluorescence measurement or X-ray diffraction (Blumenthal *et al*, 2002; Aeffner *et al*, 2012). The application of cryo-electron microscopy, a major focus of my work, has made it possible to directly capture and visualize the populated structures during fusion, leading to new mechanistic insights into this dynamic process (Diao *et al*, 2012; Hernandez *et al*, 2012; Lee *et al*, 2011; Chlanda *et al*, 2016; Bonnafous *et al*, 2014).

My thesis focuses on direct structural characterization of viral fusion proteins and interplay between fusion proteins and membrane during fusion. In Chapter 2, I have combined cryo-electron tomography (cryo-ET) and fluorescence spectroscopy to investigate the 3-dimensional organization and kinetics of the intermediates during fusion of influenza virus with membranes. I observed that progression of membrane reorganization proceeded through an extended contact zone with tightly apposed virus-target membrane interactions. This study provided the first demonstration of the sequence of membrane reorganzations during fusion based upon imaging of fusion interactions with sufficient resolution to identify membrane leaflets and fusion proteins.

In Chapter 3, HA fusion peptide-induced membrane deformation for isolated fusion proteins was compared with the behavior on whole viruses. I also examined the influence of cholesterol on the type of membrane deformations that are induced by activated HA. This study showed that isolated, soluble HA ectodomain by itself could induce significant membrane

deformation and that cholesterol had a very noticeable effect in stabilizing the target membrane against fusion protein-induced membrane deformation.

In Chapter 4, I examined a parallel enveloped virus system to influenza virus by studying the organization of surface glycoproteins on human parainfluenza virus 3 (HPIV3). Using a combination of negative-staining and cryo-ET I was able to resolve the distribution of receptor binding proteins and fusion proteins, even to identify the conformational states of these proteins on the virus surface in some cases. My observations are consistent with a model for fusion in which prefusion fusion proteins associate with receptor binding proteins prior to receptor engagement (Gui *et al*, 2015).

In the context of recent work from other groups, our results suggest novel directions for future research, which will ideally provide new insights into mechanisms of virus fusion machinery and protein-mediated membrane fusion.

5.1 Erythrocyte ghost membranes as the target membranes

Liposomes are widely used as artificial target membranes in the studies of virus membrane fusion because the researchers can image the fusion process under control of experimental parameters (e.g. pH, temperature and liposome lipid compositions)(Lee, 2010; Lee *et al*, 2011; Fontana & Steven, 2015; Kanaseki, 1997). In our current experiments dioleoylphosphatidylcholine (DOPC) was selected as the main target membrane component for 2 main reasons: 1) phosphatidylcholine (PC) is a major component of the host membrane; and 2) DOPC in our experimental situations is in the disordered liquid crystalline rather than ordered gel state, due to its low transition temperature (-17 °C). It is important to note however that DOPC tends to form planar bilayers and resists the formation of curved structures due to the molecular shape of DOPC consisting similar sizes of the polar heads with the unsaturated hydrocarbon tails (Chernomordik & Kozlov, 2008; Jahn *et al*, 2003). Given the fact that significant membrane remodeling has been observed during fusion of influenza virus with DOPC liposomes, we

anticipate that influenza virus HA will induce similar or even greater deformations in other less resilient membranes that contain for example phosphatidylethanolamine (PE), which tends to form curved membranes with smaller headgroups and promotes membrane fusion.

In a synthetic liposomal system, it is challenging to replicate the complexity of a true biological membrane due to the complicated mixture of lipids, sterols and other components as well as the asymmetric distribution of those components on the two leaflets. Indeed, several important factors were absent from the simplistic DOPC target membrane would be present in authentic biological membranes. For instance, biological membranes for viral fusion are complex mixtures of different types of phospholipids including PC, PE and phosphatidylserine (PS). Sterols such as cholesterol and sphingomyelin are also important components of authentic biological membranes (van Meer *et al*, 2008). Moreover, the asymmetric distribution of the components between the two leaflets can influence the physical properties of the membranes (Verkleij *et al*, 1973; van Meer *et al*, 2008). Finally, our synthetic liposomes lack the sialic acid receptor for virus engagement. It is widely accepted that human-adapted HA subtypes preferentially bind to α2,6-linked sialic acid, whereas the avian-adapted HA subtypes preferentially recognize α2,3-linked sialic acid. This difference is thought to be a key determinant for host cell tropisms (García-Sastre, 2010). Previous fluorescence studies suggested that removal of cell membrane sialic acid resulted in a reduction in both viral binding and fusion (de Lima *et al*, 1995). But other reports have demonstrated that influenza virus membrane fusion proceeds similarly with or without sialic acid receptors, although a slightly faster rate is observed with receptors present (Ramalho-Santos & Pedroso De Lima, 2004; Ellens *et al*, 1990). In experiments I have performed (not included in this thesis), I have found that the efficiency of fusion was indeed enhanced but only by ~20% when 5% ganglioside that presents sialic acid receptors was included. We infer that receptor on the target membrane helps to adsorb the virus particles prior to HA activation, but may not play an important role during the HA-mediated fusion process. Other data from members of our group have shown that the HA1 receptor binding domain loses significant structural integrity under

fusion-activating acidic conditions (Garcia *et al*, 2015), which likely would reduce its interaction with sialic acid receptors, which already is relatively weak with ~mM binding affinity.

In order to use a more authentic target membrane, I have performed preliminary experiments using vesicles prepared from erythrocyte ghost membranes. Erythrocyte ghost membranes can be prepared from the lysis of fresh erythrocytes and have been widely used as model target membranes for enveloped viral fusion. The lipid composition of erythrocyte ghost membranes is similar to membranes found in early endosomes, though it is important to notice that after maturation, endosomes have ~50% less cholesterol and added a new lipid component known as bis(monoacylglycero)phosphate (BMP) that promotes membrane fusion at acidic pH (Kobayashi *et al*, 2002) (see Chapter 2). In the presence of Mg-ATP, the asymmetry of membrane lipid can be preserved during the lysis step (Connor *et al*, 1990; Seigneuret & Devaux, 1984). Many previous fusion studies have used sealed ghost membranes that contained intact spectrin membrane skeleton, but the dimensions of sealed ghost membranes (usually several μm) are too large for cryo-ET imaging (Reda *et al*, 2009; Herrmann *et al*, 1988; Nir *et al*, 1986). We have adapted methods first reported by Steck and colleagues for generating spectrin-depleted vesicles with 200-500 nm dimensions that are suitable for cryo-ET (Steck *et al*, 1970; Steck, 1974). The workflow for generating these vesicles proceeds as follows: 1) erythrocyte ghost membranes are prepared by hypotonic lysis in the presence of Mg-ATP and isolated from cellular contents by low-speed spin; 2) The ghost membranes are then homogenized using 27-gauge needles to form spectrin-depleted vesicles that are predominantly right side out (R.O.V.); 3) R.O.V. can be further separated from erythrocyte ghost membranes and inside-out vesicles (I.O.V.) using a dextran density gradient. 4) Purified R.O.V. then can serve as the target membranes in fluorescence assays and cryo-ET. As a control, vesicles with scrambled lipid distribution (without Mg-ATP) can be examined. Leaflet asymmetry would be monitored using sialidase and susceptibility assay. A panel of antibodies that can distinguish protein components found on inner and outer leaflets can also be used to confirm the asymmetric orientation of leaflets and their components. I was able

to generate preliminary data with R.O.V. and influenza virus, but a more complete study will require optimization of vesicle production and optimization of fusion assays.

Liposomes containing more complete mixtures of lipids and cholesterol can also be tested to determine whether the observed membrane deformation and fusion pathway I found with DOPC-based liposomes is generally representative. One such formulation described by Lentz and colleagues called “Nature’s own fusogenic lipid bilayer”, containing DOPC:DOPE:SM:Chol in 35:30:15:20 molar ratios was found to be highly fusogenic (Haque *et al*, 2001). Our previous experiments (Chapters 2 and 3) focused on the role of cholesterol in influenza virus membrane fusion, but it has been reported that sphingomyelin and cholesterol act together to influence membrane properties such as rigidity and fluidity.

By comparing fusion between virus and authentic biological target membranes derived from erythrocytes with model target membranes of a range of defined compositions, we aim to test the generality of our fusion model raised in Chapter 2 and enhance our understanding of the lipidic determinants of membrane fusion.

5.2 The role of matrix layer during viral membrane fusion

The M1 matrix layer of influenza A virus underlies the viral membrane and is thought to mediate the interactions between the envelope and the viral ribonucleoproteins (RNPs). During the step of viral assembly, M1 is recruited to the plasma membrane by the cytoplasmic tails of membrane proteins and serves as a docking site for further recruitment of RNPs at the docking sites (Rossman & Lamb, 2011). Recent work has revealed another role of the M1 protein in membrane fusion (Lee, 2010; Fontana & Steven, 2013). Exposure of influenza virions to low pH in the endosomes initiates membrane fusion and results in the release of RNPs into the cytoplasm. One consequence of acidic conditions is to trigger the structural rearrangements in the HA glycoprotein on the surface of virions. Following exposure to acidic pH conditions, the virus interior (inside the membrane) also becomes acidified resulting from the passage of protons

through the viral M2 ion channel (Pinto *et al*, 1992; Skehel, 1992). Our recent cryo-ET efforts have shown that (i) at pH 5.5, the matrix layer associates with the viral envelope and maintains the integrity and shape of the virus particles, acting like endoskeleton. As a result, membrane deformations are focused on the target membrane while the viral membrane is stabilized at early stages of the fusion reaction (Lee, 2010); (ii) at pH 5.25 or lower, M1 detaches from the membrane, which is thought to make the membrane more pliable, enabling the membranes to merge (see Chapter 2). We also found that at the late stages of membrane fusion (pH 5.25, 30 minutes after acidification), the majority of influenza virus particles (more than 80%) lacked the matrix layer and formed postfusion influenza-liposome complex, while a small percentage of unfused influenza virus particles (less than 20%) exhibited matrix layer that was still associated with the viral envelope (see Chapter 2). From these data we conclude that both the HA fusion protein and M1 matrix protein are tuned to respond to acidic pH conditions and that the sequence of HA refolding and M1-envelope interactions may be important for mediating efficient membrane fusion.

A key piece of information that is not yet available relates to the nature of interaction between the M1 protein and the cytoplasmic tails of the two viral membrane glycoproteins, HA and NA. Some studies have provided suggestive evidence of a direct interaction between these components (Enami & Enami, 1996; Jin *et al*, 1997; Ali *et al*, 2000; Lee, 2010), but this interaction has not been characterized at a structural level. We hypothesize that the M1 matrix layer influences HA's refolding process during fusion through its interactions with the HA cytoplasmic tail and the closely associated transmembrane anchor domain that is embedded in the viral membrane. It has been proposed that target-membrane inserted fusion peptide needs to associate with this HA transmembrane domain (TMD) in order to complete the fusion process (Kemble *et al*, 1993; 1994). In the presence of an intact matrix layer, the HA TMD that is connected the tail would be restrained. As pH is lowered towards 5.0, the M1 matrix layer dissociates from the viral envelope and releases the HA cytoplasmic tails. This would allow the TMD to associate

with fusion peptide locking in the hairpin, post-fusion form of HA and promoting the completion of membrane merging. Based on our tomographic observations, we assume that the matrix layer dissociation releases the final constraints that allow the membranes to transition past the tightly docked interfaces (Type-III) into the postfusion complex (Type-IV).

To better characterize the M1/HA tail interaction, in it will be of interest to carry out sub-tomogram averaging of cryo-electron tomograms gathered for X31 virus particles by cryo-ET under neutral (pH 7.5), early fusion (pH 5.5) and late fusion (pH 5.0) conditions. We would expect to directly observe the co-localization of M1 and HA cytoplasmic tails at neutral pH, but this type of co-localization may vanish at acidic pH. By averaging boxed sub-tomographic regions together, it is possible to improve the resolution of some features and to better characterize how these components interact with each other (Briggs, 2013). Bald virus particles in which the surface HA spikes are removed by Bromelain digestion would be favorable reagents to use because bald viruses are not fusogenic at acidic pH and are ideal specimens embedded in the thin ice for high contrast imaging (BRAND & Skehel, 1972).

5.3 Molecular architecture of the extended interface

In Chapter 2, we identified a striking membrane-virus interaction of sandwiched membranes extending over broad spans of the virus surface. Our kinetics experiments demonstrated that these states were on-pathway intermediates leading to efficient membrane fusion, rather than off-pathway trapped states. In these zones, the two proximal leaflets (virus and liposome outer leaflets) in many cases became indistinguishable from a single leaflet, however the detailed spatial organization of lipids in the tightly docked contact zones remains beyond the resolution of cryo-ET. In computational simulations, other groups reported that when two liposomes approach, the water layer between vesicles thinned until a transition state was attained in which the two lipids tails could be splayed with one tail in each membrane and the head group positioned between the two (Kasson *et al*, 2010; Smirnova *et al*, 2010). Their observation is

consistent with our cryo-ET observation that the width of this electron dense zone is no thicker than one would expect for the electron-dense phosphate head group layer of a single leaflet (~2nm; Figure 2.5). It isn't clear the extent to which lipid mixing takes place across this type of boundary.

We hypothesize that lipids are able to exchange or flip between the tightly associated layers. Our rationale for this is based upon the kinetics of lipid mixing reported by the fluorescence fusion assays. These consistently take place on a faster time scale than we observed by cryo-ET despite similar experimental conditions (as close as possible given the limitations of each technique). In future fluorescence assays, it will be valuable to test different types of lipidic probes to test whether all fluorescent probes report on the same lipid mixing process. Some studies have reported discrepancies of fusion monitored for different fluorescent reporters (Stegmann *et al*, 1993; Nunes-Correia *et al*, 2002; Blumenthal *et al*, 2002).

The fluorescence probes should meet the following requirements: (i) pH-independent fluorescence over the range of pH (5.0-7.5) examined in these studies; (ii) curvature-independent because of the membrane deformation and curvature changing during viral membrane fusion; (iii) non or little non-specific probe transfer from labeled membranes to unlabeled membranes upon prolonged incubation. Examples of these probes that might be useful in our self-quenching studies are octadecylrhodamine B chloride (R18) with solo bilayer-anchoring chain and phosphatidylethanolamine (Ph-PE) which has two long fatty acid chains. It is quite likely that the fluorescent lipid probes could also exchange at the tightly docked interfaces and the rate of the exchange is expected to be related with the structures of the probes (Nunes-Correia *et al*, 2002; Willem *et al*, 1990). We anticipate that the dequenching of high-frequency exchanging dye will be monitored during the formation of the extended docking contacts, while the dequenching of low-frequency exchanging dye will result from the complete membrane fusion. In addition, lipid-conjugated probes based fluorescence resonance energy transfer (FRET) which have been widely used in lipid mixing assays will also be tested (Struck *et al*, 1981; Domanska *et al*, 2013).

In a final experiment I also plan to freeze cryo-EM samples directly from my fluorescence assays at time points that indicate the fluorescence signal has plateaued. I will assess the cryo-electron tomograms of these specimens to determine whether the virus particles have completed fusion (post-fusion complexes) or are still predominantly in the extended contact zone state (type III contacts).

5.4 HPIV3 fusion with liposomes

Viral membrane fusion is driven by specialized fusion glycoproteins that bring viral envelope and target membrane in close apposition and form a fusion pore. The trigger that initiates a series of conformational rearrangements in the fusion glycoproteins leading to membrane merger varies depending on the pathway that the virus uses to enter the cell and thus whether fusion occurs at the surface at neutral pH or in the endosome. For influenza virus, the fusion glycoprotein HA is triggered when the virus is exposed to low pH inside the late endosomes. However, in paramyxoviruses, the F proteins are activated when the adjacent receptor binding protein binds to cellular receptor, initiating the fusion process (Lamb & Jardetzky, 2007; Jardetzky & Lamb, 2014; Harrison, 2015). In Chapter 4, we have revealed the organization of surface glycoproteins on human parainfluenza virus 3 (HPIV3) and built a model in which receptor binding proteins (hemagglutinin-neuraminidase, HN) associates with fusion (F) proteins before receptor engagement (Gui *et al*, 2015). But another key question has still eluded characterization: what are the structural changes in HN after HN binding to the receptor? How the structural changes in HN are relevant to the triggering of F proteins?

In order to better define the activation mechanism between HN and F, our hypothesis is that the receptor engagement encourages oligomerization of HN subunits into functional HN that activate F. This hypothesis can be tested by mixing the whole HPIV3 virions with receptor-presenting liposomes. Previous *in vivo* and *in vitro* studies of HPIV3 have shown that the HPIV3 bound predominantly to receptors containing α2,3-linked sialic acid and receptor engagement

resulted the release of fusion peptides of F proteins (Moscona & Peluso, 1993; Connolly *et al*, 2006). Liposomes containing gangliosides or erythrocyte-derived vesicles should be able to promote fusion in this system. A combined approach including fluorescence assay to monitor fusion reaction kinetics and cryo-ET to visualize the oligomerization of HN upon receptor engagement analogous to what I have used to study influenza virus would be an effective way to study this parallel system.

We also note that in the absence of HN, heat has reported as as a surrogate F trigger and F proteins alone could induce liposome association at 50 °C (Connolly *et al*, 2006; 2009). Other studies suggested that HPIV3 HN stabilizes the prefusion F protein with respect to thermal triggering (Porotto *et al*, 2012). Thus, it may be of interest to image the surface organization of HN and F proteins after heat shock perhaps in the presence of liposomes as target membranes. Overall, imaging the viral fusion nano-machinery will deepen our understanding of paramyxovirus membrane fusion and will allow us to identify strategies for interfering with the process and arresting the infection cycle.

5.5 Concluding remarks

My studies have shown that a combination of biophysical and structural approaches can provide new insights into the process of protein-mediated membrane fusion. The findings I described for viral systems likely also will apply in some fashion to other protein-mediated fusion systems such as SNARE and dynamin-driven cases. Central to addressing all of these systems and membrane fusion at a mechanistic level will be the use of methods such as cryo-ET to directly image the membranes as they are being remodeled during fusion and the fusion proteins that mediate this essential biological process.

Reference:

Aeffner S, Reusch T, Weinhausen B & Salditt T (2012) Energetics of stalk intermediates in membrane fusion are controlled by lipid composition. *Proc. Natl. Acad. Sci. USA* **109:** E1609–18

Ali A, Avalos RT, Ponimaskin E & Nayak DP (2000) Influenza virus assembly: effect of influenza virus glycoproteins on the membrane association of M1 protein. *J. Virol.* **74:** 8709–8719

Blumenthal R, Gallo SA, Viard M, Raviv Y & Puri A (2002) Fluorescent lipid probes in the study of viral membrane fusion. *Chem. Phys. Lipids* **116:** 39–55

Bonnafous P, Nicolaï M-C, Taveau J-C, Chevalier M, Barrière F, Medina J, Le Bihan O, Adam O, Ronzon F & Lambert O (2014). Treatment of influenza virus with Beta-propiolactone alters viral membrane fusion. *BBA - Biomembranes* **1838:** 355–363

BRAND CM & Skehel JJ (1972) Crystalline Antigen from the Influenza Virus Envelope. *Nature New Biology* **238:** 145–147

Briggs JAG (2013) Structural biology in situ--the potential of subtomogram averaging. *Curr. Opin. Struct. Biol.* **23:** 261–267

Chan DC & Kim PS (1998) HIV entry and its inhibition. *Cell* **93:** 681–684

Chernomordik LV & Kozlov MM (2008) Mechanics of membrane fusion. *Nat. Struct. Mol. Biol.* **15:** 675–683

Chlanda P, Mekhedov E, Waters H, Schwartz CL, Fischer ER, Ryham RJ, Cohen FS, Blank PS & Zimmerberg J (2016) The hemifusion structure induced by influenza virus haemagglutinin is determined by physical properties of the target membranes. *Nat. Microbiol* **50:** 16050–8

Connolly SA, Leser GP, Jardetzky TS & Lamb RA (2009) Bimolecular complementation of paramyxovirus fusion and hemagglutinin-neuraminidase proteins enhances fusion: implications for the mechanism of fusion triggering. *J. Virol.* **83:** 10857–10868

Connolly SA, Leser GP, Yin H-S, Jardetzky TS & Lamb RA (2006) Refolding of a paramyxovirus F protein from prefusion to postfusion conformations observed by liposome binding and electron microscopy. *Proc. Natl. Acad. Sci. U.S.A.* **103:** 17903–17908

Connor J, Gillum K & Schroit AJ (1990) Maintenance of lipid asymmetry in red blood cells and ghosts: effect of divalent cations and serum albumin on the transbilayer distribution of phosphatidylserine. *BBA - Biomembranes* **1025:** 82–86

de Lima MC, Ramalho-Santos J, Flasher D, Slepushkin VA, Nir S & Düzgüneş N (1995) Target cell membrane sialic acid modulates both binding and fusion activity of influenza virus. *Biochim. Biophys. Acta* **1236:** 323–330

Diao J, Grob P, Cipriano DJ, Kyoung M, Zhang Y, Shah S, Nguyen A, Padolina M, Srivastava A, Vrljic M, Shah A, Nogales E, Chu S & Brunger AT (2012) Synaptic proteins promote

calcium-triggered fast transition from point contact to full fusion. *eLife* **1:** e00109–e00109

Domanska MK, Wrona D & Kasson PM (2013) Multiphasic effects of cholesterol on influenza fusion kinetics reflect multiple mechanistic roles. *Biophys J.* **105:** 1383–1387

Ellens H, Bentz J, Mason D, Zhang F & White JM (1990) Fusion of influenza hemagglutinin-expressing fibroblasts with glycophorin-bearing liposomes: role of hemagglutinin surface density. *Biochemistry* **29:** 9697–9707

Enami M & Enami K (1996) Influenza virus hemagglutinin and neuraminidase glycoproteins stimulate the membrane association of the matrix protein. *J. Virol.* **70:** 6653–6657

Fontana J & Steven AC (2013) At low pH, Influenza virus matrix protein M1 undergoes a conformational change prior to dissociating from the membrane. *J. Virol.* **87:** 5621–5628

Fontana J & Steven AC (2015) Archives of Biochemistry and Biophysics. Influenza virus-mediated membrane fusion: structural insights from electron microscopy. *Arch. Biochem. Biophys.* **581:**86-97

Garcia NK, Guttman M, Ebner JL & Lee KK (2015) Dynamic changes during acid-induced activation of influenza hemagglutinin. *Structure* **23:** 665–676

García-Sastre A (2010) Influenza virus receptor specificity: disease and transmission. *Am. J. Pathol.* **176:** 1584–1585

Gui L, Jurgens EM, Ebner JL, Porotto M, Moscona A, Lee KK (2015) Electron tomography imaging of surface glycoproteins on human parainfluenza virus 3: association of receptor binding and fusion proteins before receptor engagement. *mBio* **6**:e02393-14.

Haque ME, McIntosh TJ & Lentz BR (2001) Influence of lipid composition on physical properties and PEG-Mediated fusion of curved and uncurved model membrane vesicles: 'Nature's Own' fusogenic lipid bilayer. *Biochemistry* **40:** 4340–4348

Harrison SC (2008) Viral membrane fusion. *Nat. Struct. Mol. Biol.* **15:** 690–698

Harrison SC (2015) Viral membrane fusion. *Virology* **479-480:** 498–507

Hernandez JM, Stein A, Behrmann E, Riedel D, Cypionka A, Farsi Z, Walla PJ, Raunser S & Jahn R (2012) Membrane fusion intermediates via directional and full assembly of the SNARE complex. *Science* **336:** 1581–1584

Herrmann A, Pritzen C, Palesch A & Groth T (1988) The influenza virus-induced fusion of erythrocyte ghosts does not depend on osmotic forces. *Biochim. Biophys. Acta* **943:** 411–418

Jahn R, Lang T & Südhof TC (2003) Membrane fusion. *Cell* **112:** 519–533

Jardetzky TS & Lamb RA (2014) Activation of paramyxovirus membrane fusion and virus entry. *Curr. Opin. Virol.* **5:** 24–33

Jin H, Leser GP, Zhang J & Lamb RA (1997) Influenza virus hemagglutinin and neuraminidase cytoplasmic tails control particle shape. *EMBO J.* **16:** 1236–1247

Kanaseki T (1997) Structural features of membrane fusion between influenza virus and liposome as revealed by quick-freezing electron microscopy. *J. Cell. Biol.* **137**:1041-56.

Kasson PM, Lindahl E & Pande VS (2010) Atomic-resolution simulations predict a transition state for vesicle fusion defined by contact of a few lipid tails. *PLoS Comput Biol* **6:** e1000829

Kemble GW, Danieli T & White JM (1994) Lipid-anchored influenza hemagglutinin promotes hemifusion, not complete fusion. *Cell* **76:** 383–391

Kemble GW, Henis YI & White JM (1993) GPI-and transmembrane-anchored influenza hemagglutinin differ in structure and receptor binding activity. *J. Cell Biol.* **122**:1253-65

Kobayashi T, Beuchat M-H, Chevallier J, Makino A, Mayran N, Escola J-M, Lebrand C, Cosson P, Kobayashi T & Gruenberg J (2002) Separation and characterization of late endosomal membrane domains. *J. Biol. Chem.* **277:** 32157–32164

Lamb RA & Jardetzky TS (2007) Structural basis of viral invasion: lessons from paramyxovirus F. *Curr. Opin. Struct. Biol.* **17:** 427–436

Lee KK (2010) Architecture of a nascent viral fusion pore. *EMBO J.* **29:** 1299–1311

Lee KK, Pessi A, Gui L, Santoprete A, Talekar A, Moscona A & Porotto M (2011) Capturing a fusion intermediate of influenza hemagglutinin with a cholesterol-conjugated peptide, a new antiviral strategy for influenza virus. *J. Biol. Chem.* **286:** 42141–42149

Martens S & McMahon HT (2008) Mechanisms of membrane fusion: disparate players and common principles. *Nat. Rev. Mol. Cell. Biol* **9:** 543–556

Moscona A & Peluso RW (1993) Relative affinity of the human parainfluenza virus type 3 hemagglutinin-neuraminidase for sialic acid correlates with virus-induced fusion activity. *J. Virol.* **67:** 6463–6468

Nir S, Klappe K & Hoekstra D (1986) Kinetics and extent of fusion between Sendai virus and erythrocyte ghosts: application of a mass action kinetic model. *Biochemistry* **25:** 2155–2161

Nunes-Correia I, Eulálio A, Nir S, Düzgünes N, Ramalho-Santos J & Pedroso De Lima MC (2002) Fluorescent probes for monitoring virus fusion kinetics: comparative evaluation of reliability. *Biochim. Biophys. Acta* **1561:** 65–75

Pinto LH, Holsinger LJ & Lamb RA (1992) Influenza virus M2 protein has ion channel activity. *Cell* **69:** 517–528

Porotto M, Salah ZW, Gui L, Devito I, Jurgens EM, Lu H, Yokoyama CC, Palermo LM, Lee KK & Moscona A (2012) Regulation of paramyxovirus fusion activation: the hemagglutinin-neuraminidase protein stabilizes the fusion protein in a pretriggered state. *J. Virol.* **86:** 12838–12848

Ramalho-Santos J & Pedroso De Lima MC (2004) The role of target membrane sialic acid residues in the fusion activity of the influenza virus: the effect of two types of ganglioside on the kinetics of membrane merging. *Cell. Mol. Biol. Lett.* **9:** 337–351

Reda T, Blumenthal R, Müller P & Herrmann A (2009) Influence of the spectrin network on fusion of influenza virus with red blood cells. *Molec. Membrane Biol.* **12:** 271–276

Rossman JS & Lamb RA (2011) Influenza virus assembly and budding. *Virology* **411:** 229–236

Seigneuret M & Devaux PF (1984) ATP-dependent asymmetric distribution of spin-labeled phospholipids in the erythrocyte membrane: relation to shape changes. *Proc. Natl. Acad. Sci. U.S.A.* **81:** 3751–3755

Skehel JJ (1992) Amantadine blocks the channel. *Nature* **358:** 110–111

Smirnova YG, Marrink S-J, Lipowsky R & Knecht V (2010) Solvent-exposed tails as prestalk transition states for membrane fusion at low hydration. *J. Am. Chem. Soc.* **132:** 6710–6718

Steck TL (1974) Preparation of Impermeable Inside-Out and Right-Side-Out Vesicles from Erythrocyte Membranes. *Methods Enzymol.* **31**:172-80.

Steck TL, Weinstein RS, Straus JH & Wallach DFH (1970) Inside-Out Red Cell Membrane Vesicles: Preparation and Puirification. *Science* **168:** 255–257

Stegmann T, Schoen P, Bron R, Wey J, Bartoldus I, Ortiz A, Nieva JL & Wilschut J (1993) Evaluation of viral membrane fusion assays. Comparison of the octadecylrhodamine dequenching assay with the pyrene excimer assay. *Biochemistry* **32:** 11330–11337

Struck DK, Hoekstra D & Pagano RE (1981) Use of resonance energy transfer to monitor membrane fusion. *Biochemistry* **20:** 4093–4099

van Meer G, Voelker DR & Feigenson GW (2008) Membrane lipids: where they are and how they behave. *Nat. Rev. Mol. Cell. Biol.* **9:** 112–124

Verkleij AJ, Zwaal RF, Roelofsen B, Comfurius P, Kastelijn D & van Deenen LL (1973) The asymmetric distribution of phospholipids in the human red cell membrane. A combined study using phospholipases and freeze-etch electron microscopy. *Biochim. Biophys. Acta* **323:** 178–193

White JM, Delos SE, Brecher M & Schornberg K (2008) Structures and Mechanisms of Viral Membrane Fusion Proteins: Multiple Variations on a Common Theme. *Crit. Rev. Biochem. Mol. Biol.* **43:** 189–219

Willem J, Beest ter M, Scherphof G & Hoekstra D (1990) A non-exchangeable fluorescent phospholipid analog as a membrane traffic marker of the endocytic pathway. *Eur. J. Cell Biol.* **53:** 173–184